2009

Boreal forest fire impacts on lower troposphere carbon monoxide and ozone levels at the regional to hemispheric scales

Kateryna Lapina
Michigan Technological University

Boreal forest fire impacts on lower troposphere CO and ozone levels at the regional to hemispheric scales

By

Kateryna Lapina

A DISSERTATION

Submitted in partial fulfillment of the requirements

for the degree of

DOCTOR OF PHILOSOPHY

(Environmental Engineering)

MICHIGAN TECHNOLOGICAL UNIVERSITY

2009

This dissertation, "Boreal forest fire impacts on lower troposphere CO and ozone levels at the regional to hemispheric scales," is hereby approved in partial fulfillment of the requirements for the degree of DOCTOR OF PHILOSOPHY (Environmental Engineering).

Geological and Mining Engineering and Sciences

Dr. Judith Perlinger, Committee Co-Chair

Dr. Detlev Helmig, Committee Co-Chair

Dr. Judith Perlinger, Non-Departmental Program Chair

Date

Dedicated to the memory of Richard Honrath.

Abstract

Tropospheric ozone (O_3) and carbon monoxide (CO) pollution in the Northern Hemisphere is commonly thought to be of anthropogenic origin. While this is true in most cases, copious quantities of pollutants are emitted by fires in boreal regions, and the impact of these fires on CO has been shown to significantly exceed the impact of urban and industrial sources during large fire years. The impact of boreal fires on ozone is still poorly quantified, and large uncertainties exist in the estimates of the fire-released nitrogen oxides (NO_x), a critical factor in ozone production. As boreal fire activity is predicted to increase in the future due to its strong dependence on weather conditions, it is necessary to understand how these fires affect atmospheric composition. To determine the scale of boreal fire impacts on ozone and its precursors, this work combined statistical analysis of ground-based measurements downwind of fires, satellite data analysis, transport modeling and the results of chemical model simulations.

The first part of this work focused on determining boreal fire impact on ozone levels downwind of fires, using analysis of observations in several-days-old fire plumes intercepted at the Pico Mountain station (Azores). The results of this study revealed that fires significantly increase midlatitude summertime ozone background during high fire years, implying that predicted future increases in boreal wildfires may affect ozone levels over large regions in the

Northern Hemisphere.

To improve current estimates of NO_x emissions from boreal fires, we further analyzed $\Delta NO_y/\Delta CO$ enhancement ratios in the observed fire plumes together with transport modeling of fire emission estimates. The results of this analysis revealed the presence of a considerable seasonal trend in the fire NO_x/CO emission ratio due to the late-summer changes in burning properties. This finding implies that the constant NO_x/CO emission ratio currently used in atmospheric modeling is unrealistic, and is likely to introduce a significant bias in the estimated ozone production.

Finally, satellite observations were used to determine the impact of fires on atmospheric burdens of nitrogen dioxide (NO_2) and formaldehyde (HCHO) in the North American boreal region. This analysis demonstrated that fires dominated the HCHO burden over the fires and in plumes up to two days old. This finding provides insights into the magnitude of secondary HCHO production and further enhances scientific understanding of the atmospheric impacts of boreal fires.

Acknowledgements

I would like to express my deep gratitude to my adviser, Dr. Richard Honrath, for his constant guidance, inspiration and support throughout my Ph.D. work. He was a great mentor, outstanding scientist and a wonderful person, who introduced me to the exciting world of atmospheric chemistry and inspired me to pursue a carreer in atmospheric research. I also would like to thank my committee, Drs. David Watkins, Will Cantrell and Simon Carn, for their contribution and guidance. I thank my research group, Dr. Maria Val Martín, Dr. Chris Owen, Dr. Jan Kleissl, Claudia Toro, Dr. Louisa Kramer and J. M. Strane for their support and contributions to my research. I would like to thank Mike Dziobak and Dr. Paulo Fialho (Azores University, Portugal) for their efforts in installing and maintaining the Pico Mountain observatory. I would like to gratefully acknowledge Gabi Pfister (UCAR) for providing MOZART simulations, Edward Hyer (NRL) for providing BWEM fire emissions inventory, Andreas Richter and Folkard Wittrock (University of Bremen, Germany) for providing SCIAMACHY data, Colette Heald (CSU) for the isoprene model simulations, Andreas Stohl (NILU, Norway) for the FLEXPART model, Diamantino Henriques (Portuguese Meteorological Institute) for the ECMWF data used for FLEXPART simulations, and NOAA Air Resources Laboratory for the HYSPLIT transport model. The MODIS data used in this work were acquired as part of NASA's Earth Science Enterprise

and obtained from the Goddard Distributed Active Archive Center. This work was supported by NOAA, Office of Global Programs, grants NA16GP1658, NA86GP0325 and NA03OAR4310002, and by National Science Foundation grants ATM-0215843, ATM-0535486 and INT-0110397, MTU Finishing Fellowship, MTU CEE department, Azores Regional Secretariat for Science and Technology (Project M1.2.1/I/006/2005), Program INTERREG IIIB, Azores, Madeira and Canaries (Project CLIMARCOST FEDER-INTERREG IIIB-05/MAC/2.3/A1) and the Portuguese Science and Technological Foundation (Project POCTI-32649-CTA-2000 and Grant SFRH/BD/9049/2002).

I would like to thank my family for their love and support. I would also like to thank Ezequiel Medici, Claudia Toro, Doug and Deb McDowell and many other wonderful friends in the UP for their support and friendship and for all the great times we had together. Special thanks to the International Folk dancing group in Hancock, MI, for many fun hours of dancing.

Contents

List of Figures

List of Tables

Chapter 1

Introduction

1.1 Background

Biomass burning is a significant source of atmospheric trace gases and particles [*e.g. Crutzen and Andreae*, 1990; *Andreae and Merlet*, 2001] with the potential to affect air quality not only at the regional but also at the hemispheric scales [*Edwards et al.*, 2004; *Yurganov et al.*, 2004; *Van der Werf et al.*, 2004; *Kasischke et al.*, 2005]. For example, global biomass burning accounts for 15-30% of the entire tropospheric CO background [*Galanter et al.*, 2000]. Fires also serve as an important source of ozone precursors, such as NO_x and non-methane hydrocarbons (NMHC) [*Goode et al.*, 2000; *Andreae and Merlet*, 2001], and were shown to explain most of the interannual variability in summer organic carbon aerosol in the western U.S. [*Spracklen et al.*, 2007].

The impact of forest fires in boreal regions (regions located north of 45° N latitude) on atmospheric composition was significantly underestimated in the past years [*Lavoue et al.*, 2000], but received considerable attention recently, as new measurements, *i.e.*, from satellites [*Stocks et al.*, 2003], became available, and a significant increase in the annual area burned across the North

American region was observed [*Gillet et al.*, 2004; *Kasischke and Turetsky*, 2006]. Boreal forests contain one third of all terrestrial carbon storage and can generate up to 20% of the global biomass burning carbon through direct and indirect (post-fire) emissions [*Conard and Ivanova*, 1997]. In the summer, CO emissions from boreal wildfires are similar in magnitude to total U.S. and European anthropogenic emissions even in average fire years [*Wotawa et al.*, 2001], and their impact on atmospheric burden can significantly exceed the impact of CO from fossil fuels during the months with extremely high fire activity [*Yurganov et al.*, 2004]. Boreal fires also emit large amounts of aerosols and contribute 10% of total anthropogenic black carbon emissions in the Northern Hemisphere, on average [*Bond et al.*, 2004]. An important feature of intense crown fires in the boreal regions is their ability to inject emissions into the upper troposphere and even stratosphere [*Fromm and Servanckx*, 2003; *Jost et al.*, 2004]. Lifting of pollution plumes into these high-altitude layers increases the lifetimes of emitted species and results in dispersion of pollutants over a large spatial scale due to faster transport [*Fromm and Bevilacqua*, 2004]. Prolonged lifetimes of particles at these altitudes may lead to changes in the radiative balance of the atmosphere [*Law and Stohl*, 2007].

Most important, in terms of the amount of generated emissions, is a small number of large fires generated by lightning in remote areas [*Stocks et al.*, 2003]. The episodic nature of these fires implies that they can release large amounts of pollutants into the atmosphere over relatively short timescales [*Stocks et al.*, 1998]. Low levels of hydroxyl radical (OH) at high latitudes result in enhanced lifetime of these pollutants [*Levine and Cofer III*, 2000], allowing formation of large, long-lasting pollution plumes. The frequency of occurrence of boreal fires varies dramatically on a year-to-year basis and is highly sensitive to changes in meteorological conditions [*Stocks et al.*, 1998; *Flannigan et al.*, 2005]. Consequently, these fires may become more frequent

in response to global warming, which will cause the largest temperature increase over the high-latitude regions [*Hassol*, 2004; *IPCC*, 2007]. General circulation models (GCMs) predict more extreme droughts and increases in lightning frequency, fire intensity and fire length in response to doubled-CO_2 concentrations in the atmosphere [*Stocks et al.*, 1998]. The resulting net loss of carbon from the biosphere to the atmosphere and changes in the albedo of areas impacted by burning have a potential for creating a positive feedback between climate warming and fire activities, which would aggravate the fire situation even further [*Stocks et al.*, 1998; *IPCC*, 2007]. It is therefore crucial to understand and quantify the impact of boreal fires on atmospheric composition in order to determine the effects of climate change on air quality.

While it has been accepted that wildfires affect the interannual variability of CO in the Northern Hemisphere [*Yurganov et al.*, 2004; *Van der Werf et al.*, 2004; *Novelli et al.*, 2003; *Kasischke et al.*, 2005], the impact of fires on tropospheric ozone (O_3) is less conclusive and it is generally recognized that ozone production in the Northern Hemisphere is dominated by anthropogenic sources. Ozone is the major source of hydroxyl radical (OH), a compound which controls the oxidizing capacity of the atmosphere, and is an important oxidant itself [*Seinfeld and Pandis*, 1998]. It is the third most important greenhouse gas [*IPCC*, 2007] and its elevated concentrations have negative impacts on health and plants. Ozone levels in the U.S. are regulated by the Environmental Protection Agency (US EPA) which recently lowered the 8-hour standard from 0.08 ppm to 0.075 ppm. Complying with these standards requires good understanding of sources contributing to the ozone budget.

Ozone is formed from the photolysis of NO_2 and subsequent reaction of the oxygen atom with molecular oxygen:

$$NO_2 + h\nu \rightarrow NO + O(^3P) \tag{1.1}$$

$$O(^3P) + O_2 \rightarrow O_3 \tag{1.2}$$

Ozone then reacts with NO to form NO_2

$$O_3 + NO \rightarrow O_2 + NO_2 \tag{1.3}$$

In addition to the above reactions, which constitute a zero cycle for O_3, additional O_3 formation can be achieved in the presence of HO_2 or organic peroxy radicals that oxidize NO to NO_2 without destroying ozone:

$$NO + PO_2 \rightarrow NO_2 + PO, \tag{1.4}$$

where peroxy radicals are formed from the oxidation of non-methane volatile organic compounds (NMVOCs). While anthropogenic sources of pollution, such as cars and industry, are known to be the dominant contributors to O_3 in the areas where standards are commonly exceeded, intense periods of fire activity, which result in release of large amounts of ozone precursors such as NO_x (sum of NO and NO_2) and NMVOCs, were found to significantly increase the frequency of such exceedances [*Pfister et al.*, 2008]. Recent work showed that boreal fires can impact summertime ozone levels in the U.S. and Europe [*Jaffe et al.*, 2004; *Simmonds et al.*, 2005; *Forster et al.*, 2001], even at the locations where anthropogenic pollution levels are normally very high [*Morris et al.*, 2006]. *Jaffe et al.* [2004] showed that in the summer of 2003, large Siberian fires contributed to an exceedance of O_3 regulatory standard at the surface site in the Northwestern US. For a few other sites in Alaska, British Columbia and Washington, these fires resulted in the highest mean summer O_3 mixing ratios since the records were kept.

Despite these given examples of the significant impacts of boreal fires on ozone, ozone production in the boreal fire plumes is still not fully understood and there is no clear picture of the average magnitude of this impact.

While *Honrath et al.* [2004] and *Bertschi and Jaffe* [2005] showed that ozone enhancement ratios ($\Delta O_3/\Delta CO$) can be very high even in very well-aged plumes (more than 10 days old), suppressed ozone formation was observed as well [*Tanimoto et al.*, 2000], and ozone enhancement ratios in the aged (7–15 days old) boreal fire plumes at the Pico Mountain Observatory (Azores) exhibited high variability [*Val Martín et al.*, 2006], implying the need for further studies.

One of the possible reasons for the observed difference in ozone enhancement ratios is the highly variable NO_x/CO emission ratio for boreal fires, which plays a determining role in the ozone production [*Goode et al.*, 2000; *McKeen et al.*, 2002; *Cook et al.*, 2007]. This ratio is believed to be lower for boreal fires, than for fires in other ecosystems, such as tropics and savanna due to the dominant role of the smoldering (as opposed to flaming) stage in the fuel burning for boreal fires, as well as to the lower nitrogen content of boreal vegetation [*Wofsy et al.*, 1992]. Smoldering combustion is especially common for the burning of the ground surface layer, which contributes a major fraction of total fuel consumption in boreal forests [*French et al.*, 2004; *Kasischke and Johnstone*, 2005]. Quantifying the fraction of fuel consumed in smoldering versus flaming combustion is critical for reliable estimates of emissions of ozone precursors and is done using the fire-derived carbon emissions models [*Kasischke et al.*, 2005; *Turquety et al.*, 2007]. Improving these models represents a challenging task due to the high variability in fuel types and fire properties and is currently an active area of research [*French et al.*, 2007]. One of the vital steps in this process is testing the derived emission products against the existing measurements of ozone, NO_x, NO_y (which includes the oxidation products of NO_x in more aged plumes) and CO in the boreal fire plumes.

In summary, research on ozone production in the boreal fire plumes is far

from being complete, and more studies on factors controlling NO_x emissions from boreal fires is needed. If fires are shown to systematically affect the ozone levels in the far away regions, and given that this impact may increase in the future as a result of climate change, more stringent ozone air quality standards will have to be introduced for cars and industry. Hence, as many Northern Hemisphere regions strive to attain these standards, studies aimed at quantifying the impact of boreal fires on ozone in the regions downwind are of critical importance.

1.2 Research objectives and approach

Pico Mountain Observatory is a measurement station at a mountaintop site in the Azores Islands in the central North Atlantic region established in 2001 by our research group in collaboration with the University of Azores, Portugal. This site is mostly located in the free troposphere [*Kleissl et al.*, 2007] and in the summer it is frequently impacted by air from arctic/subarctic regions from North America and Eurasia carrying emissions from boreal wildfires [*Honrath et al.*, 2004]. Nearly continuous measurements of NO_x, NO_y O_3, BC, and CO are available for the boreal fire seasons in 2001, 2003, 2004 and 2005. This dataset is unique as it represents multi-year and multi-species measurements downwind of boreal regions.

In the previous section it was shown that the magnitude of boreal fire impact on ozone levels in the regions downwind is poorly quantified. Therefore, **the first objective of this work is to quantify the impact of boreal wildfires on midlatitude lower free tropospheric background O_3 during summer.** To accomplish this objective, observations made at the Pico Mountain Observatory were analyzed together with HYSPLIT backward trajectories and modeling of the boreal fire impact at the observatory using

MOZART chemical transport model. Analysis was performed for summertime observations of CO and O_3 during three years, which included two years of high fire activity (2003 and 2004) and one year of low fire activity (2001). The studied air masses represented pollution plumes that had already undergone considerable photochemical processing, but were not completely mixed in background air. This allowed the study of ozone production within well aged (7–15 days old) biomass burning plumes.

The previous section also discussed the need to improve the existing inventories of ozone precursors released from boreal fires and the effect of fire burning properties on these emissions. Hence, **the second objective of this work was to assess the impact of seasonal trends in fuel consumption and flaming/smoldering ratios in the boreal wildfires on emissions of NO_x (species dominated by flaming combustion) and CO (species dominated by smoldering combustion).** To accomplish this objective we used $\Delta NO_y/\Delta CO$ measurements in the several-days-old fire plumes at the Pico Mountain Observatory during the active boreal fire seasons of 2004 and 2005. Airmass history for the studied periods was analyzed using the FLEXPART transport model simulations.

To learn about the impact of boreal fires on ozone precursors in the fire region and immediately downwind of fires, the third objective of this work, we utilized satellite measurements of NO_2 and formaldehyde (HCHO), made with the SCIAMACHY instrument, over the regions of active boreal fires in Alaska and Canada in 2004. These measurements were combined with modeling of fire emissions. Emissions of NO_x and HCHO were estimated using the BWEM model, and simulations of fire emissions transport were performed using FLEXPART.

1.3 Dissertation overview

The following chapters convey methods, analyses, results and conclusions to address the research objectives of this work. Chapter 2 presents analysis of the multi-year (2001, 2003 and 2004) measurements of CO and ozone made at the Pico Mountain Observatory to which address the first research objective. Chapter 3 presents analysis performed to assess the seasonal trend in emissions from boreal forest fires. Chapter 4 presents analysis of the impact of boreal fires on atmospheric levels of formaldehyde and NO_2 in the North American boreal region during summer of 2004. The appendix includes figures used for this analysis.

Chapter 2

Evidence of significant large-scale impacts of boreal fires on ozone levels in the midlatitude Northern Hemisphere free troposphere[†]

[†]This chapter is based on material previously published as Lapina, K., R. Honrath, R. C. Owen, Val Martín M. and G. Pfister (2006), Evidence of significant large-scale impacts of boreal fires on ozone levels in the midlatitude Northern Hemisphere free troposphere, *Geophys. Res. Lett., 33*, L10815, doi:10.1029/2006GL025878.

2.1 Introduction

Boreal wildfires are known to significantly impact tropospheric composition [*e.g.*, *Van der Werf et al.*, 2004; *DeBell et al.*, 2004]. CO emissions have gained considerable attention in recent years, as the resulting impacts on tropospheric background CO levels are significant [*Novelli et al.*, 2003; *Edwards et al.*, 2004]. Recent studies have also identified increased mean summertime O_3 at boundary layer (BL) sites in northwest N. America and at Mace Head, Ireland during years of exceptionally large area burned [*Jaffe et al.*, 2004; *Simmonds et al.*, 2005], suggesting that boreal fires may also significantly impact background O_3. However, loss of ozone from the BL may mute this signal at BL sites [*DeBell et al.*, 2004], and the large-scale impact of boreal fires on FT O_3 levels remains poorly characterized.

O_3 plays a central role in tropospheric chemistry as a major source of hydroxyl radical. O_3 is phytotoxic, harmful to health and an important greenhouse gas [*Houghton et al.*, 2001]. Tropospheric O_3 production in the NH midlatitudes is dominated by anthropogenic sources, which impact tropospheric O_3 over large regions [*e.g.*, *Chandra et al.*, 2004]. However, northerly regions can be a substantial source of the O_3 precursors nitrogen oxides (NO_x, NO + NO_2), CO and volatile organic compounds [*Goode et al.*, 2000] during the boreal fire season (May–September). Quantifying the resulting impact of boreal fires on tropospheric O_3 is a challenging task, due to the large degree of variability in the type of fire and fuel [*Kasischke et al.*, 2005], which leads to variability and uncertainty in emissions of NO_x, a limiting factor for O_3 production. As a result, the magnitude of O_3 production from boreal fires is highly variable and uncertain, with the limited number of studies available reporting O_3 enhancements ranging from high [*e.g.*, *Bertschi and Jaffe*, 2005; *Honrath et al.*, 2004; *Law et al.*, 2005], to very low [*e.g.*, *Tanimoto et al.*, 2000]

in several-days-old fire plumes.

Most studies of O_3 in aged fire plumes are based on observations obtained during the sampling of individual plumes and therefore characterize a specific combination of fire type, meteorological conditions and plume age, or a limited number of such combinations. In contrast, this work utilizes multi-year (2001, 2003 and 2004) measurements at a site far downwind from the boreal fire region. Thus, the resulting dataset includes observations of fire plumes characteristic of multiple sources that have aged and dispersed during 5–15 days of transport [*Honrath et al.*, 2004]. In addition, this work utilizes FT measurements, a key distinction as BL O_3 loss may obscure the true magnitude of boreal fire O_3 impacts. It therefore provides a sampling of the large-scale impacts of boreal fires on FT O_3 levels.

2.2 Methods

To characterize the impact of boreal fires on O_3 mixing ratios in regions well downwind, we combine analysis of observations made at the PICO-NARE station with backward trajectories and the results of global simulations of fire emissions transport and chemistry.

2.2.1 Measurements

The PICO-NARE station is located on the summit caldera of Pico mountain in the Azores Islands (Portugal) in the central North Atlantic Ocean (38°N, 28°W). This station is frequently impacted by air from high-latitude regions, often without downwind transport over anthropogenic source regions [*Honrath et al.*, 2004]. It is therefore well suited to study the outflow from N. American and Siberian boreal wildfires. Station altitude (2225 m) is well above the marine boundary layer (MBL). To ensure that the measurements analyzed

here are characteristic of the FT, we have excluded from this analysis all periods potentially affected by upslope flow of MBL air [*Kleissl et al.*, 2005]. (This screening removed 30% of the measurements, but did not affect the results significantly.)

CO was determined using a modified non-dispersive infrared absorption instrument (Thermo Environmental, Inc., Model 48C-TL), calibrated daily with standards referenced to the NOAA CMDL standard [*Novelli et al.*, 2003]. O_3 was determined with commercial ultraviolet absorption instruments (Thermo Environmental Instruments Inc., Franklin, Massachusetts; Model 49C) referenced to the NOAA CMDL network ozone standard (S. Oltmans, NOAA/ESRL, personal communications, 2001, 2004). As a result of instrument damage due to water ingestion following heavy icing the previous winter, no O_3 data are available for summer 2002. Additional details on the instruments and calibration methods are provided elsewhere [*Honrath et al.*, 2004; *Owen et al.*, An analysis of transport mechanisms of North American emissions to the central North Atlantic, submitted to *J. Geophys. Res.*] Data were recorded as one-minute averages, and were further averaged to obtain the 1-hour averages used in this work.

2.2.2 Transport Analysis

To identify airmass transport pathways, we calculated hourly backward trajectories using the HYbrid Single-Particle Lagrangian Integrated Trajectories (HYSPLIT) model [*Draxler and Rolph*, 2003]. The model uses hourly wind vectors interpolated from 6-hourly National Weather Service National Center for Environmental Prediction FNL output [*Stunder*, 1997]. For each hour, a set of six trajectories was initiated: one terminating at the station, four terminating at end points separated by 1° of latitude and longitude from the

station, and one terminating directly below the station, at a height of 2000 m. Trajectories were run for 10 days backward in time, with trajectory locations recorded every hour.

We selected time periods potentially affected by outflow from boreal regions by picking hours when one or more of the trajectories passed over Alaska or Canada north of 50°N. These flow periods are referred to as northern N. American periods (abbreviated as NNA periods). They include multiple intervals of time impacted by N. American or Siberian fires, which last from hours to days [*Honrath et al.*, 2004].

2.2.3 MOZART Simulations

The global chemical transport model MOZART (Model for OZone And Related chemical Tracers) was used to simulate the impact of emissions from the 2004 N. American boreal fires on CO at the PICO-NARE station. MOZART was driven by 6-hourly meteorological fields from the National Centers for Environmental Prediction (NCEP) dataset. The spatial resolution is approximately $2.8° \times 2.8°$ with 28 vertical levels between the surface and 2 hPa. The chemical time step of the model is 20 minutes. The MOZART simulation results presented in this work are mixing ratios averaged over 2-hour windows and interpolated to the location and pressure of the PICO-NARE observatory. These simulations utilized updated N. American boreal fire emissions that were optimized using MOPITT (Measurements Of Pollution In The Troposphere) CO columns as described by *Pfister et al.* [2005]; CO emissions were injected between 0 and 9 km. To infer the magnitude of the fire impact at the PICO-NARE station, we use the MOZART-simulated ratio of CO fire tracer (CO that was emitted from the N. American boreal fires) to total CO mixing ratio at the PICO-NARE station, $([CO_f]/[CO])_{MOZART}$. A second

model run, in which N. American boreal fire emissions were turned off, was also conducted. Simulation results for O_3 from this run were used to assess the importance of processes other than boreal fire emissions on O_3 levels.

2.3 Results

Figure 2.1a shows the distribution of summer CO mixing ratios for the years of 2001, 2003 and 2004. In 2003 and 2004 CO exhibited maximum levels nearly twice as high as in 2001 (Table 2.1). High mixing ratios were also more frequent. Median values increased from 67 ppbv in 2001 to 108 and 87 ppbv in 2003 and 2004, respectively. We have shown previously [*Honrath et al.*, 2004] that 2001 was a low-fire year, while the highest CO levels in 2003 were the result of extreme Siberian fires that year. These fires consumed the largest area burned in more than ten years [*Jaffe et al.*, 2004]. 2004 was also a high-fire year, with the largest fire season on record in Alaska [*Pfister et al.*, 2005]. To confirm these fires as the primary cause of the high CO that year, we have inspected the backward trajectories for CO observations exceeding the 70th percentile of the 2004 summer measurements (98 ppbv). At least 75% of these cases were consistent with transport from the region of active fires in Alaska and/or western Canada based on MODIS (MODerate resolution Imaging Spectroradiometer) fire counts, with haze in the upwind region clearly visible in MODIS true-color images. Thus, the considerably higher CO mixing ratios observed in both 2003 and 2004 were the result of emissions from large fires transported to the Azores region in NNA flow. This conclusion is in accordance with recent works showing that boreal wildfires strongly affect the NH summer CO background during years of high fire activity [*Novelli et al.*, 2003; *Edwards et al.*, 2004; *Van der Werf et al.*, 2004; *Kasischke et al.*, 2005].

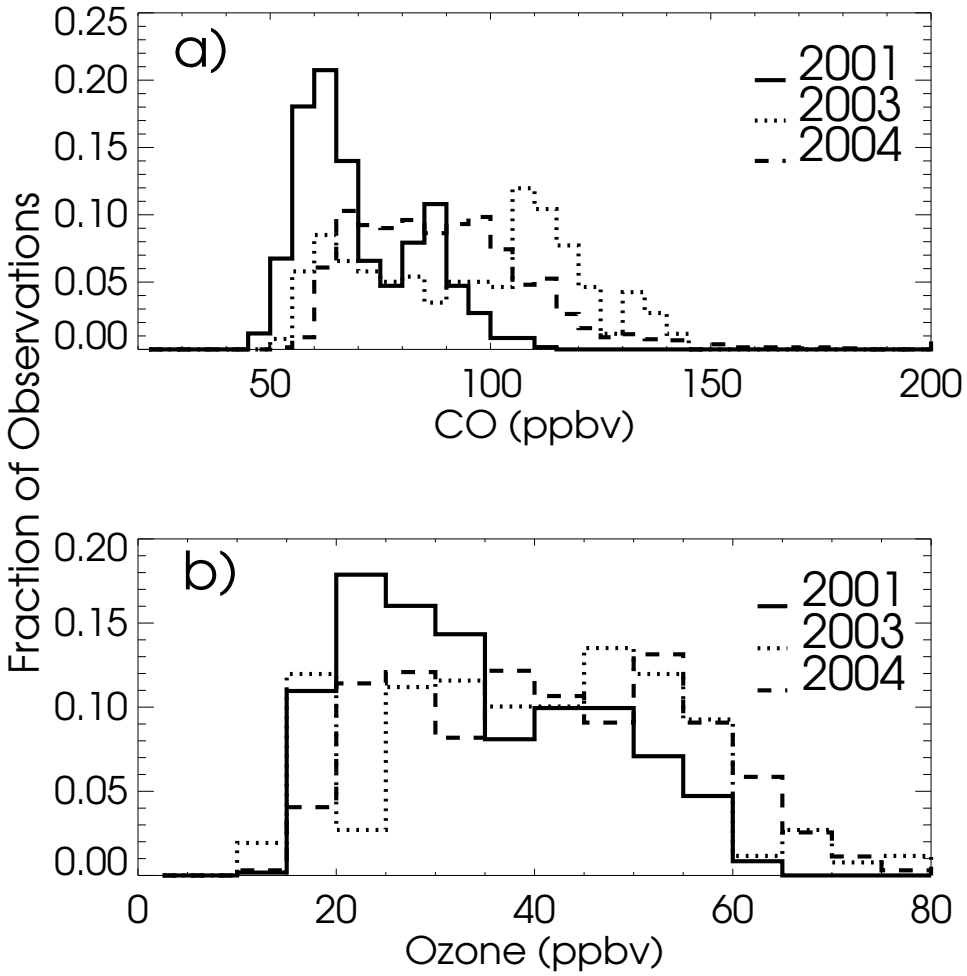

Figure 2.1 Distributions of (a) CO and (b) O_3 including all measurements for each summer. A small number of CO observations greater than the maximum value shown are included in the rightmost bin..

Table 2.1 Statistics of CO and O_3 distributions by year (all concentrations are in ppbv).

	CO					O_3					
Data subset	N	Mean	Median	Min	Max	N	Mean	Median	Min	Max	ΔMedian[c]
2001, All data[a]	606	70	67	47	111	593	34	31	14	65	
NNA[a]	187	82	85	57	111	184	42	44	14	65	
Non-fire, NNA[b]	50	71	69	61	82	50	32	32	14	59	
Fire, NNA[b]	25	97	96	88	111	25	53	55	37	65	24
2003, All data[a] 442	104	108	54	201	259	40	40	12	78		
NNA[a]	263	114	114	56	201	153	45	46	13	78	
Non-fire, NNA[b]	37	80	79	56	108	37	35	30	13	69	
Fire, NNA[b]	33	130	130	117	142	33	52	53	39	59	23
2004, All data[a]	1362	90	87	51	233	1332	41	41	13	79	
NNA[a]	852	97	95	56	233	842	45	46	15	79	
Non-fire, NNA[b]	200	76	76	56	90	200	33	30	15	69	
Fire, NNA[b]	248	122	114	99	233	248	51	52	32	74	22

N, Number of hourly average data points. [a]Measurements with either CO or O_3 are included. [b]Non-fire and fire subsets were selected using the 40th and 60th percentiles of the "NNA" CO distribution, MOZART simulations, and previously identified fire periods. The cutoffs are equal to the non-fire maximum and the fire minimum, respectively. [c]Difference between medians of the fire and non-fire O_3 subsets.

The distributions of summer O_3 mixing ratios were also shifted toward higher levels in 2003 and 2004 relative to 2001 (Figure 2.1b). Median O_3 increased from 31 ppbv in 2001 to 40 ppbv in 2003 and 41 ppbv in 2004 (Table 2.1). Given the prior observations of O_3 enhancements in individual boreal fire plumes noted above and the presence of elevated levels of nitrogen oxides in fire plumes sampled at the PICO-NARE station during 2004 [*Val Martín et al.*, 2005], O_3 production in the fire plumes may have contributed to the higher O_3 levels in 2003 and 2004. To evaluate this, we now test the hypothesis that boreal fire emissions result in significantly increased O_3 levels in the highly aged fire plumes sampled at the PICO-NARE station.

To assess the impact of boreal fires on O_3 levels, we analyze only those measurements obtained during NNA periods. This minimizes the potential impact of latitudinal O_3 gradients on the results. We selected from the full set of NNA periods those apparently impacted by fire emissions (termed "fire" airmasses) and those with clean background conditions (referred to as "non-fire" airmasses). Fire periods were identified based on the occurrence of significantly enhanced CO levels, confirmed by simulations of fire emissions transport. Non-fire periods were identified based on the occurrence of low CO levels and absent or minimal model-simulated fire impacts. The 40th and 60th percentiles of CO measurements in NNA flow periods (Table 2.1) were used for the non-fire and fire CO cutoff values, respectively. For 2004, we required $([CO_f]/[CO])_{MOZART} > 0.1$ for the fire periods; no intervals with $([CO_f]/[CO])_{MOZART} > 0.09$ were included within non-fire periods. For 2001 and 2003, we used the results of previous analyses [*Honrath et al.*, 2004], in which the NRL Aerosol Analysis and Prediction System model was used to identify PICO-NARE measurements potentially impacted by upwind boreal fires. Fire periods were required to be within those previously identified intervals, and non-fire periods were required to exclude those previously identified

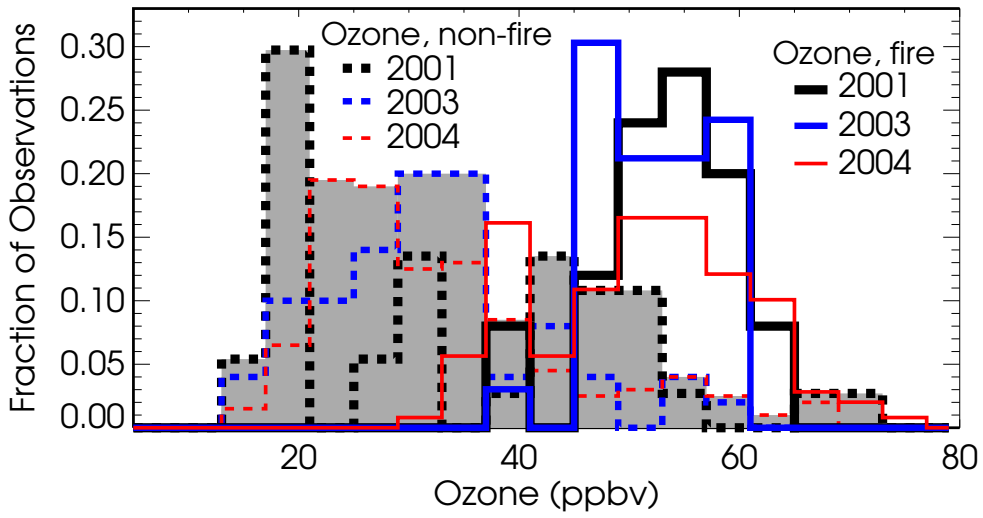

Figure 2.2 O_3 frequency distribution in Northern N. American (NNA) flow, fire and non-fire subsets. The area under the non-fire O_3 distributions is shaded..

intervals.

Histograms of O_3 for fire and non-fire periods in each year are shown in Figure 2.2. For each year, the two distributions are clearly different. Table 2.1 presents the medians, means and ranges of each distribution. To confirm that the O_3 distributions in the fire airmasses were significantly different from the O_3 distributions during the non-fire periods, we performed a nonparametric Wilcoxon Sum-rank test. We also performed a two-sample t-test to test for differences between the means of two distributions. These two tests gave consistent results at the 0.01 level of significance, indicating that the distributions were significantly different, with significantly higher mean values in the fire subset.

The differences between the median O_3 values in the non-fire and fire subsets each year (ΔMedian) are shown in Table 2.1. To estimate the contribution to ΔMedian resulting from latitudinal or altitudinal O_3 gradients not caused by fires, we repeated the analysis with the following difference.

Instead of using measured O_3 mixing ratios, we used [O_3] simulated at Pico in the 2004 MOZART simulation that excluded N. American boreal fire emissions. The resulting ΔMedian was 3 ppbv—14% of the actual value (22 ppbv: Table 2.1). To assess potential impacts of anthropogenic O_3 production, we repeated the original analysis but excluded periods with trajectories passing over N. America south of 48°N. ΔMedian changed by <1 ppbv. (Both reanalyses were conducted for 2004, the only year with sufficient data and MOZART simulations.) These results support the hypothesis that a majority of the observed fire minus non-fire O_3 differences is the result of boreal wildfire emissions.

We discussed above the effect of high fire activity in 2003 and 2004 on CO. Here, we see evidence of fire impacts in 2001 as well. This is the result of a relatively small number of 2001 events in which Siberian fire emissions reached the Azores, as noted previously [*Honrath et al.*, 2004]. These 2001 events had little effect on the overall CO and O_3 distributions, but nevertheless provide additional evidence of fire-enhanced O_3.

It is possible to obtain ozone enhancement ratios by dividing the values of ΔMedian (corrected by the MOZART-based estimate of 2004 non-fire contribution) by the difference between median CO in the fire and non-fire subsets. For 2004, the ratio is 0.5. This value is relatively large, but is in the range of the highest values measured in aged boreal fire plumes by the sources cited in the Introduction. However, further work is required to explain the mechanism leading to these high ozone enhancements.

2.4 Conclusions

By separating multi-year summertime O_3 observations impacted by outflow from high-latitude regions into two subsets composed of fire-affected and non-

fire (relatively clean) periods, we found that O_3 levels in the North Atlantic lower FT are significantly increased when boreal fire impacts are present. O_3 production from boreal fire precursors was therefore at least partially responsible for significant shifts in the O_3 distributions toward higher mixing ratios during the high-fire-activity summers of 2003 and 2004, when median O_3 values were 9–10 ppbv greater than during the summer of 2001 (a low-fire year). Given the long distance from the fires in northwestern N. America and Siberia to the Azores where our measurements were made, these results imply that boreal fires affect background O_3 levels over a very large region of the NH midlatitudes.

Surface temperatures in the boreal regions have risen more rapidly than global average temperatures over recent decades [*Hassol*, 2004], and Global Circulation Model simulations predict that boreal climate warming will lead to increased boreal fire danger in future decades [*Stocks et al.*, 1998]. Our results imply that increased boreal fire magnitudes would lead to (or may have already led to) an increase in the summertime O_3 background over large regions of the NH, providing a climate forcing feedback (as O_3 is a greenhouse gas) and negatively affecting the ability of downwind nations to meet O_3 air quality standards.

Chapter 3

Late-summer changes in burning conditions in the boreal regions and their implications for NO_x and CO emissions from boreal fires[†]

[†]This chapter is based on material previously published as Lapina, K., R. Honrath, R. C. Owen, Val Martín M., Hyer, E. J. and Fialho, P. (2008), Late-summer changes in burning conditions in the boreal regions and their implications for NO_x and CO emissions from boreal fires, *J. Geophys. Res., 113*, D11304, doi:10.1029/2007JD009421.

3.1 Introduction

Research in recent years has shown that the impact of boreal fires on tropospheric CO background levels is significant [*Novelli et al.*, 2003; *Edwards et al.*, 2004]. Measurements in fire plumes and modeling studies have also confirmed boreal fires as an important source of ozone precursors [*Val Martín et al.*, 2006; *Pfister et al.*, 2006; *Real et al.*, 2007], resulting in significant impacts on midlatitude lower free troposphere (FT) background O_3 during summer [*Lapina et al.*, 2006]. Large boreal wildfires can significantly affect tropospheric composition even in populated areas thousands of miles away, where anthropogenic sources usually dominate air quality impacts [*Wotawa et al.*, 2001; *Sapkota et al.*, 2005; *Colarco et al.*, 2004; *DeBell et al.*, 2004; *Morris et al.*, 2006].

Quantifying and modeling fire emissions is a challenging task, due to the large degree of variability in the types of fire and fuel [*Kasischke et al.*, 2005]. Burning in the boreal forests is typically separated into two components with significantly different fuel characteristics and associated combustion processes: burning of aboveground vegetation and burning of organic soil layers (the ground layer) [*French et al.*, 2004]. The ground layer is located on the top of mineral soil and is made of litter, lichen, moss and organic soils [*Kasischke et al.*, 2005]. The amount of ground-layer carbon is twice the amount of aboveground carbon, on average [*French et al.*, 2004], and therefore ground-layer carbon may be a major contributor to the total amount of carbon emissions released during fires. Ground-layer emissions are especially difficult to quantify, as the fraction of soil layer consumed is one of the most uncertain parameters in fire modeling [*Kasischke and Bruhwiller*, 2002; *French et al.*, 2004]. For example, recent field studies that measured the depth of burning in Alaskan fires indicate that current fire models significantly underestimate the degree

of consumption of surface layer fuels [*French et al.*, 2007].

Burning of peatlands (*i.e.*, sparsely forested lowlands) is another major source of emissions from fires [*Duncan et al.*, 2003; *Turquety et al.*, 2007]. Peatlands occupy 15–20% of the area of North American boreal regions, and research in the recent years has shown that they are as susceptible to burning as are well-drained upland ecosystems [*Turetsky et al.*, 2004].

While CO emissions are greatest during smoldering combustion, NO_x ($NO+NO_2$), a limiting factor for O_3 production, is mainly produced during the flaming stage of burning [*Lobert et al.*, 1991]. Therefore the emission ratio of NO_x/CO is related to the relative amounts of flaming and smoldering combustion. Because the NO_x/CO ratio (currently highly uncertain) plays an important role in estimates of NO_x emissions and therefore O_3 production [*e.g.*, *McKeen et al.*, 2002; *Cook et al.*, 2007], understanding the processes affecting its magnitude in fire plumes is of primary importance.

The extent of ground-layer burning in boreal regions increases through the growing season. Early in the season, soil layers are still frozen or saturated, and only dry vegetation on the surface is susceptible to burning. However, by late summer deeper soil layers have dried out and become flammable [*Kasischke and Johnstone*, 2005; *Turetsky et al.*, 2004]. As burning of ground layers occurs mostly via smoldering combustion [*Miyanishi*, 2001], this change in fuel properties is expected to result in an increase in both total carbon consumption and the relative importance of smoldering combustion, relative to flaming combustion. In particular, the increase in ground-layer burning during the late fire season is expected to drive down the overall emission ratio of NO_x/CO (while increasing the total emissions of CO and possibly NO_x).

The aim of this work is to use measurements in boreal fire plumes downwind of the source fires to assess the magnitude of this effect. Following emission, NO_x is converted to nitric acid (HNO_3), peroxyacetyl nitrate (PAN) and

other members of the NO_y (total reactive nitrogen oxides) family. We therefore use $\Delta NO_y/\Delta CO$ enhancement ratios in aged boreal fire plumes sampled during summers of 2004 and 2005 at the Pico Mountain observatory in the central North Atlantic to constrain NO_x/CO emission ratios in the upwind fires. The Boreal Wildland-Fire Emissions Model (BWEM) [*Kasischke et al.*, 2005], a current model of boreal fire emissions of CO and NO_x, is also applied, together with the FLEXPART transport model, to estimate emissions and determine their consistency with the observations.

3.2 Methods

This section starts with the description of the Pico Mountain observatory and measurements used in this work. The estimation of CO and NO_x fire emissions for the 2004 and 2005 fire seasons using BWEM is described in section 4.3.1, and use of the FLEXPART transport model to generate time series of CO and NO_x fire tracers at the observatory is described in section 4.3.2. Identification of fire events and selection of background levels of CO and NO_y are described in sections 3.2.4 and 3.2.5.

3.2.1 Pico Mountain station and measurements

The Pico Mountain observatory is located on the summit caldera of Pico Mountain in the Azores Islands (Portugal) in the central North Atlantic Ocean (38.78°N, 28.67°W). The observatory is frequently impacted by air from high-latitude regions, often without downwind transport over anthropogenic source regions [*Honrath et al.*, 2004]. It is therefore well suited to study the outflow from North American and Siberian boreal wildfires. The observatory's altitude (2225 m) is well above the marine boundary layer (MBL) during summer

[*Kleissl et al.*, 2007] and the impact of island pollution on measurements is negligible [*Kleissl et al.*, 2007; *Val Martín et al.*, 2006].

CO was determined using a non-dispersive infrared absorption instrument (a modified Thermo Environmental, Inc., Model 48C-TL), calibrated daily with standards referenced to the NOAA Global Monitoring Division standard [*Novelli et al.*, 2003]. CO data were recorded as one-minute averages, and were further averaged to obtain the 30-min averages used in this work. Additional details on the instrument and calibration methods are provided in the works of *Honrath et al.* [2004] and *Owen et al.* [2006].

NO, NO_2 and NO_y were determined by an automated $NO_{x,y}$ system developed at Michigan Technological University, using established techniques: NO detection by O_3 chemiluminescence, NO_2 by conversion to NO via ultraviolet photodissociation and NO_y by Au-catalyzed reduction to NO in the presence of CO. Measurements were recorded as 30-s averages (NO and NO_2) and 20-s averages (NO_y) every 10 min, and were averaged to obtain the 30-min averages used here. A detailed description of the system can be found elsewhere [*Val Martin et al.*, 2006; *Val Martin et al.*, Seasonal variation of nitrogen oxides in the central North Atlantic lower free troposphere, submitted to *J. Geophys. Res.*, 2007].

To ensure that NO_y observations were representative of air in the surrounding FT, we have excluded from this analysis (1) all periods potentially affected by upslope flow of MBL air [*Kleissl et al.*, 2007], (2) measurements made during low to calm winds (wind speed < 2 m/s), to avoid including NO_y observations with potential for HNO_3 to be removed on the mountain surface, and (3) measurements with high ambient variability, to avoid including nitrogen oxides resulting from volcanic emissions, sometimes observed at this site under near-calm conditions [*Val Martín et al.*, 2006]. For this purpose, periods with high ambient variability were defined as in the work of *Val Martín*

et al. [2006].

3.2.2 Boreal Wildland-Fire Emissions Model

BWEM is a model specifically developed to calculate emissions from boreal fires in the high-latitude regions of the Northern Hemisphere. The main feature that distinguishes BWEM from other wildland fire emissions models is its explicit consideration of surface organic layer consumption, which is a major contributor to fire emissions in boreal regions.

Emissions were estimated separately for burning of aboveground vegetation and burning of the surface organic layer. There is no peatland category, although the deeper surface organic material and lower aboveground biomass of peatlands are accounted for by the forest inventory and soil carbon database used in the model [*Kasischke et al.*, 2005]. For aboveground vegetation, BWEM employs a standard bottom-up approach, in which emission factors of CO and other species are applied to the estimated fuel consumption. To estimate emissions from ground layer consumption, BWEM accounts for variation in the depth of burning according to the month of burning and fire type (surface or crown) and for variations in carbon density of the surface layer.

The potential carbon emissions (*i.e.*, carbon emissions released if burning takes place) from burning of aboveground vegetation, $C_{p\_a}(t)$, and of the ground layer, $C_{p\_g}(t)$, are calculated as follows:

$$C_{p\_a}(t) = B_a f_{c\_a} F_{b\_a} \beta_a(t) \tag{3.1}$$

and

$$C_{p\_g}(t) = \int_0^{d_b(t)} C_g(x) dx, \tag{3.2}$$

where B_a is aboveground carbon density, f_{c_a} represents the biomass carbon content ($f_{c\_a} = 0.45$), F_{b_a} is the biomass fraction available for burning, $\beta_a(t)$ is

the fractional fuel consumption (a function of biomass density and fire type), $C_g(x)$ is the carbon density of the surface organic layer as a function of depth, x, and $d_b(t)$ is the depth of burning.

Crown and surface fires are considered separately by the BWEM, and the prevalence of crown fires increases from 70% of area burned early in the fire season (before 1 June) to 90% of area burned after 1 August. Crown fires consume more aboveground vegetation (have high $\beta_a(t)$) and the depth of ground-layer burning is also higher, because they typically burn in drier conditions compared to surface fires. The depth of burning was varied seasonally within BWEM by using different values of $d_b(t)$ for early (before 1 June), mid-season (1 June–31 July) and late (August and later) fires. Late-season fires have values of $d_b(t)$ twice those of fires earlier in the season (1 June–31 July). As a result of these assumptions, greater carbon emissions (*i.e.*, emissions of CO_2, CO, hydrocarbons and carbonaceous particles) are generated by fires occurring later in the growing season [*Kasischke et al.*, 2005].

In the BWEM as applied in this work, the ratio of flaming to smoldering was 80:20 for aboveground biomass and 20:80 for the surface organic layer. Potential emissions of other species can be obtained from potential carbon estimates using emission factors relative to total carbon as a function of combustion type: EF_f, for flaming, and EF_s, for smoldering. For CO, we used the BWEM emission factors: 460 and 190 grams of CO per kilogram of carbon burned for smoldering and flaming, respectively [*Kasischke and Bruhwiller*, 2002]. For NO_x, emission factors were selected based on a review of available literature, as described in section 3.2.2.2 below. Potential emissions were then combined with estimates of area burned using a geographic information system (GIS). Emissions of any species, $E(t)$, were obtained using:

$$E(t) = A(t)\{EF_f[0.8C_{p\_a}(t)+0.2C_{p\_g}(t)]+EF_s[0.2C_{p\_a}(t)+0.8C_{p\_g}(t)]\}, \quad (3.3)$$

where $A(t)$ is the area burned. Early in the season (June–July) an overall smoldering/flaming ratio in the model is 1.3, on average, and later in the season it is 2.0, as the prevalence of smoldering increases due to higher levels of fuel consumption in surface organic layers. This results in enhanced emissions (per unit fuel combusted) of compounds with larger emission factors for smoldering combustion (*e.g.*, CO and hydrocarbons) and reduced emissions (per unit fuel combusted) of flaming combustion products (*e.g.*, NO_x). NO_x/CO emission ratios drop correspondingly (see section 4.5.2).

Burned area and fire locations for Alaska were obtained from the Alaska Fire Service [*Kasischke et al.*, 2002]. For Canada, burned area was obtained from the Canadian Forest Service (http://cfs.nrcan.gc.ca/regions/nofc). Because these data were available at the provincial level only, fire locations were determined from MODIS hot spots. Information on the temporal distribution of the fires in both regions was obtained from MODIS hot spot data. Despite incomplete information due to satellite coverage limitations, this approach has been shown to adequately represent day-to-day variability in emissions time series for atmospheric modeling applications [*Hyer et al.*, 2007a; *Roy et al.*, 2007].

Emissions were calculated on a $1^\circ \times 1^\circ$ grid, on a daily basis and assuming typical burning conditions (moderate severity scenario) [*Kasischke et al.*, 2005]. A more detailed description of the model can be found in the work of *Kasischke et al.* [2005].

3.2.2.1 Fires in Siberia

The emissions simulated by BWEM and used in this work include North American emissions only. Large areas burn every year in Siberia (approximately three times those in North America, on average [*Soja et al.*, 2007]). Although Siberian fire emissions can impact the Pico Mountain measurement

site [*Honrath et al.*, 2004; *Lapina et al.*, 2006], such impacts have been reported during exceptionally large fire years (*i.e.*, 2003). The impact of Siberian emissions at the Pico Mountain station during 2004 is expected to be small relative to the North American fires, as 2004 was a low-fire year in Siberia. 2005 was a relatively high-fire year for Siberia [*Soja et al.*, 2007]. Therefore, it is possible that some impact of Siberian emissions was present during the summer 2005. However, during time periods affected by fires from both source regions, we expect the impact of North American fires to be larger due to their relative proximity to the observatory. Hence, the fire periods discussed below, selected based on North American fire impacts, are expected to be characteristic of North American fires.

3.2.2.2 NO_x emission factors

Daily NO_x fire emissions were obtained using equation (3), which requires knowledge of NO_x emission factors. NO_x is a flaming-stage compound [*Lobert et al.*, 1991] and is produced in smaller amounts during smoldering combustion, as laboratory studies have shown [*Yokelson et al.*, 1997]. The combustion temperatures in biomass fires are insufficient for significant conversion of atmospheric N_2 to NO_x [*Andreae*, 2004]. Hence, NO_x emissions reflect the nitrogen content of the fuel, which is considered to be relatively low in boreal vegetation [*Wofsy et al.*, 1992]. This, and the fact that a large fraction of biomass in the boreal fires is consumed via smoldering combustion, result in lower NO_x emission factors for boreal fires compared to fires in other regions. However, currently there are few field observations of NO_x from boreal fires available, and the existing emission factors exhibit large variability, making the modeling of NO_x emissions a challenging task.

Goode et al. [2000] performed field measurements of NO_x emission factors from boreal wildfires in Alaska. They reported an average emission factor

(which includes fire observations made by *Nance et al.* [1993]) of 1.54 grams NO_x as NO per kilogram fuel burned. In the units reported in this work this corresponds to 3.42 grams NO_x as NO per kilogram carbon burned. The measured fires were predominantly flaming crown and surface fires, and emission factors for predominantly smoldering fires, such as peat fires, are expected to be lower.

While many studies use a single NO_x emission factor that incorporates both smoldering and flaming combustion processes [*Andreae and Merlet*, 2001], we took advantage of BWEM's ability to allocate emissions by combustion type. To obtain emission factors for the flaming and smoldering stages of combustion, we referred to laboratory measurements, reported by *Yokelson et al.* [1996], because the field studies report only fire-integrated estimates. We chose the emission factors for smoldering and flaming combustion obtained for fuel described as "broadcast" by *Yokelson et al.* [1996], 0.0656 NO and 0.0189 NO_2 for flaming combustion and 0.0167 NO and 0.0019 NO_2 for smoldering combustion, in units of moles per kilogram fuel. These correspond to $EF_f = 5.64$ and $EF_s = 1.24$ (g NO_x as NO per kilogram carbon) for flaming and smoldering combustion, respectively. The broadcast fuel was made up of a mixture of decomposing organic matter, pine needles, twigs, and wood. To test whether the selected values of EF_f and EF_s are reasonable, we input them into BWEM under the average fuel consumption scenario to derive fire-integrated emission factors. The derived estimates were in a good agreement (within 25%) with the field observations [*Goode et al.*, 2000].

Based on the selected emission factors, the NO_x/CO emission ratio for purely smoldering combustion in the model was 3×10^{-3} mol mol^{-1}, while the emission ratio for purely flaming combustion was 28×10^{-3} mol mol^{-1}. This results in NO_x/CO emission ratios of 18×10^{-3} mol mol^{-1} for aboveground vegetation and 5×10^{-3} mol mol^{-1} for the surface organic layer.

3.2.3 FLEXPART simulations

The Lagrangian particle dispersion model FLEXPART [*Stohl et al.*, 2005] was used to calculate mixing ratios of CO and NO_x tracers at the Pico Mountain observatory resulting from the BWEM-estimated fire emissions, to assess the potential impact of wet deposition on nitrogen oxides levels in the fire plumes and to evaluate emissions injection height scenarios. FLEXPART (version 6.2) was driven with data from the European Centre for Medium Range Weather Forecasts (ECMWF) [*ECMWF*, 2005] with a $1^\circ \times 1^\circ$ horizontal resolution, 61 vertical levels and a temporal resolution of 3 hours, using meteorological analysis at 0000, 0600, 1200, and 1800 UTC, and ECMWF 3-hr forecasts at intermediate times (0300, 0900, 1500, 2100 UTC).

Forward FLEXPART runs were used to simulate the advection and dispersion of fire emissions tracers. These results were used to analyze the vertical distribution of emissions. Particles representing fire emissions were released over 3-hour intervals above the locations of active fires, at altitudes determined by the height scenarios (see section 3.2.3.1). The number of particles released into each grid cell was scaled by the mass of emissions in each grid cell. Particles were dropped from the simulation after 20 days and were conserved up to that time. Thus, the simulations model only enhancements caused by fire emissions over the previous 20 days.

Backward FLEXPART simulations (*i.e.*, retroplumes) were used to calculate mixing ratios of fire tracers at the measurement site and to determine the transport pathways of air before arriving at the observatory. Retroplumes were initiated every three hours using 4,000 particles released over a 1-hour time interval into a $1^\circ \times 1^\circ$ grid box centered on the observatory, over an altitude range of 2000–2500 m asl. Particles were followed backward in time for 20 days. In order to account for differences in air density between the

release cell and upwind sources, the upwind residence times of the particles were normalized by the local air density. Normalized particle residence times were convolved with North American boreal fire CO emissions (section 4.3.1) according to the technique described by *Seibert and Frank* [2004] to obtain CO fire tracer mixing ratios at the Pico Mountain station, CO_{BB_T}. Emissions were convolved with the retroplumes from the surface layer up to the maximum injection height of emissions. The same approach was employed to obtain simulations of NO_{xBB_T}, an inert tracer representing NO_x fire emissions. Since particles are tagged with their release times, the travel time of air sampled at the observatory can be estimated.

To identify periods when anthropogenic impacts were significant (in order to omit these periods from the analyses presented below), we performed FLEXPART simulations of anthropogenic tracers. Anthropogenic tracers representing North American, European, and Asian emissions, were obtained in a manner similar to the fire tracers, except that emissions were convolved with the retroplumes in the footprint layer only (0–300 m). All three sources had significant impacts, although North American emissions were dominant. Anthropogenic emissions were based on the EDGAR 3.2 Fast Track 2000 dataset [*Olivier and Berdowski*, 2001] with 1° resolution.

3.2.3.1 Injection height of fire emissions

The injection height plays an important role in the fate of fire emissions, as it influences their long-range transport and lifetime. It is affected by numerous factors, which include not only fire characteristics (*e.g.*, intensity and type) but also meteorological conditions present at the time of burning [*Trentmann et al.*, 2006; *Luderer et al.*, 2006].

Because of this complex behavior, we selected an arbitrary scenario, consistent with our understanding of processes that affect fire injection height in the

boreal regions. In this scenario, emissions were released between the surface and 7.5 km with a constant mixing ratio throughout the column. This choice is consistent with limited field observations and was based on the results of other recent boreal fire modeling studies, most of which have distributed emissions with constant mixing ratio between the surface and a selected maximum height [*Damoah et al.*, 2006; *Pfister et al.*, 2005; *Stohl et al.*, 2006; *Cook et al.*, 2007]. For example, *Cook et al.* [2007] distributed emissions from surface up to 10 km, while *Stohl et al.* [2006] injected emissions into the lowest 3 km of the model atmosphere. *Hyer et al.* [2007a] found that emissions injected by constant mixing ratio through the tropospheric column or injected into the midtroposhere (∼500 hPa) resulted in the best agreement with MOPITT observations. An alternative approach is to distribute emissions within selected layers of the modeled atmosphere to account for significant contributions from a particular fire type. For example, to simulate large contributions from peat fires, *Turquety et al.* [2007] released 40% of the emissions into the boundary layer (with the remaining 60% evenly divided between the middle and upper troposphere), while *Generoso et al.* [2007] implemented a scheme in which the fraction of total emissions increased with height up to a maximum level (which varied from 3 to 6.5 km), similar to the impact of convection generated by intense crown fires. *Turquety et al.* [2007] performed a sensitivity study of chemical transport model simulations of the 2004 North American fires, which showed that at least half of the emissions needed to be injected above the model boundary layer to match MOPITT CO data. By choosing a maximum injection height of 7.5 km, we place a major fraction of emissions (about 70%) above the boundary layer.

The 2004 North American fires were also studied by *Mazzoni et al.* [2007] who determined the injection heights of individual fire plumes using satellite data and found somewhat lower numbers, with a maximum height of

5.2 km and a mean of 2.4 km. However, these results may be biased by inherent limitations of the spaceborne sensor, including exclusion of cloudy pixels and undersampling due to the infrequent overpasses. For example, no pyroconvective events lofting emissions to the upper troposphere or lower stratosphere [*Fromm and Servanckx*, 2003; *Jost et al.*, 2004; *Fromm et al.*, 2005] were observed, while such occurrences were documented in 2004 [*Damoah et al.*, 2006].

For comparison purposes, an additional run in which all emissions were injected into the lowest layer of the model (0–300 m) was also conducted. In all cases the model was run with the FLEXPART convective scheme turned on. Previous work has demonstrated the effectiveness of this scheme to transport emissions as high as the stratosphere for specific extreme events, even when a relatively low initial injection height (3 km) was used [*Damoah et al.*, 2006]. As will be discussed below (section 3.3.4), the comparison between these two runs showed that simulations employing a 7.5 km maximum injection height best reproduced the observations at the Pico Mountain observatory, indicating the importance of placing a significant fraction of emissions above the boundary layer. The higher release height also resulted in faster model transport and reduced wet removal (section 3.2.3.2). However, the choice of injection height was not critical for the conclusions presented below, as the choice of fire periods and modeled NO_x to CO enhancement ratios did not significantly change when the 300 m injection height simulations were used instead.

3.2.3.2 Assessment of wet removal

To compare the fire-affected periods in terms of the amount of precipitation during transport to the Pico Mountain observatory, which may have affected NO_y levels, we performed a "wet" run, in which NO_{xBB_T} underwent wet removal in the model. As the emphasis was on a plume-to-plume comparison,

rather than accurate modeling of NO_y deposition, and since interconversion among NO_y species is not modeled in FLEXPART, a simplified method was employed.

FLEXPART allows the choice of species and their first-order physico-chemical parameters in the modeling of wet deposition, which takes the form of an exponential decay process during precipitation [*Stohl et al.*, 2005]. We applied the default NO_2 wet scavenging parameters, provided in FLEXPART, to all NO_y in the model, and computed removal that would have occurred if all NO_y were scavenged as is NO_2. These simulations are defined as NO_{xBB_w}. NO_2 was chosen because of its moderate removal efficiency. The results are presented below in terms of f_{WET}, the fraction of NO_x tracer removed in the wet run, relative to the NO_{xBB_T} (inert tracer) simulation (*i.e.*, $(NO_{xBB_T} - NO_{xBB_w})/NO_{xBB_T}$). While f_{WET} is not meant to be an accurate estimate of wet deposition of NO_y in the fire plumes, the calculated values are instructive as an indication of the relative importance of precipitation among the events analyzed.

Runs performed using 300 m and 7.5 km release heights showed similar event-to-event differences, although the lower release height resulted in higher NO_{xBB_T} removed (f_{WET} in the range of 0.45–0.85, with the mean value of 0.55, compared to the range of 0.26–0.70 and the mean value of 0.41 for the base run). This higher removal was a result of the longer residence time of emissions in the boundary layer during transport to Pico. Also, as no wet removal was assumed to occur in the initial step when emissions were injected up to 7.5 km, f_{WET} in this run can be underestimated if there were precipitation in the fire cloud.

3.2.4 Fire-affected events selection

Fire-affected time periods were identified on the basis of high CO observations and enhanced FLEXPART CO fire tracer. CO was considered to be high when the 30-min average mixing ratio exceeded the estimated boreal CO background (section 3.2.5) by at least 5 ppbv. For a high-CO period to be considered a fire-affected event, the presence of fire emissions had to be confirmed by elevated CO_{BB_T} mixing ratios and CO_{BB_T} had to exceed anthropogenic CO tracers during the event period or within ± 6 hours. In this way we limited our analysis to periods affected predominantly by fire emissions. We excluded periods when high relative humidity (above 96%) was observed at the observatory, as such conditions favor removal of the nitric acid component of NO_y thus potentially biasing the $\Delta NO_y/\Delta CO$ analysis.

When averaging model results for the fire-affected periods, the start and end of each event were adjusted by up to ±6 hours relative to the original start and end of the event, in order to maximize the average CO_{BB_T} over the period of same length. This was done in order to account for errors in transport modeling, e.g. periods when the model simulated an event a few hours earlier or later than it occurred in reality.

3.2.5 Estimation of background levels and enhancement ratios

Enhancement ratios of NO_y for the fire-affected periods are presented below (section 3.3.5). Enhancement ratios of NO_y ($\Delta NO_y/\Delta CO$) were calculated by averaging ΔNO_y and ΔCO for each period and taking their ratios, where ΔNO_y and ΔCO are defined as enhancements over the background levels of these species. Enhancement ratios depend critically on the background

values used. Therefore, the remainder of this section discusses the estimation of the background levels for the fire-affected periods.

To estimate the CO background values in the boreal fire plumes, we averaged CO monthly observations at two boreal stations, Alert and Barrow. These CO measurements are made by the NOAA Earth System Research Laboratory, Global Monitoring Division (available at http://www.esrl.noaa.gov/gmd), and are screened for non-background values. We obtained daily varying CO boreal backgrounds by linearly interpolating between the monthly values. Responding to a seasonal change in OH concentrations, CO background levels drop sharply from June to July and then increase slowly in the late summer. Since this seasonal process continues to affect air during its transport to the Pico Mountain observatory, the effective CO boreal background is different from the one when the airmass left the source region (approximately 10 days prior, on average). To account for this change, we used boreal background values corresponding to the day the measurements were made. CO background values obtained in this way ranged from 87 to 97 ppbv for the studied time periods, with the mean of 92 ppbv.

To assess whether these background values are reasonable, we compared them to CO mixing ratios observed during boreal outflow in the absence of fires. We identified three such periods prior to the start of large fires: 0500–0900 UTC June 7, 2004, 0800–1900 UTC June 19, 2004, and 0530–1200 UTC May 31, 2005. Model simulations indicated near-zero fire impact during these times. The difference between the estimated background levels and the mean observed CO mixing ratios in boreal outflow without the presence of fire emissions was not significant, less than 8 ppbv. This estimation may be an upper limit on the potential bias of the background calculation as this comparison was obtained during the late spring/early summer season when ambient CO levels undergo fast transition due to a sharp rise in OH levels.

For the NO_y background, we used the mean mixing ratio observed at the Pico Mountain station during the same periods (except the period on June 19, when NO_y measurements were unavailable). The resulting NO_y background mixing ratios were 139 ppbv for 2004 and 214 ppbv for 2005. These mixing ratios were close to the lowest values observed during the fire-affected periods. During most events, ΔNO_y was only weakly sensitive to uncertainty in these background values, since NO_y enhancements in the fire plumes were usually large. For example, a 25% change in the presumed NO_y backgrounds would result in a 13% change of ΔNO_y on average, and would not significantly affect the results presented below.

3.3 Results and Discussion

We start this section with the discussion of the generated CO fire inventory and its comparison to other existing inventories. Next, simulated fire NO_x/CO emission ratios are discussed in the context of measurements and modeling studies (section 4.5.2). Fire tracers at the Pico Mountain station are compared with observations during the fire-affected periods for two injection height scenarios in sections 3.3.3 and 3.3.4. Finally, the variability in observed $\Delta NO_y/\Delta CO$ enhancement ratios is used to assess the presence of seasonality in NO_x/CO emission ratios from fires.

3.3.1 BWEM CO emissions estimates

Figures 3.1a and b present the calculated daily emissions of CO from boreal fires in North America for the summers of 2004 and 2005. These seasons were the largest and third-largest on record in Alaska, respectively (Center for International Disaster Information, www.cidi.org/wildfire). Large areas were also burned in Canada (National Forestry Database Program,

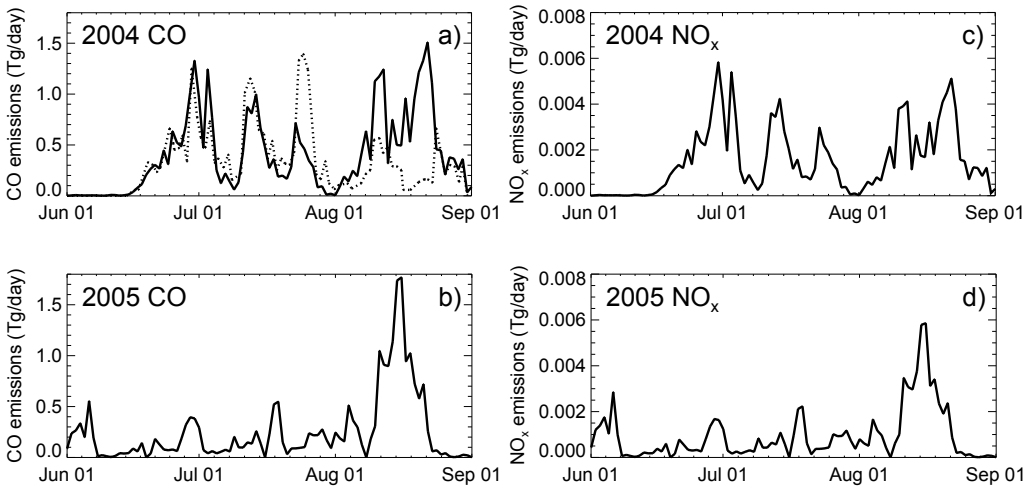

Figure 3.1 Estimated emissions from North American boreal fires during the summers of 2004 and 2005, derived with BWEM (solid lines) for CO (a and b, in units of Tg day^{-1}) and NO$_x$ (c and d, in units of Tg N day^{-1}). The prior CO emissions estimate of *Pfister et al.* [2005] is plotted for comparison (dotted line in part a)..

http://nfdp.ccfm.org/compendium/fires), thus making 2004 and 2005 large fire years in boreal North America [*Pfister et al.*, 2005; *Stohl et al.*, 2006; *Turquety et al.*, 2007; *Soja et al.*, 2007]. Here we compare our CO inventory for Alaskan and Canadian wildfires with other existing inventories, and discuss the reasons for observed differences.

Two other independent CO emission inventories were developed for the 2004 North American boreal fire season. *Pfister et al.* [2005] used an inverse modeling approach to constrain 2004 fire CO emissions using MOPITT observations and MOZART chemical transport model simulations. They applied a weekly adjustment to their a priori emissions estimate, which resulted in more than a twofold increase in the total summer emissions. Another inventory for the 2004 fires was developed by *Turquety et al.* [2007], who used a bottom-up approach with emphasis on the large deduced contribution of peat burning. Although these approaches differed, both inventories resulted in an estimate of 30 Tg CO released from Alaskan and Canadian fires over 2004

summer season, with *Pfister et al.* [2005] reporting an uncertainty of ±5 Tg CO. We obtained a somewhat higher estimate of 37 Tg CO using BWEM. (For comparison, anthropogenic CO emissions for the entire continental U.S. during the same period were approximately 25 Tg CO [*Pfister et al.*, 2005]). In addition, there are significant differences in the timing of these emissions. For example, while all three inventories predict large peaks in CO emissions at the end of June and throughout July, BWEM emissions stay high throughout August (Figure 3.1a). A decrease in burned area in August resulted in the decline in emissions in the previous inventories, while the higher August emissions in BWEM are the result of accounting for deeper burning of the organic soil layer in late summer.

Turquety et al. [2007] introduced a linearly increasing daily scaling factor (ranging from 0.67 on 1 June to 1.33 on 31 August) to account for an increase in peat fuel consumption due to drying as summer progressed. However, no such increase was applied to the burning of surface organic layer in the upland forests. Consequently, their late-season estimates are likely too low. *Pfister et al.* [2005] noticed that their adjustment to the a priori emissions increased as summertime advanced. They suggested a further thawing of surface layers and intensifying peat fires as a possible explanation for this increase. However, their a posteriori August CO emissions were still significantly lower (by 11 Tg) than the BWEM-estimated emissions for the same time period. To further investigate this difference, we used FLEXPART simulations (section 4.3.2) of the vertical distribution of fire emissions over the region and time period used for inversion by *Pfister et al.* [2005]. On average, 30% of the CO mass in the studied region was present below 2 km, where MOPITT's sensitivity is low. This number increased to more than 50% for the run with emissions injected within the lowest 300 m. Provided a late-season increase in smoldering emissions is associated with much of emissions to be released near the

ground, this change may therefore have contributed to an underestimation of total CO by the MOPITT-based inversion. (For a discussion of the effects of MOPITT vertical sensitivity on estimated source magnitudes, see the work of *Hyer et al.* [2007b]). However, smoldering emissions, the production of which is expected to increase in the late summer, do not necessarily originate from the low-intensity ground fires, typically characterized by low injection height, but they can be a result of more frequent high-energy crown fires in the late season [*Kasischke et al.*, 2005]. Therefore, although changes in the injection height of emissions are possible, there is not enough information available at present to draw conclusions regarding the nature of these changes.

A more detailed intercomparison of CO inventories, which would account for differences in methodologies (including, for example, the fact that each inventory used different sources for burned areas) is beyond the scope of this work. Current methods used for building fire emission inventories have very large uncertainties, making it challenging to find the best estimate.

We are not aware of any other existing inventories for 2005 boreal fire season available for comparison with this work. Fire activity in North American boreal regions during 2005 was lower than in 2004, and we derived 23.5 Tg CO for the total summer 2005 emissions.

3.3.2 NO_x emissions and NO_x/CO emission ratios

We estimated total NO_x emitted from the North American boreal fires during the summers of 2004 (Figure 3.1c) and 2005 (Figure 3.1d) as 0.145 Tg N and 0.088 Tg N, respectively.

Daily fire NO_x/CO emission ratios were calculated by dividing total NO_x fire emissions by total CO fire emissions for that day. Emission ratios depend on multiple model parameters, which include the depth of burning,

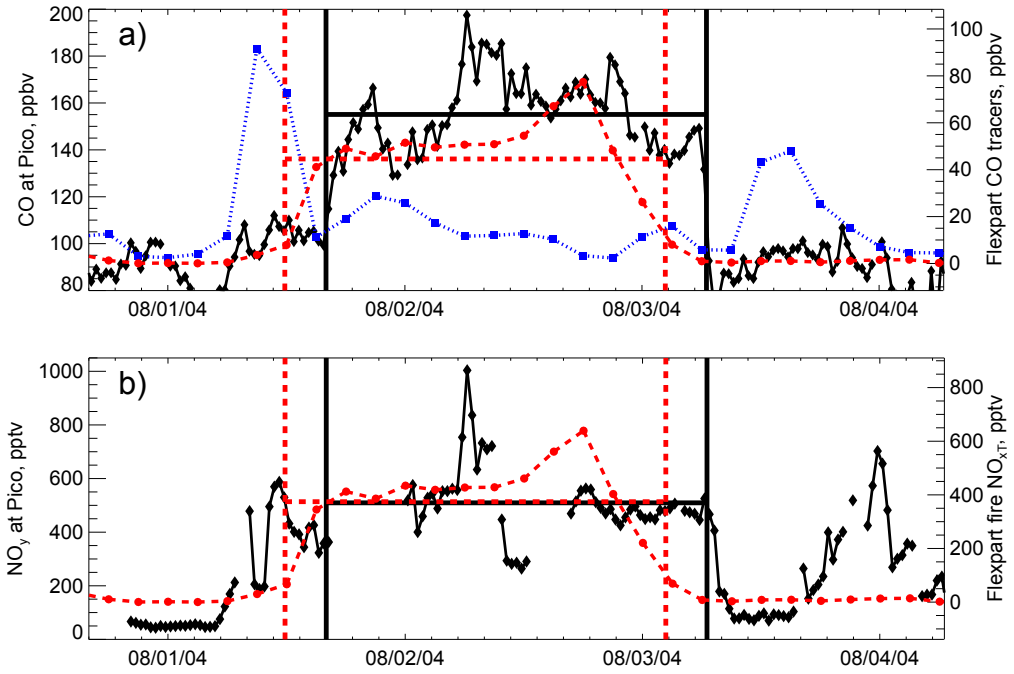

Figure 3.2 Comparison of measurements with modeled fire tracers during the fire event on August 1–3, 2004, for (a) CO and (b) NO_y. Measurements (black), modeled fire tracer (dashed line) and North American anthropogenic CO tracer (dotted line in a) are shown. Horizontal lines show the average values for the event. Vertical lines indicate the beginning and end of the actual event (solid lines) and of the period corresponding to the modeled event in the FLEXPART (dashed lines). The right axis is offset so that zero tracer mixing ratio is aligned with the estimated boreal background..

allocation of flaming/smoldering, and choice of emission factors for CO and NO_x. The average emission ratio dropped from 9×10^{-3} mol mol^{-1} in June and July to 7×10^{-3} mol mol^{-1} in August, with the summer average of 8×10^{-3} mol mol^{-1}, for both 2004 and 2005. The drop in the emission ratio in August is a result of the increase in the amount of organic soil layer consumed later in the burning season, as described above (section 4.3.1).

Although previous boreal fire emission inventories have not considered a seasonal decline in NO_x/CO emission ratios, their ratios are in general agreement with the BWEM seasonal-average value. For example, *Cook et al.* [2007] selected 8×10^{-3} mol mol^{-1} as the optimal NO_x/CO emission ratio for their model to best match the aircraft and satellite observations of the 2004 Alaskan and Canadian fire plumes in July. *McKeen et al.* [2002] reported $\Delta NO_y/\Delta CO$ observations of 7×10^{-3} mol mol^{-1} in late June in North American fire plumes less than 50 hours old and used this number as a reasonable fit for the emission ratio in their model simulations. Observations of fresh (less than one day old) Alaskan fire plumes by *Wofsy et al.* [1992] give a lower value, 5.6×10^{-3} mol mol^{-1}, which the authors suggested may have indicated smoldering tundra fires as the source. *Goode et al.* [2000] sampled air over the Alaskan fires in the late June and measured NO_x/CO ratio of 18×10^{-3} mol mol^{-1}. The same value was obtained by *Wofsy et al.* [1994] who sampled fire-affected air masses in NE Canada from the middle to late July. These high numbers were likely the result of predominantly flaming nature of sampled fires.

3.3.3 Fire-affected periods and comparison of model to observations

Twelve fire-affected periods satisfying the criteria described in section 3.2.4 were identified: seven events in 2004 and five events in 2005 (see Table 1 for the start and end times of the events). NO_y levels were significantly enhanced in all selected periods. (The 2004 periods selected here are nearly identical to those previously identified by *Val Martín et al.* [2006].)

The majority of the fire plumes observed at the Pico Mountain station have a finely detailed structure, characterized by short-term variability in CO and NO_y that is typically not reproduced by the FLEXPART simulations. An example of this is shown in Figure 3.2. (For additional examples of measurements obtained during the fire-affected periods and time periods in the absence of fire emissions, see Figures 1 and 3 in the work of *Val Martín et al.* [2006].) However, averaging over the events' duration leads to a reasonably good agreement between the observations and simulated tracers. Scatter plots of the mean FLEXPART tracer mixing ratios for each event versus the event-mean CO and NO_y enhancements are shown in Figure 3.3. FLEXPART generally captured the timing and relative magnitudes of the fire events ($r = 0.76$ and $r = 0.89$ for CO and NO_y, respectively). The better correlation for NO_y was likely the result of reduced sensitivity to variability in the background, as discussed in section 3.2.5.

The regression slopes are 1.1 for CO and 1.3 for NO_y. The slopes were calculated using the geometric mean (reduced major axis) two-sided regression technique [*Ayers*, 2001; *Draper and Smith*, 1998]. To use these slopes to evaluate the consistency of the measurements with the BWEM emissions, it is necessary to consider the fact that losses during transport to the station are possible. For CO, loss of less than 20% by reaction with OH is expected

over the 7–15 day transport period, if OH concentrations in the fire plumes are low as was concluded by *de Gouw et al.* [2006] ([OH]=4.5×10^5 cm^{-3}). This would produce a tracer/observed enhancement slope of $\leq$1.25, if the emissions inventory and transport model were accurate. The regression slope of 1.1 thus indicates rather good agreement.

For NO_y, significant removal is expected, mainly via wet scavenging of HNO_3 and therefore a slope significantly greater than unity is expected. For anthropogenic emissions, a majority of NO_y ($> 80\%$) is typically lost before or during transport out of the boundary layer [*Stohl et al.*, 2002; *Parrish et al.*, 2004; *Li et al.*, 2004; *Hudman et al.*, 2007]. The fraction of NO_y from the fires that is lost may be significantly lower, however, for several reasons [*Val Martín et al.*, 2006]. First, PAN/HNO_3 ratios in boreal fire plumes are larger than those in typical anthropogenic source regions, due to lower NO_x/NMHC emission ratios and cooler temperatures [*Jacob et al.*, 1992; *Mauzerall et al.*, 1998; *Mason et al.*, 2001]. For example, the airborne measurements of the North American fire plumes over the eastern U.S. determined that more than half of the NO_y in the plumes was in the form of PAN. Nitric acid and aerosol nitrate were also significantly elevated, while NO_x concentrations were low [*Singh et al.*, 2007]. Since PAN is not effectively removed by wet deposition, this is expected to increase NO_y transport efficiency. Second, rapid convection associated with large fires may result in relatively ineffective removal of soluble species—for example, relatively significant amounts of black carbon particles can survive such uplift [*Stohl et al.*, 2006]. Third, convection-induced injection into the cold FT leads to a long lifetime for PAN, which can then be transported long distances [*Singh et al.*, 2007; *Cook et al.*, 2007]. Finally, dry conditions during transport in the FT can also lead to inefficient removal of nitric acid.

Since the magnitude of NO_y loss during lofting and transport to the Pico

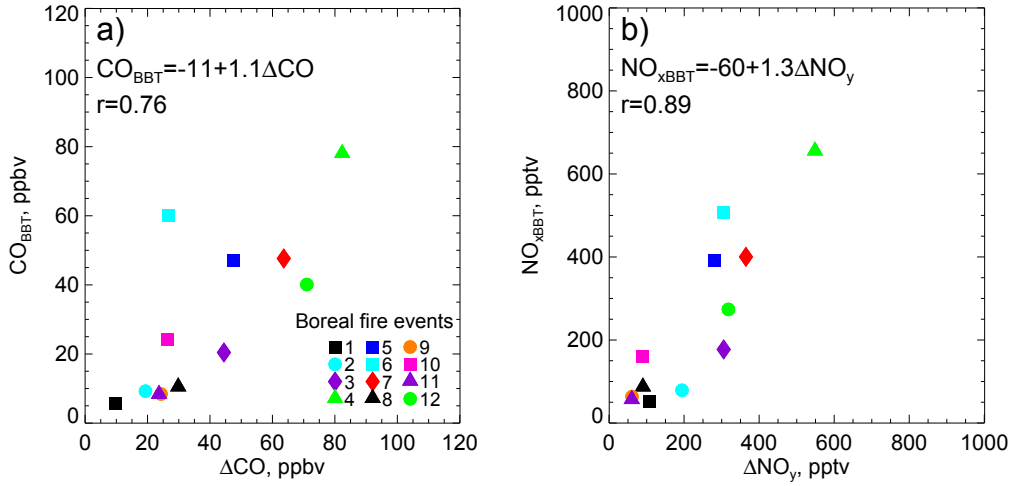

Figure 3.3 Scatter plot of simulated tracer mixing ratios against observed enhancements, averaged over each event: (a) CO_{BB_T} versus ΔCO and (b) NO_{xBB_T} versus $\Delta\mathrm{NO}_y$. Fire events (Table 1) are coded as shown in the legend..

Mountain station is not known, it is not possible to quantitatively evaluate the NO_y regression slope. The slope of 1.3 is consistent with $\sim$25% loss, and suggests that either NO_y loss was low and of that approximate magnitude, or loss was greater but NO_x emissions were underestimated.

3.3.4 Impact of emission injection height

To determine the sensitivity of the simulations to the emissions injection height, we compared the standard FLEXPART simulation results to those from the run in which all emissions were released within the lowest 300 m layer. The correlation of the resulting tracer simulations was significantly worse than in the base run (Figure 3.3): the correlation coefficient dropped by more than 30% for both species and the regression slopes dropped by nearly 40%. Hence, use of the low maximum release height resulted in underestimation of mixing ratios at the Pico Mountain station. While this comparison to the Pico Mountain observations alone is insufficient to constrain the mag-

nitude and injection height of all emissions [*Leung et al.*, 2007], these results support the conclusions of previous research that releasing emissions above the boundary layer is important for adequate modeling of boreal fires [*Turquety et al.*, 2007; *Hyer et al.*, 2007b].

To determine whether there is a relationship between the magnitude of ΔCO observed at the observatory and the initial injection height, we divided fire-affected periods into two groups: high-CO events, characterized by $\Delta\text{CO} > 60$ ppbv (three events total), and moderate-CO events, with $\Delta\text{CO} < 30$ ppbv (a group of six events). We compared the ratios of modeled to observed CO enhancements ($\text{CO}_{BB_T}/\Delta\text{CO}$) for these groups, using both simulations (300 m and 7.5 km injection height). Average $\text{CO}_{BB_T}/\Delta\text{CO}$ for high-CO events dropped from 0.8 (for the 7.5 km simulations) to 0.4 (for the 300 m simulations), while no change was observed for moderate-CO events (with the average $\text{CO}_{BB_T}/\Delta\text{CO}$ of 0.6 for both runs). These results imply that high-CO events at the Pico Mountain observatory resulted from large, intense fires that injected emissions well above the boundary layer. Injection of emissions at higher altitude likely led to a shorter travel time and, possibly, to less dilution of CO during transport.

3.3.5 $\text{NO}_{xBB_T}/\text{CO}_{BB_T}$ vs $\Delta\text{NO}_y/\Delta\text{CO}$

The tracers mixing ratios, NO_{xBB_T} and CO_{BB_T}, have uncertainties resulting from both transport modeling errors and errors associated with the emissions estimation. In the remainder of this paper, we analyze enhancement ratios, observed and simulated, in order to minimize the effects of uncertainties in the transport simulations, and focus on the consistency of the observations with estimated emission ratios.

The tracer ratios ($\text{NO}_{xBB_T}/\text{CO}_{BB_T}$) are presented in Figure 3.4a (black

asterisks) by day of year. These simulated enhancement ratios are somewhat higher in the early summer season (8.5×10^{-3} mol mol^{-1} in June–July) compared to the late summer season (7.3×10^{-3} mol mol^{-1} from August to early September) as a result of the increased smoldering combustion simulated in August, and are very similar (within 5%) to the spatially-averaged NO_x/CO emission ratios, since the species are treated as conserved tracers. Measured NO_y enhancement ratios ($\Delta NO_y/\Delta CO$) are also shown in Figure 3.4a (solid symbols). While the measured ratios follow a similar pattern, they exhibit more scatter and a larger decline in August than NO_{xBB_T}/CO_{BB_T}.

To assess the consistency of the observations with the model, we computed the ratio of observed to modeled enhancement ratios $(\Delta NO_y/\Delta CO)/(NO_{xBB_T}/CO_{BB_T})$. If CO were treated as conserved and the modeled emissions are correct, the deviation of this ratio from unity would indicate the degree of NO_y loss between emission and sampling. The mean ratio between observed and modeled enhancement ratios, $(\Delta NO_y/\Delta CO)/(NO_{xBB_T}/CO_{BB_T})$, dropped from 0.90 in June–July to 0.50 in August. If the emissions were correct, this would indicate NO_y loss of about 10% in June–July and about 50% in August. Although the magnitude of NO_y loss after emission is poorly characterized, it is very likely that the loss is significantly greater than 10%, as discussed in section 3.3.3. This implies that the modeled NO_x/CO emission ratio is an underestimate, at least in the early season, and therefore that the NO_x emission factors are too low, the CO emission factors are too high, or the ratio of flaming to smoldering is too low in the early season.

The increased scatter in the measurements, relative to the simulated NO_{xBB_T}/CO_{BB_T}, may be due to fire-to-fire variability in emissions and injection height not captured by the model, and/or varying degrees of NO_y removal during transport. The impact of wet removal is analyzed further in

the next section, followed by a discussion of the seasonal $\Delta NO_y/\Delta CO$ decline.

3.3.6 Impact of removal on $\Delta NO_y/\Delta CO$

To test whether the observed scatter in $\Delta NO_y/\Delta CO$ is a result of varying degrees of removal of nitric acid from the fire plumes during their multi-day transport to the observatory, we used f_{WET}. Figure 3.4b shows f_{WET} by event as an indicator of potential wet removal. The correlation between f_{WET} and $\Delta NO_y/\Delta CO$ was low ($r = -0.38$). Based on this, we conclude that most of the scatter in $\Delta NO_y/\Delta CO$ apparent in Figure 3.4a was not the result of varying NO_y removal, but was most likely the result of a fire-to-fire variability in emissions and/or initial NO_y export efficiency during lofting into the FT near or above the fires.

3.3.7 NO_x/CO seasonal trend

The decline in $\Delta NO_y/\Delta CO$ observed during the late fire season is consistent with expectations based on an increase in the relative importance of smoldering combustion, as discussed in section 4.3.1. To quantify the magnitude of this decline, we first divided the fire plumes into early- and late-summer subsets. These subsets were divided using the late-season start day used by BWEM (1 August), and taking into account that the shortest transport time from fire source regions to the observatory is 7 days, as modeled by FLEXPART. Therefore, all measurements made at the Pico Mountain observatory prior to 8 August were included into the early-summer subset, and the measurements made after that date constitute the late-summer subset. Although this division is somewhat arbitrary, it is consistent with the decline in the observed ratios. One event was located on the border between these subsets, on 8 August. This event also had the largest wet removal value (f_{WET}=0.7). Al-

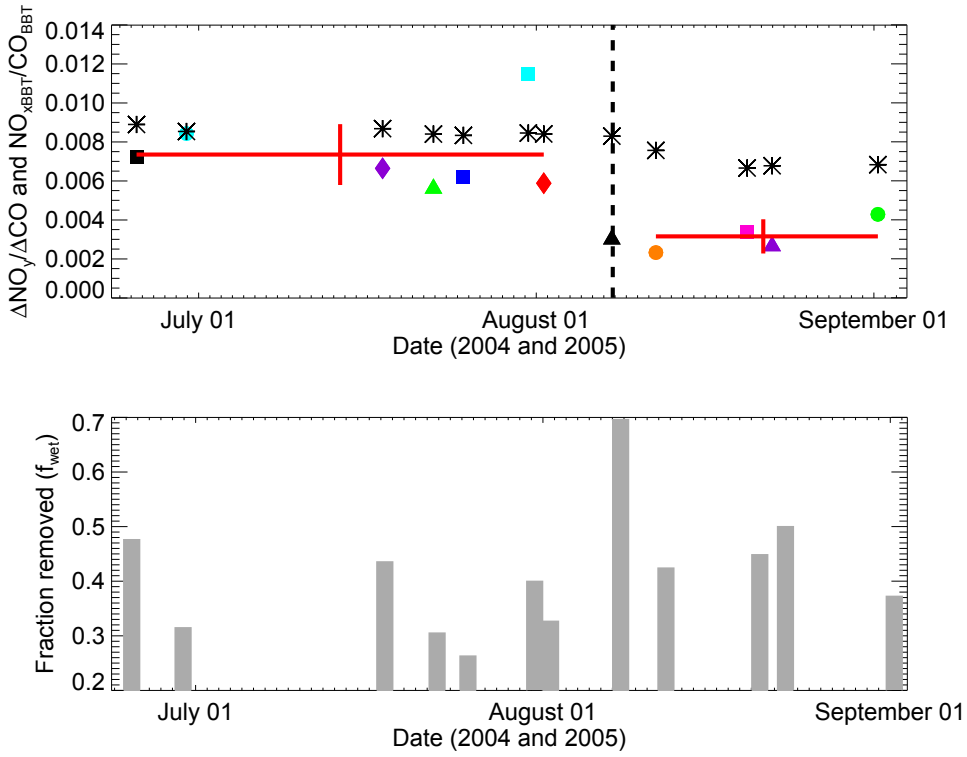

Figure 3.4 (a) Measured and modeled enhancement ratios during the fire-affected periods at the Pico Mountain observatory, in units of $\times 10^{-3}$ mol mol^{-1}. Shown are $\mathrm{NO}_{xBB_T}/\mathrm{CO}_{BB_T}$, simulated without wet removal (asterisks), and measured $\Delta\mathrm{NO}_y/\Delta\mathrm{CO}$ enhancement ratios (coded as shown in Figure 3.3). Solid lines represent early- and late-summer averages of $\Delta\mathrm{NO}_y/\Delta\mathrm{CO} \pm 2$ standard error of the mean. (b) f_{WET}, an indicator of wet-removed fraction..

though $\Delta\mathrm{NO}_y/\Delta\mathrm{CO}$ during this event was similar to that in the late-summer events, this event was excluded from further analysis.

The mean $\Delta\mathrm{NO}_y/\Delta\mathrm{CO}$ ratios for the early and late summer subsets are plotted on Figure 3.4 using solid lines. We employed a non-parametric Wilcoxon Sum-rank test and a two-sample t-test to test for differences between two means. The early- and late-summer means are significantly different (α=0.01), with significantly higher values in the early-summer subset (7.3×10^{-3} mol mol^{-1}) relative to the late-summer subset (2.8×10^{-3} mol mol^{-1}).

3.4 Conclusions

Using $\Delta NO_y/\Delta CO$ enhancement ratios observed in aged fire plumes, this work presents the first evidence of a seasonal trend in NO_x/CO emission ratios from boreal fires, with higher values in early summer and lower values in late summer. This trend is consistent with our understanding of the seasonal progression of boreal fire activity, in particular an increase in the amount of fuel consumed by smoldering combustion later in the growing season due to deeper burning of the drier surface layer fuels. This change in burning properties affects the relative proportions of species released from fires, leading to enhanced emissions of compounds with larger emission factors for smoldering combustion and reduced emissions of flaming combustion products. A major growth in overall fuel consumption in the late summer is also expected, due to higher levels of fuel consumption in surface organic layers. These changes are not accounted for in prior inventories of boreal forest fire NO_x emissions, but they can result in considerable differences in estimated emissions and, hence, are expected to significantly affect the results of modeled ozone production rates.

Tracer transport simulations of CO and NO_x emissions from fires were in reasonably good agreement with the measurements. The NO_x emission factors used in this work represent the best information currently available in the published literature. However, comparison of simulated NO_{xBB_T}/CO_{BB_T} with $\Delta NO_y/\Delta CO$ in the aged fire plumes suggests that NO_{xBB_T}/CO_{BB_T} ratios were underestimated in the early season. This indicates that either NO_x emission factors were underestimated, CO emission factors were overestimated, the model's ratio of flaming to smoldering combustion in the early season was too low, or a combination of these errors was present. The seasonal trend in this disagreement favors the third cause, which would imply

Table 3.1 Boreal wildfire events observed at the Pico Mountain station.

Event number	Start time	End time
1	June 25 07:30, 2005	June 27 01:00, 2005
2	June 29 21:20, 2005	July 1 09:30, 2005
3	July 17 21:30, 2004	July 18 07:10, 2004
4	July 22 13:30, 2004	July 23 11:00, 2004
5	July 25 07:15, 2004	July 25 23:30, 2004
6	July 31 06:30, 2004	July 31 13:00, 2004
7	August 1 16:00, 2004	August 3 06:30, 2004
8	August 7 22:30, 2004	August 8 12:00, 2004
9	August 11 23:00, 2005	August 13 16:00, 2005
10	August 20 08:30, 2005	August 21 20:30, 2005
11	August 22 15:00, 2005	August 23 11:00, 2005
12	September 1 08:30, 2004	September 2 18:00, 2004

that the magnitude of the seasonal drop in emission ratios from boreal fires might be even larger than simulated. The inability of the model to simulate the observed drop indicates that further research on the depth of ground-layer burning in the boreal regions and on boreal fire NO_x emission factors is needed.

High $\Delta NO_y/\Delta CO$ enhancement ratios measured at the Pico Mountain observatory and the poor correlation of these ratios with f_{WET}, an indicator of wet removal, implies efficient lofting and transport of NO_y from boreal fires.

There was a better agreement between measurements and simulated mixing ratios when emissions were released up to 7.5 km compared to the case when the maximum injection height of 300 m was used, implying the importance of pyro-convection in the boreal region. The presumed injection height was most important for the events with the highest ΔCO, pointing to large intense fires as their source.

There is evidence of an increase in area burned in boreal regions in recent years, and further increases are predicted [*Flannigan et al.*, 2005; *Kasischke and Turetsky*, 2006; *Soja et al.*, 2007]. In addition, deeper seasonal thawing of permafrost and increased depth of burning are predicted [*Kasischke and Turetsky*, 2006]. The results presented here indicate that this would further shift the relative amounts of species emitted during flaming and smoldering combustion and increase total emissions with implications for atmospheric impacts.

Chapter 4

Observing boreal wildfire impacts on HCHO and NO_2 from space[†]

4.1 Introduction

In recent years, the impact of boreal wildfires on atmospheric composition has received increased attention [*e.g.*, *Wotawa et al.*, 2001; *Novelli et al.*, 2003; *Jaffe et al.*, 2004; *Pfister et al.*, 2005; *Lapina et al.*, 2006; *Stohl et al.*, 2006]. In addition to being a major source of CO [*Edwards et al.*, 2004; *Yurganov et al.*, 2004; *Kasischke et al.*, 2005], measurements in fire plumes and modeling studies have confirmed that boreal fires are an important source of ozone precursors, *i.e.*, VOCs and NO_x (NO + NO_2) [*Goode et al.*, 2000;

[‡]This chapter is based on material to be submitted, with minor changes, as K. Lapina, R. Honrath, R. C. Owen, A. Richter, F. Wittrock, E. Hyer and J. Burrows (2009), Observing boreal wildfire impacts on HCHO and NO_2 from space, *J. Geophys. Res.*

Val Martín et al., 2006; *de Gouw et al.*, 2006; *Pfister et al.*, 2006; *Real et al.*, 2007; *Verma et al.*, 2009], resulting in significant ozone impacts [*Jaffe et al.*, 2004; *Simmonds et al.*, 2005; *Lapina et al.*, 2006].

Building emission inventories for fires in boreal regions is a challenging task due to large uncertainties in fuel availability and consumption [*French et al.*, 2007] and variability in fire burning properties. Estimating production of secondary compounds from fire emissions, such as formaldehyde (HCHO), is further complicated by uncertainties in the complex chemical mechanisms of VOC oxidation [*de Gouw et al.*, 2006; *Mason et al.*, 2006]. HCHO from biomass burning is an important source of HO_x radicals, which control the oxidizing capacity of the atmosphere [*Lee et al.*, 1998], and contributes to ozone formation in the presence of NO_x [*Seinfeld and Pandis*, 1998]. Large amounts of HCHO are released by fires directly [*Lee et al.*, 1997] and formed downwind from fire-emitted VOCs (which include oxygenated compounds, such as methanol) [*Stavrakou et al.*, 2009]. Because HCHO is produced as an intermediate during the oxidation of VOCs emitted from fires, its high concentrations can serve as an important tracer of recent photochemical activity in fire plumes [*Fried et al.*, 2008].

While methane oxidation is the main source of formaldehyde in the remote atmosphere, biomass burning and biogenic emissions control HCHO levels near source regions [*Marbach et al.*, 2005; *Wittrock et al.*, 2006], and space-based HCHO data can be used to constrain these emissions [*Palmer et al.*, 2003; *Meyer-Arnek et al.*, 2005; *Palmer et al.*, 2006; *Millet et al.*, 2008]. Enhanced HCHO is commonly observed by satellites over fire regions [*W. Thomas et al.*, 1998; *Wittrock*, 2006; *Marbach et al.*, 2005; *Meyer-Arnek et al.*, 2005; *Spichtinger et al.*, 2004; *Fu et al.*, 2007; *De Smedt et al.*, 2008], and studies over boreal fires in Siberia and North America showed that HCHO was well-correlated with the locations of the fire hot spots [*Wittrock*, 2006; *Spichtinger*

et al., 2004].

Large post-emission increases in HCHO were previously observed in field studies [*Yokelson et al.*, 2003, 2009], especially in the plumes processed by clouds, due to heterogeneous methanol loss [*Tabazadeh et al.*, 2004]. VOC oxidation in fire plumes is initiated by reaction with OH, and eventually leads to the production of HCHO for most compounds. This secondary production can sustain enhanced HCHO in the fire plumes for many hours or days after release from fires [*Stavrakou et al.*, 2009]. Thus, despite the relatively short HCHO lifetime of several hours at midday, *Fried et al.* [2008] observed high HCHO concentrations in an Alaskan plume 3–4 days old during the INTEX-NA campaign off the coast of North America. *Stavrakou et al.* [2009] estimated that directly released HCHO contributes only 14% to the total HCHO production over the first day since emission, by which time half of the total HCHO that will be produced from these emissions has been formed. They based their estimate on model simulations which included an explicit speciation profile of VOCs released from fires. They went further to compare modeled annually averaged HCHO columns with SCIAMACHY data, but boreal fire regions were excluded from the analysis due to the poor model agreement and high noise.

Fires are also an important source of NO_x and can be a major contributor to NO_2 columns in regions with low impact of anthropogenic emissions, such as the tropics [*Boersma et al.*, 2008]. NO_x emissions per unit carbon consumed are lower from boreal fires compared to fires in other regions, due to the lower nitrogen content of the fuel and a higher fraction of smoldering combustion [*Lobert et al.*, 1991; *Wofsy et al.*, 1992]. Despite this, large wildfires in boreal North America have been shown to be responsible for significant impacts on the summer distribution of nitrogen oxides observations in the remote atmosphere over the central North Atlantic [*Val Martín et al.*,

2006, 2008]. Elevated NO_2 tropospheric columns were occasionally observed by OMI over Siberian fires in 2006 [*Verma et al.*, 2009] and by GOME over Canadian fires in 1998 [*Spichtinger et al.*, 2001]. While the signal from the latter was not detectable on a seasonal basis, enhanced NO_2 columns, averaged from July to August, were distinguishable over the area with the most intense fires in Siberia [*Spichtinger et al.*, 2004]. This implies that the strength of the produced NO_2 signal depends on fire properties and/or spatial distribution. Dependence of the tropospheric NO_2 signal on the type of fire was further confirmed by *Marbach et al.* [2005], who used a combination of HCHO and NO_2 measurements from GOME to study global biomass burning in the summer of 1997. They found that while monthly HCHO columns were consistently correlated with fire counts from the Along Track Scanning Radiometer (ATSR), only grassland fires resulted in enhanced tropospheric NO_2 amounts.

In this work, we use HCHO and NO_2 tropospheric columns from SCIAMACHY to assess the impact of fires on the atmospheric burdens of these species in the Alaskan and Canadian regions. Our study is performed for the summer of 2004, which was a large fire season in boreal North America and the largest on record in Alaska (Center for International Disaster Information, www.cidi.org/wildfire). Another objective of this work was to improve our understanding of secondary HCHO production occurring in the fire plumes and to compare its magnitude to direct HCHO fire emissions.

4.2 SCIAMACHY measurements

SCIAMACHY HCHO and NO_2 tropospheric columns used in this study are the products of the University of Bremen. SCIAMACHY is an absorption spectrometer covering the spectral range from the ultraviolet to the near infrared. It was launched on ENVISAT in 2002 and has an equator crossing

time of 10 AM local time. Scan width in the nadir view is 960 km and global coverage is achieved within 6 days. The ground pixel size is 30 km × 60 km for NO_2 and 60 km × 120 km for HCHO and only ground scenes having less than 20 percent cloud cover are considered. To estimate slant columns, the Differential Optical Absorption Spectroscopy (DOAS) method is applied in the spectral region of 334–348 nm for HCHO and 425–450 nm for NO_2. Stratospheric correction for NO_2 was performed using the reference sector method, *i.e.*, measurements from a clean air region (140–180W) were subtracted from the slant column at each latitude prior to conversion to vertical columns. In order to compensate for the offsets introduced by solar reference measurements [*Richter and Burrows*, 2002], the slant HCHO columns were normalized to the mean background value of 3.5×10^{15} molec cm^{-2} over the 150–180W reference sector. More details on retrieval technique and error analysis are given in the works of *Wittrock* [2006] and *Richter et al.* [2005].

Due to the sparse coverage of SCIAMACHY observations (see Figures A.1, A.2, A.3, A.4 and Figure A.5 in the Appendix A), 5-day composites were used in this study. HCHO and NO_2 data were gridded at a 1-degree resolution and each grid cell with at least one pixel over the 5-day period was assigned the mean value of all pixels in that cell. A total of eighteen composites were analyzed in this work, with the earliest 5-day period centered on June 3 and the latest on August 27. SCIAMACHY data were analyzed for the region extending from 180W to 90W and from 55N to 70N, covering a major portion of the North American boreal region.

4.3 Modeling transport of fire emissions

4.3.1 The Boreal Wildland-Fire Emissions Model

BWEM [*Kasischke et al.*, 2005] was used to estimate HCHO primary emissions (emissions directly released during biomass burning). This model was specifically developed to calculate emissions from boreal fires and it explicitly considers surface organic layer consumption, which is a major contributor to fire emissions in boreal regions.

Emissions in the model are estimated separately for burning of aboveground vegetation (at a ratio of 80% flaming/20% smoldering) and the surface organic layer (at a ratio of 20% flaming/80% smoldering). The depth of surface layer burning during the late season (August) is twice the depth during the early season (June–July), resulting in an increase in emissions, especially for smoldering compounds [*Lapina et al.*, 2008]. Emissions of NO_x and HCHO were calculated by applying emission factors (EF) to carbon emissions separately in flaming (EF_f) and smoldering (EF_s) categories. Field studies report only fire-integrated estimates of emission factors. Therefore we derived EF_f and EF_s to match the fire-integrated EF of 1.85 $\pm$ 0.38 g HCHO/kg C reported for the Alaskan wildfires in late June by *Goode et al.* [2000]. By using the typical ratio of EF_s to EF_f of 2 for HCHO (based on the laboratory measurements by *Yokelson et al.* [1996]), and assuming the overall fuel consumption breakdown of 43% flaming/57% smoldering in June predicted by BWEM, we derived $EF_f = 2.6$ and $EF_s = 5.3$ g HCHO/kg C burned.

Emission factors for NO_x were selected as described in work by *Lapina et al.* [2008]. We used $EF_f = 5.64$ and $EF_s = 1.24$ (g NO_x as NO per kilogram carbon).

Emissions were calculated on a $1^\circ \times 1^\circ$ grid, on a daily basis. Burned area and fire locations for Alaska were obtained from the Alaska Fire Service

[*Kasischke et al.*, 2002]. For Canada, burned area was obtained from the Canadian Forest Service (http://cfs.nrcan.gc.ca/regions/nofc). Because these data were available at the provincial level only, fire locations were determined from MODIS hot spots. Information on the temporal distribution of the fires in both regions was obtained from MODIS hot spot data. In a recent paper, we showed that BWEM CO emission estimates for the North American boreal fires in 2004 and 2005 were in good agreement with CO observations in the fire plumes 7–15 days downwind [*Lapina et al.*, 2008]. More information on BWEM can be found elsewhere [*Kasischke et al.*, 2005].

4.3.2 FLEXPART simulations

The Lagrangian particle dispersion model FLEXPART [*Stohl et al.*, 2005] was used to simulate the advection and dispersion of BWEM-estimated emissions of HCHO and NO_x, treated as inert tracers in the model. These simulations were used to remove the effect of transport on calculated HCHO and NO_2 burdens by analyzing burdens within transported plume regions, identified as described in section 4.3.3. Model results were also used to quantify the mass of emissions over selected locations and to distinguish between fresh and more aged emissions for calculations of HCHO burden due to directly released fire emissions.

Particles representing fire emissions were released on a daily basis above the locations of active fires, between the surface and 7.5 km with a constant mixing ratio throughout the column, as described by *Lapina et al.* [2008]. Forward FLEXPART runs (version 6.2) were driven with data from the European Centre for Medium Range Weather Forecasts (ECMWF) [European Centre for Medium-Range Weather Forecasts, 2005] with a $1^\circ \times 1^\circ$ horizontal resolution, 61 vertical levels and a temporal resolution of 3 hours, using me-

teorological analyses at 0000, 0600, 1200, and 1800 UTC, and ECMWF 3-h forecasts at intermediate times (0300, 0900, 1500, 2100 UTC). The number of particles released into each grid cell was scaled by the mass of emissions in that cell.

At every location, the tracer concentration was modeled as a sum of the contributions of transported fire emissions released (emitted) upwind at earlier times, at 6-h resolution. These separate contributions grouped by the upwind release time are referred to as the age spectrum. The model only simulates tracer concentrations caused by fire emissions not older than the longest upwind time stored in the model, *i.e.*, the maximum age of the tracer, after which particles were dropped from the simulation. The choice of the maximum age for the fire tracers, t_{hcho} and t_{no_x}, is described in sections 4.3.2.1 and 4.3.2.2.

We used FLEXPART output at 18 UTC, the mean SCIAMACHY overpass time in the study region, which corresponds to 10 AM in Alaska. For a meaningful comparison of model to satellite observations it is necessary to take into account the presence of a large number of missing values in the SCIAMACHY data. Using FLEXPART as a tool to model the downwind locations of the transported emissions, we sampled FLEXPART tracer maps for each day only at the locations where SCIAMACHY measurements were available on that day. The resulting daily maps were then combined to obtain 5-day FLEXPART composites used in this work. These FLEXPART composites thus include values at the same locations and times as were included in the SCIAMACHY 5-day composites described in section 4.2. FLEXPART maps generated in this way were in better agreement with satellite observations than the maps obtained by averaging 5 days of simulations at every grid cell, based on a visual examination.

4.3.2.1 Maximum age of tracer for HCHO analysis

One of the objectives of this work was to investigate the timescale over which the impact of fires on HCHO columns remains significant. This timescale is not well defined, as in addition to being directly released from fires, HCHO can be produced through secondary production in the plumes, as discussed in more detail in section 4.4.1.3. To simulate fire impacts on HCHO, the maximum age of the HCHO tracer needs to be set equal to the typical maximum age of fire plumes maintaining high HCHO levels. This age was determined by analyzing SCIAMACHY HCHO columns together with transport simulations of fire emissions.

The maximum age of the tracer was varied between 24 and 72 hours, with a 12-h resolution. For each simulation, we analyzed FLEXPART composite maps to assess how well they matched SCIAMACHY observations. This was done based on a visual examination and by using values of the Pearson coefficients, R, for spatial correlation between the modeled and observed HCHO column maps on a $1^\circ \times 1^\circ$ grid. This analysis was conducted only for the periods with high fire activity, defined as 5-day periods with mean daily HCHO emissions exceeding 4 Gg. First, we analyzed how well each simulation reproduced the location of the enhanced HCHO levels downwind of fires. A maximum age of 24 hours was found to be insufficient for most cases, as these simulations failed to reproduce high HCHO present at locations further away from the sources. However, 72-h simulations often overstretched the plumes' extent to locations where the satellite data showed HCHO columns reduced to background levels. Improved spatial correlation between the model and SCIAMACHY HCHO maps was confirmed by the correlation analysis. The average value of R increased from 0.47 to 0.55, when t_{hcho} was increased from 24 to 48 hours. Simulations using a larger values of t_{hcho} did not result in further im-

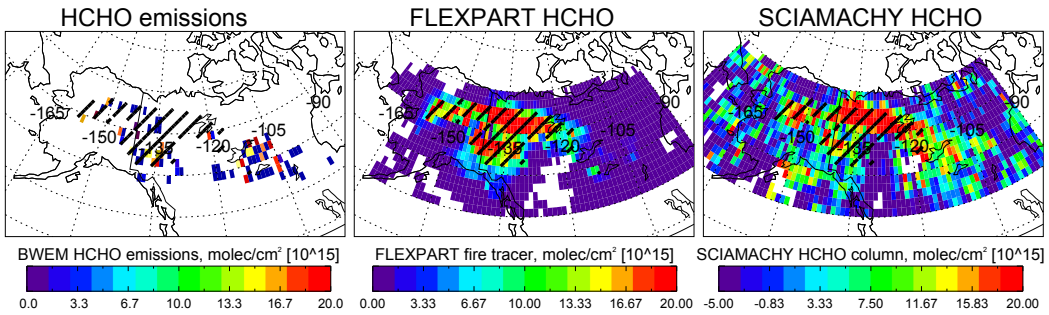

Figure 4.1 An example 5-day composite (July 11–July 15, 2004) of FLEXPART HCHO tracer simulations (center) and HCHO SCIAMACHY columns (right). Left: mean 5-day HCHO emissions over the fire locations released over the 48-hour period prior to the SCIAMACHY overpass. The plume region defined based on high values of the fire HCHO tracer (see text for description) is hatched in black. White areas inside the study region indicate either zero fire tracer concentrations (for FLEXPART) or missing satellite observations (for both SCIAMACHY and FLEXPART).

provement. (R remained below 0.56 for t_{hcho} as large as 72 hours.) Although a single maximum age did not produce the best match for all composites, we picked the value that showed the best agreement for most composites and set t_{hcho} equal to 48 hours for the final analysis. As the lifetime of HCHO is only a few hours, the presence of high HCHO levels at locations more than a day downwind demonstrates the importance of secondary HCHO formation from oxidation of the fire-emitted VOCs.

4.3.2.2 Maximum age of tracer for NO_2 analysis

To study the impact of fires on NO_2 levels and to model transport of the NO_x fire emissions, we took into account that NO_x is directly released from fires and its lifetime is on the order of few hours. We selected a maximum age for the NO_x tracer of 6 hours, with this value being a typical lifetime of NO_x oxidation against HNO_3 at these latitudes [*Martin et al.*, 2003]. Although it is possible for NO_x to last longer, especially if the plumes are lifted above the boundary layer, we found no evidence of enhanced NO_2 in SCIAMACHY maps at the transport distance of greater than 6 hours away which could be linked to the fire source.

4.3.3 Determining plume regions

FLEXPART simulations with the final values of t_{hcho} and t_{no_x} were used to locate plume regions for the analysis of fire impact on HCHO and NO_2 levels downwind. Each of the FLEXPART 5-day composite maps was analyzed separately to define locations of transported emissions for that time period, *i.e.*, the plume region. Plume regions were identified based on the presence of high levels of simulated fire tracer columns. Two separate plume regions were identified for each 5-day composite, one for NO_2 and one for HCHO.

For HCHO, a grid cell was defined as being part of a plume if the value of the fire HCHO tracer exceeded 1.0×10^{16} molec cm^{-2}. Using this criterion, the average value of corresponding SCIAMACHY cells in each 5-day composite varied between 2.6×10^{15} molec cm^{-2} and 2.1×10^{16} molec cm^{-2} with an overall average of 1.3×10^{16} molec cm^{-2}, which is higher than 90% of all summer HCHO values in the study region, confirming that we selected locations within fire plumes with greatly enhanced HCHO levels. An example of a selected plume region is shown in Figure 4.1. We evaluated the accuracy of the FLEXPART simulations by including an additional 2-degree buffer around the identified plume locations, and comparing the results for the case when no buffer was added. The addition of the buffer had no effect on the results of analysis presented in this work and, therefore, the results below are presented for the plume area without the buffer.

To define plume regions for the NO_2 analysis, a grid cell was defined as being part of the plume if the FLEXPART NO_x tracer exceeded 5.0×10^{15} molec cm^{-2}. By using this criterion combined with a choice of a shorter maximum residence time for the NO_x tracer, *i.e.*, t_{no_x} of 6 hours, we identified only regions over the fires and immediately downwind where the impact of fires on NO_2 levels is likely to be the strongest. The mean NO_2 value for the se-

lected grid cells in each 5-day composite varied between 1.0×10^{14} molec cm^{-2} and 1.2×10^{15} molec cm^{-2}, with an overall average of 5.0×10^{14} molec cm^{-2}, which corresponds to the 80^{th} percentile of all summer NO_2 values in the study region.

The fire tracer cutoffs used to identify fire plumes were somewhat arbitrary, but the selected locations were not sensitive to the moderate changes in the values used (within ±20%). Higher cutoffs produced plume areas of smaller size and, in the case of HCHO, appeared to exclude multiple grid cells with enhanced HCHO downwind of fires.

4.4 Burden in fire plumes

We define plume burden as the total mass of HCHO or NO_2 contained in the plume region, calculated as

$$B = f \sum_i a_i C_i, \tag{4.1}$$

where B is the burden (in Gg), a_i is area of the grid cell i, C_i is a SCIAMACHY or FLEXPART-derived tropospheric column value (molec cm^{-2}) in cell i, and f is a unit conversion factor.

4.4.1 Contributions to the HCHO burden in fire plumes

The total HCHO burden in the plume, B, can be separated into the burden enhancement due to fires, and the background burden —B_{bk}, the burden that would be present in the absence of fires. Fire burden is composed of the burden contributed by the directly released HCHO emissions, B_{direct}, and the burden resulting from secondary HCHO production from precursors emitted from fires, $B_{secondary}$. Therefore, the total HCHO burden can be expressed as

$$B = B_{bk} + B_{direct} + B_{secondary} \tag{4.2}$$

B_{direct} can be estimated using the FLEXPART transport simulations of HCHO emissions and information on HCHO destruction as described in section 4.4.1.2 below. Knowing B, B_{bk} and B_{direct}, we can deduce the burden resulting from secondary HCHO production, $B_{secondary}$.

4.4.1.1 Background HCHO burden

B_{bk} was estimated by determining the HCHO burden corresponding to an area of the same size as each plume, but not containing fire emissions. The impact of fire emissions in a grid cell was considered to be minimal if the level of FLEXPART-simulated HCHO tracer was below 1.0×10^{14} molec cm^{-2}. This threshold was sufficiently low to select locations at a significant distance away from the fire sources that were not contaminated by fire emissions, as was evident from their low levels in SCIAMACHY HCHO maps. (The value of B_{bk}, as calculated here, reflects the combination of the true HCHO background, originating from the presence of VOCs from non-fire sources, *e.g.*, methane and biogenic emissions, and bias in the satellite data.)

The analysis was performed for the summer, when biogenic emissions of isoprene are at their maximum and contribute to the HCHO budget in the study region. To test for the evidence of a HCHO signal due to isoprene, which could interfere with our estimation of B_{bk}, we used estimates of isoprene fluxes for the summer of 2004 (Colette Heald, Colorado State University, personal communication, 2009). The fluxes were simulated with a global chemical transport model (GEOS-Chem, version 7.04) using the MEGAN (Model of Emissions of Gases and Aerosols from Nature) version 2 model [*Guenther et al.*, 2006]. We selected five HCHO composites during periods when fire

emissions were low and the SCIAMACHY HCHO signal from fires was minimal (periods centered on June 3, June 8, June 13, July 3 and August 2). Next, we selected the region where GEOS-Chem predicted enhanced isoprene emissions (greater than 6×10^{11} atoms C cm^{-2} sec^{-1} in July) and an area of similar size (approximately $13^\circ \times 4^\circ$) with low isoprene emissions (less than 2×10^{11} atoms C cm^{-2} sec^{-1} in July; see Figure A.6 in the Appendix A). The mean HCHO columns in the regions with high and low isoprene emissions were not significantly different (with the mean HCHO column in the region with low isoprene emissions even exceeding the mean HCHO column with high isoprene emissions for three periods), implying that impact of isoprene on HCHO columns was within the noise level of the SCIAMACHY data (see Table A.1 and Figure A.7 in the Appendix A).

Out of all the background locations in each 5-day composite, we selected 300 grid cells and divided their HCHO burden by the total area. The resulting value (background burden per unit area) was multiplied by the area of the plume to obtain the B_{bk} value for that composite. The grid cells were selected randomly. (HCHO levels outside of the fire plumes were relatively homogeneous and there was no evidence of major HCHO sources in the study area other than fires.) HCHO columns for the background cells exhibited variability due to noise in the SCIAMACHY data, but the standard error of the obtained mean was relatively low due to the large number of grid cells used for averaging (Figure 4.2). On several occasions the background is negative, implying a negative bias for these periods in the retrieved columns, likely as a result of the correction for offset error performed during retrieval.

4.4.1.2 Burden due to direct HCHO emissions

To estimate B_{direct} we reduced the contributions of emitted HCHO according to the HCHO destruction rate constant, using the FLEXPART age spectra to

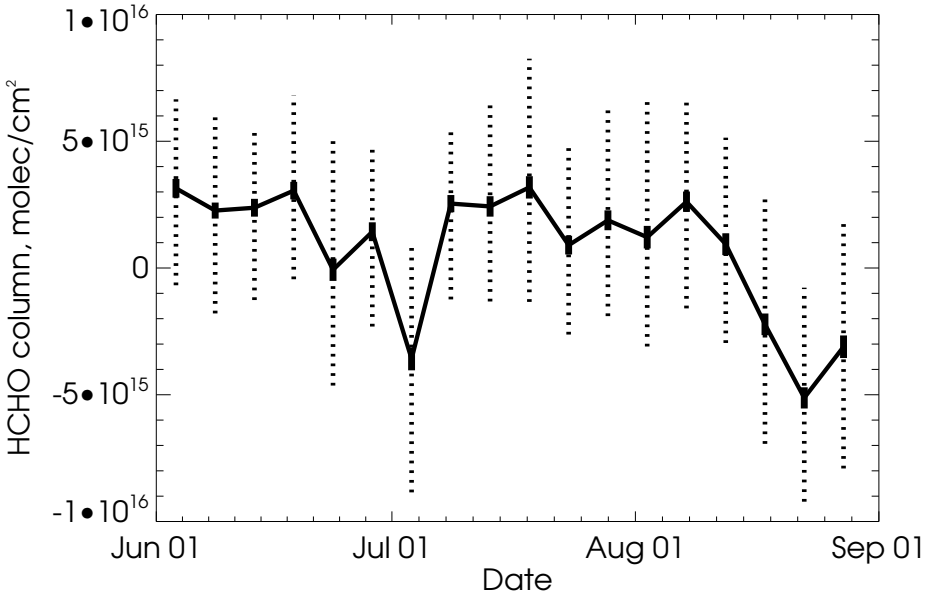

Figure 4.2 Mean HCHO tropospheric background column for each of the 5-day HCHO composites. The standard error of the mean is shown with solid vertical lines, and the 25^{th} and 75^{th} percentiles of the HCHO columns in the background grid cells are indicated with the dotted lines .

define the distribution of times since emission [*Parrish et al.*, 2007; *Honrath et al.*, 2008]. Thus, the contribution of emissions released at time t_E to the total HCHO concentration at the time of measurement, t_M, can be expressed as

$$[A]_{t_E} = [A]_{0,t_E} \exp(-k'\Delta t), \tag{4.3}$$

where $[A]_{0,t_E}$ is the concentration increment that the emissions would have contributed in the absence of removal, k' is the mean value of the diurnally-varying rate constant for pseudo-first order HCHO loss between t_E and t_M, which describes the main HCHO removal mechanisms (the reaction with OH and photolysis [*Fried et al.*, 2008]), and Δt is the time since emission.

The total burden in grid cell j can be obtained by summing up the incremental contributions over all values of Δt between the SCIAMACHY overpass time and up to several e-folding time periods earlier:

$$B_{direct_j} = \sum_{t_M-\infty}^{t_M} [A]_{0,t_E} \exp(-k'\Delta t) \tag{4.4}$$

Because of the dependence of k' on sunlight, we calculated a diurnal profile of k', which varied between a maximum daytime value k'_{max} for overhead conditions and zero during night. k'_{max} was selected based on estimates of the column-averaged τ (with τ defined as $1/k'$) at overhead conditions, which range from 1.5 to 3 hours [*Macdonald et al.*, 2001; *Palmer et al.*, 2003; *Wittrock et al.*, 2006; *De Smedt et al.*, 2008]. Here we report results using this range to reflect the associated uncertainty.

For the τ values adopted here, only primary emissions released within the last 18–24 hours made a significant contribution to the HCHO burden, while HCHO released 24 to 48 hours upwind decayed to negligible levels (with contributions of less than 0.5% for a τ of 1.5 hours and less than 5% for a τ of 3 hours) by the time of the satellite overpass.

4.4.1.3 Burden due to secondary HCHO

The burden of secondary HCHO, $B_{secondary}$, is estimated by subtracting B_{direct} and B_{bk} from the total burden B, calculated from the SCIAMACHY data. Precise estimation of the amount of secondary HCHO produced would require knowledge of the lifetimes and relative emission rates of the VOCs that contribute to secondary HCHO formation, as well as information on atmospheric levels of OH and NO_x [*Stavrakou et al.*, 2009], and is beyond the scope of this work. However, an approximate estimate can be obtained by assuming that the ratio of burden to HCHO emitted or produced is the same for both primary and secondary HCHO, hence,

$$E_{secondary} = E_{direct}(B_{secondary}/B_{direct}), \tag{4.5}$$

where E_{direct} is the total primary HCHO emissions contributing to the region. The sum of $E_{secondary}$ and E_{direct} gives a lower limit estimate of the total amount of HCHO from fires, as we consider secondary production only within the first 48 hours after the release of emissions.

4.4.2 Contributions to the NO_2 burden

Similarly to HCHO, the NO_2 burden in the fire plumes can be separated into contributions of several factors, including fires. However, NO_2 levels aside from fires were highly variable, precluding selection of background locations. As the background contribution in the plumes could not be inferred, we analyzed the total NO_2 plume burden to determine whether fires had a detectable impact on NO_2 tropospheric columns as seen from space.

4.5 Results and discussion

4.5.1 HCHO and NO_2 in the study region

To learn about the factors controlling the variability of HCHO and NO_2 in the study region, we first visually compared 19-day HCHO and NO_2 composites for the periods before and after the start of major fires in the region. (We chose 19 days as this is the length of the period in June before the start of fires.) The top row of Figure 4.3 presents early- to mid-June composites for the period prior to the start of the main fire season. HCHO columns during this period were generally very low. However, there are highly enhanced NO_2 column densities in the northeastern part of the region, indicating the presence of the non-fire sources of NO_x. As fire activity increased later in the summer (Figure 4.3, lower rows), widespread HCHO enhancements in the region of active fires became apparent. For NO_2, the relationship is less obvious: highly enhanced NO_2 columns were seen over the fire locations in late June/early July, but not over the August fires; during late July and August, high NO_2 was present over the southeastern part of the region, away from fires, implying that fires were not the dominant source of NO_x in the region.

Visual analysis of the 5-day SCIAMACHY composite maps further demonstrated that areas of highly enhanced HCHO were closely collocated with the locations of transported FLEXPART fire tracer. NO_2 data, on the other hand, did not exhibit a consistent response to fires: enhancement over the fire locations was present only occasionally.

4.5.2 Modeling HCHO plume locations

FLEXPART identified plumes on thirteen out of eighteen 5-day composites. The locations of the modeled plumes agreed well with the locations of en-

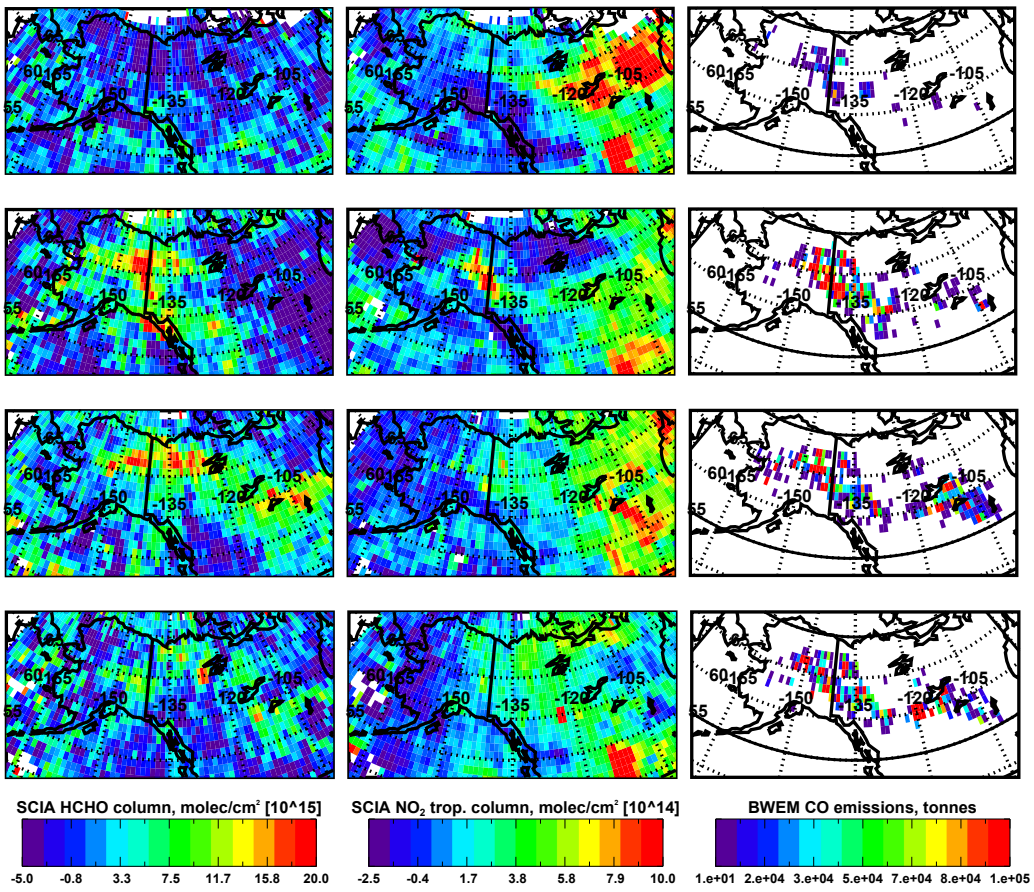

Figure 4.3 19-day composites of HCHO (left), NO_2 (center) and BWEM CO emissions over the fire locations (right) for four periods in 2004. From the top: June 1–June 19, June 20–July 8, July 9–July 27, July 28–August 15. The black border in the image on the right indicates the study region analyzed in this work.

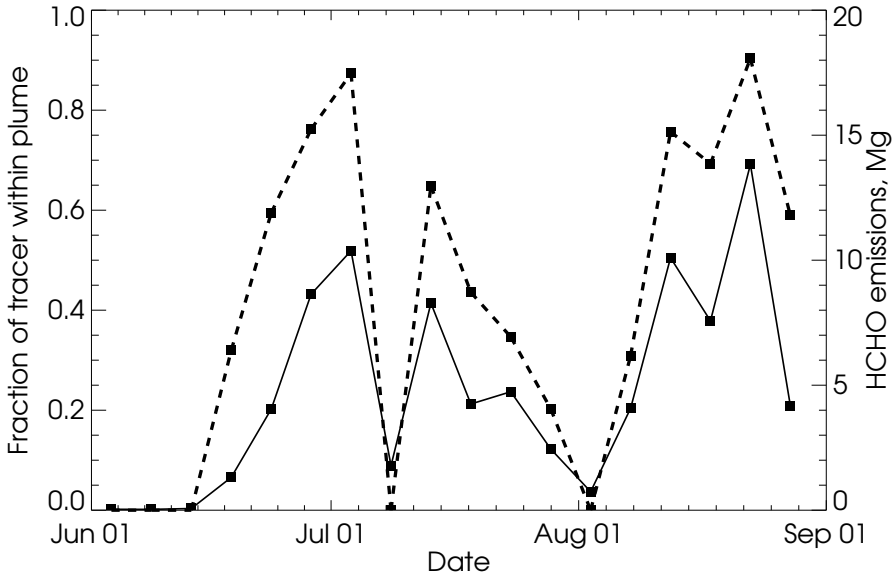

Figure 4.4 5-day-average daily BWEM emissions of HCHO in the study region (solid line) and the corresponding fraction of HCHO tracer mass contained within the plume area in the FLEXPART 5-day composites (dashed line).

hanced SCIAMACHY HCHO columns on all but two 5-day periods. The exceptions were the plumes for the periods centered on August 7 and August 27, when the model missed the locations of elevated HCHO, possibly due to the errors in the fire emissions inventory. Of the five composites in which FLEXPART identified no plumes, three were in early June, prior to the start of large fires. Low SCIAMACHY HCHO columns confirmed the absence of fire signal for four out of these five periods, with some moderately enhanced HCHO present for the fifth period. Hence, the emissions and transport models performed well overall, and simulations agreed with observations on fifteen out of eighteen periods.

Figure 4.4 shows daily emissions of primary HCHO released from fires calculated by BWEM and the fraction of these total emissions that is present in the analyzed plumes. It is apparent that during the periods with high fire activity most of the HCHO mass (that is, at least 50%, and more than

70% for the nine composites with greater than 14 Gg) is contained within the plume region. (Zero mass indicates periods when no plume regions were identified due to low fire emissions.) The spatial correlation between the modeled and observed HCHO column maps was significant ($R > 0.55$) for each composite with high fire activity (with the exceptions of the periods centered on August 7 and August 27, as described above), indicating that the FLEXPART model and BWEM inventory generally performed well in terms of the plume locations and relative magnitude of the emissions.

4.5.3 Impact of fires on the HCHO burden

Figure 4.5 presents the fire burdens in the transported fire plumes in each 5-day composite. The correlation between the SCIAMACHY-estimated burdens ($B - B_{bk}$, solid black line) and the total HCHO fire emissions released over the 48-hour period preceding the measurement and transported with the fire plume (E_{direct}, dotted black line), was high (R=0.91), implying that fires greatly affected HCHO levels over the plume regions. The total HCHO burden in the fire plumes (B, red dashed line) also tracked the variations in E_{direct} relatively well (R=0.82), consistent with the expectation that fires were the major source of variability in the SCIAMACHY HCHO columns in the identified plume regions. The background burden in the plumes, B_{bk}, (not shown on the plot) was not correlated with E_{direct}.

The blue line with error bars in Figure 4.5 shows B_{direct}, the burden contribution due to directly released HCHO emissions, calculated using equation 4.4 with two different estimates of k'_{max}. These values differed by a factor of 1.5. The significant difference between the fire burden ($B - B_{bk}$, solid black line) and B_{direct} indicates a considerable contribution of secondary HCHO production. The mean ratio of the burden attributed to secondary production

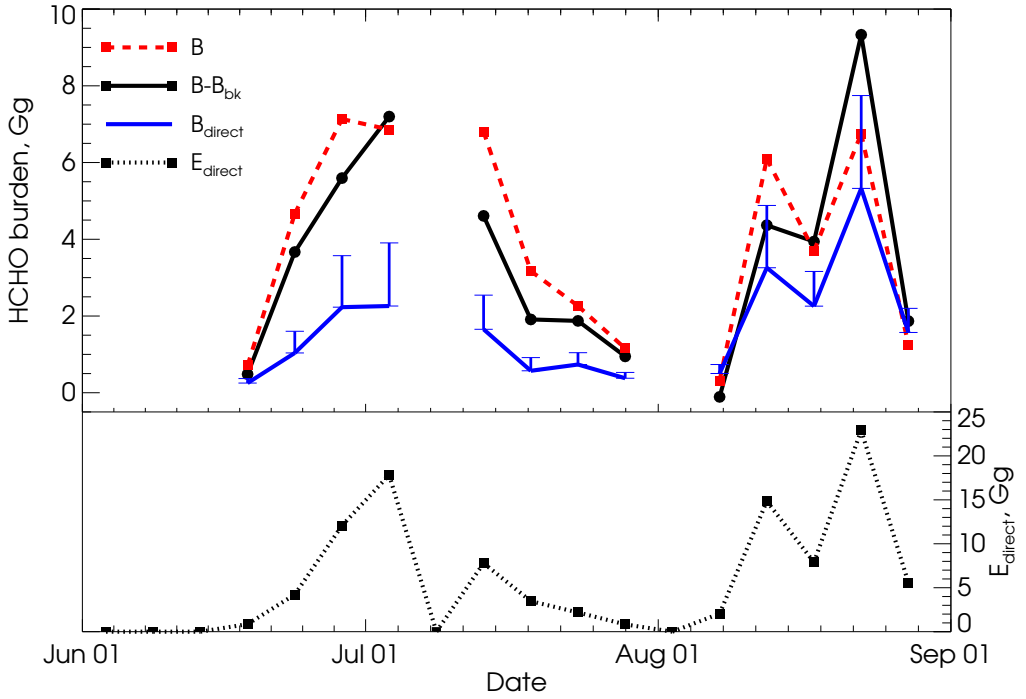

Figure 4.5 HCHO burdens in the identified fire plumes in each 5-day composite: the total HCHO burden calculated from SCIAMACHY HCHO composite maps (B, red dashed line), the HCHO fire burden ($B - B_{bk}$, black solid line), and HCHO burden from primary emissions, B_{direct} (blue line with error bars for two different values of k'_{max} used in calculation). Total emissions contributing to the fire plumes, E_{direct}, is shown with the black dotted line. Burdens are shown only for the periods with identified fire plumes (that is, 5-day composites with non-zero fraction of tracer mass within the plume area, as shown in Figure 4.4).

($B_{secondary} = B - B_{bk} - B_{direct}$) and B_{direct} was 0.7 or 1.5, depending on the choice of k'_{max} used in the calculation. Thus, the contribution of secondary HCHO production from the oxidation of the fire-emitted VOCs was of a magnitude similar to the contribution of directly emitted HCHO.

Although the relationship between VOC emissions and the mass of HCHO produced, and the relationship between HCHO produced and the resulting atmospheric burden, $B_{secondary}$, are complex, $B_{secondary}$ was rather well correlated to E_{direct} ($R = 0.75$, using k'_{max}=1/1.5 hours for the calculation of B_{direct}). This may be explained as a result of the fact that the emissions of VOCs that contribute to secondary HCHO production are expected to be

approximately proportional to the emissions of primary HCHO.

It needs to be noted that our calculation of B_{direct} may be biased, as our emissions model did not account for a diurnal cycle in fire activity. Emissions from boreal fires, similar to other regions [*Giglio*, 2007; *Boersma et al.*, 2008; *Stavrakou et al.*, 2009], are likely to be higher in the late afternoon and lower in the periods of the night and morning hours. The latter are immediately prior to SCIAMACHY overpass and, hence, are least affected by the removal and currently contribute most to the estimate of B_{direct} (see section 4.4.1.2). Thus, *Stavrakou et al.* [2009] found that neglecting the diurnal fire cycle in their model simulations led to local increases in modeled HCHO columns on the order of 10%. An overestimation of B_{direct} for this reason would imply that the impact of secondary HCHO production relative to the impact of directly-released HCHO is even larger than inferred from this analysis.

The BWEM-based amount of directly-released HCHO in the entire study region is 0.42 $\pm$0.09 Tg. By applying equation 4.5 we estimate that an additional 0.23–0.76 Tg were formed in the fire plumes, bringing the total amount of fire HCHO released or produced in the region to 0.6–1.3 Tg. As HCHO production from the slower oxidizing VOCs continues for days after fires [*Fried et al.*, 2008; *Stavrakou et al.*, 2009], this range represents a lower limit on the total fire HCHO.

To compare these numbers to other HCHO sources in the region, we computed total summer HCHO emissions from isoprene over the study region. Using one-day yields of HCHO molecule per isoprene C reacted of 0.28 for low-NO_x conditions [*Dufour et al.*, 2009], we calculate that the total amount of HCHO produced from isoprene in the entire study region during summer of 2004 was 1.6 Tg. This number exceeds the estimate of total HCHO from fires over the same time period, while above (section 4.4.1.1) we found no detectable signal in SCIAMACHY over the areas with high isoprene emissions.

To determine whether this result could be due to a difference in column concentration such that the more episodic fires produced a stronger signal in the SCIAMACHY observations, we estimated the average daily mass of HCHO per unit area in the fire plumes and over the areas of high isoprene emissions in July. Using a secondary to primary HCHO ratio for fires of 1, we found that the average estimated daily flux due to isoprene in the high-emissions area (extending from 124W to 111W and from 57N to 61N, as shown in Figure A.7 in the Appendix A), 0.46 mg HCHO m^{-2} $hour^{-1}$, is comparable to the average estimated daily fire HCHO flux within the fire plumes, 0.50 mg HCHO m^{-2} $hour^{-1}$. This result implies that the finding of clear HCHO enhancements associated with fire emissions, but not over areas of high expected isoprene emissions, is not due to a lower HCHO flux in the case of isoprene emissions. We do not yet understand the cause of this discrepancy. It could indicate overestimated isoprene fluxes or, alternatively, it could indicate that our estimates of fire HCHO impacts are too low.

To determine the impact of fires on HCHO levels outside of the plumes, we used SCIAMACHY data to compute the total HCHO burden in the entire study region. The mean ratio of HCHO burden in the fire plumes to the HCHO burden in the whole region was 0.65. (Because of a large number of negative values in HCHO data, the total burden for a large region was not always higher than the burden over a small region.) This, and the fact that the area of the simulated fire plumes exceeded 10% of the study area on seven out of thirteen periods, implies a very large fire impact on the HCHO burden in the whole North American boreal region.

4.5.4 Impact of fires on the NO_2 burden

Although highly enhanced NO_2 columns (1.0×10^{15} molec cm^{-2} and higher) were occasionally observed over the fire locations, the effect of fires on NO_2 levels in the plumes was not as apparent as their impact on HCHO.

The total NO_2 burden in the fire plumes was correlated with the mass of the fire tracer in the plumes ($R = 0.57$), but this relationship was not as strong as for the HCHO burden. Conversion of NO_x emissions to NO_y may be one of the possible explanations for this result.

NO_2 columns in the study region showed issues similar to HCHO, with several periods having a very large number of negative column amounts. This was probably due to an incorrect assumption for stratospheric correction, as the reference sector used was affected by NO_x fire emissions over Alaska. Therefore, it is likely that this issue has further weakened a modest impact of fires on the NO_2 burden.

4.6 Conclusions

Analysis of plumes from the 2004 Alaskan and Canadian fires has shown that fires dominated the HCHO burden in regions affected by emissions up to 2-days upwind. By comparing FLEXPART simulations of BWEM-estimated emissions to SCIAMACHY observations, we concluded that high HCHO levels in the outflow from fires can be sustained for at least 48 hours, due to continuing secondary production. This production was responsible for an increase in the HCHO burden, with a magnitude at least comparable to that due to directly emitted HCHO.

Model simulations successfully predicted the locations of transported fire emissions. Comparisons with SCIAMACHY tropospheric HCHO and NO_2

columns indicate that the BWEM inventory performed well in terms of the timing and relative magnitude of fires. Fire emissions released over the 48-hour period prior to the satellite overpass were significantly correlated with estimates of the HCHO burden due to secondary production from VOCs, which were constrained by SCIAMACHY HCHO columns. We estimated that at least 0.6–1.3 Tg of HCHO was added to the atmosphere from the Alaskan and Canadian fires in 2004. This amount is somewhat lower than estimates of HCHO from isoprene in the studied region. However, we were able to discern no difference in SCIAMACHY HCHO columns when comparing areas of high isoprene to areas of low isoprene emissions. In contrast, SCIAMACHY observed large differences in HCHO columns due to fire emissions. Therefore, we conclude that fire emissions had larger impact on HCHO tropospheric columns than did isoprene during the extended period of fire activity. Further studies are needed to quantify HCHO production from isoprene and fire HCHO in the boreal regions in order to determine the reasons for the observed discrepancy in the satellite data signal.

While highly elevated NO_2 levels were occasionally observed over fire locations, fires had a relatively moderate impact on the NO_2 burden, even in fresh plumes over and immediately downwind of fire locations. Observations of highly enhanced NO_2 away from the fires imply the presence of other dominant sources of NO_2 in the region studied.

Chapter 5

Summary and Conclusions

5.1 Summary and Conclusions

This work produced several major results. First, it demonstrated that O_3 levels in the North Atlantic free troposphere are significantly increased when boreal fire impacts are present. Next, it showed that there is a seasonal trend in the NO_x/CO emission ratio from boreal fires, that is due to the change in the burning properties of fires taking place in boreal regions. Finally, it showed that boreal fires dominated the burden of HCHO, an important ozone precursor, over fire locations and in plumes up to two days old, during the summer of 2004. These conclusions are presented below in more detail, followed by a general summary and recommendations for future work.

5.2 Impacts of boreal fires on tropospheric ozone levels

Analysis of the multi-year O_3 and CO measurements in several-day-old plumes at the Pico Mountain Observatory showed that boreal fires had a major im-

pact on summer distributions of CO and were at least partially responsible for significant shifts in the summer distributions of O_3 in the high-fire years (2003 and 2004) compared to the low-fire year (2001). The average increase in ozone levels during the periods affected by fire emissions, compared to the relatively clean periods, was on the order of 20 ppbv. As the Pico Mountain Observatory is located thousands of kilometers away from the fire source regions, the magnitude of this impact implies that boreal fires can affect very large regions in high-fire years. As fires raise the background ozone levels over the Northern Hemisphere, the number of ozone exceedances is expected to increase and this will negatively affect the ability of downwind nations to meet their ozone air quality standards. Summertime ozone levels are likely to be enhanced even more in the future, as boreal fire activity is amplified by the changing climate.

5.3 Seasonal trend in the fire NO_x/CO emission ratio

Analysis of the $\Delta NO_y/\Delta CO$ enhancement ratios measured in several-days-old boreal fire plumes at the Pico Mountain Observatory demonstrated the presence of a significant decreasing seasonal trend in NO_x/CO emission ratio from fires. This trend is consistent with the current understanding that the relative magnitude of ground burning significantly increases in late summer. As the ground layer is consumed predominantly via smoldering combustion and the ratio of CO to NO_x is much higher in smoldering than in flaming fires, this late-season change leads to a drop in the NO_x/CO emission ratio.

This finding is an important step in improving the existing boreal fire emission inventories and it shows that the use of a single NO_x/CO emission

ratio (as is commonly done in atmospheric modeling) introduces a significant bias in the estimated emissions. This seasonal trend also implies a higher fuel consumption per unit area burned in late summer, leading to a major overall increase in fire emissions.

A combination of the BWEM-estimated emissions with the FLEXPART transport model predicted well the fire impact at the Pico Mountain Observatory and was in good agreement with the measurements, especially when the maximum injection height of emissions in the model was increased from 300 m to 7.5 km, implying that most of the observed plumes were lifted high into the atmosphere, likely as a result of intense crown fires.

5.4 Impacts of fires on HCHO and NO_2

A combined analysis of the SCIAMACHY HCHO columns and the FLEXPART transport simulations using the BWEM emissions showed that fires were the dominant source of HCHO in plumes up to two days old. No such impact was observed for NO_2. Observed HCHO columns were larger than expected from the primary HCHO fire emissions, implying a significant secondary HCHO production from the fire-released VOCs. While the amount of HCHO from fire, both emitted and produced, was similar in magnitude to the HCHO assumed to result from isoprene emissions in the studied region, the analysis was able to discern no signal from isoprene, which may indicate a significant shortcoming in the current emission estimates.

5.5 Summary and future research

The evidence presented for the North Atlantic free troposphere region helps to assess the impact of boreal fires on the chemical environment in the Northern

Hemisphere in general. By demonstrating a significant impact of boreal fires on ozone levels, this work results in an improved understanding of the sources affecting the Northern Hemisphere summer ozone budget. Increase in the background concentrations of ozone, which is an important greenhouse gas, over very large regions of the Northern Hemisphere implies a positive feedback on the climate in boreal region, which has a potential to aggravate the fire situation even further.

This work also demonstrates the need for further research on quantifying fuel consumption in the boreal regions, especially the ground fuel, as this knowledge helps to constrain and improve the fire emission inventories of ozone precursors, such as NO_x, HCHO and CO.

Satellite data analysis used in this work was an important step in quantifying the impacts of fires over the boreal regions. Tropospheric data products from more recent satellite instruments, such as GOME-2 and OMI, have an improved spatial and temporal resolution and thus can provide a better picture of the atmospheric impact of fires. These data should be used in the future analysis of fire effects over remote boreal regions.

Further monitoring of boreal fire impacts on atmospheric composition is crucial, as the climate change will lead to an increase in fire activity which will further affect the background concentrations of atmospheric pollutants.

References

Andreae, M. O., Assessment of global emissions from vegetation fires, *International Forest Fire News (IFFN)*, *No.31*, 112–121, 2004.

Andreae, M. O., and P. Merlet, Emission of trace gases and aerosols from biomass burning, *Global Biogeochem. Cycles*, *15*, 955–966, 2001.

Ayers, G., Comment on regression analysis of air quality data, *Atmos. Environ.*, *35*, 2423–2425, 2001.

Bertschi, I. T., and D. A. Jaffe, Long-range transport of ozone, carbon monoxide, and aerosols to the NE Pacific troposphere during the summer of 2003: Observations of smoke plumes from Asian boreal fires, *J. Geophys. Res.*, *110*, 2005.

Boersma, K. F., D. J. Jacob, H. J. Eskes, R. W. Pinder, J. Wang, and R. J. van der A, Intercomparison of SCIAMACHY and OMI tropospheric NO2 columns: Observing the diurnal evolution of chemistry and emissions from space, *J. Geophys. Res.*, *113*, 2008.

Bond, T. C., D. G. Streets, K. F. Yarber, S. M. Nelson, J.-H. Woo, and Z. Klimont, A technology-based global inventory of black and organic carbon emissions from combustion, *J. Geophys. Res.*, *113*, 2004.

Chandra, S., J. R. Ziemke, X. Tie, and G. Brasseur, Elevated ozone in the troposphere over the Atlantic and Pacific oceans in the Northern Hemisphere, *Geophys. Res. Lett.*, *31*, 2004.

Colarco, P. R., M. R. Schoeberl, B. G. Doddridge, L. T. Marufu, O. Torres, and E. J. Welton, Transport of smoke from Canadian forest fires to the surface near Washington, D.C.: Injection height, entrainment, and optical properties, *J. Geophys. Res.*, *109*, 2004.

Conard, S., and G. A. Ivanova, Wildfire in Russian boreal forests - potential impacts of fire regime characteristics on emissions and global carbon balance estimates, *Environ. Pol.* , *98*, 305, 1997.

Cook, P. A., et al., Forest fire plumes over the North Atlantic: p-TOMCAT model simulations with aircraft and satellite measurements from the ITOP/ICARTT campaign, *J. Geophys. Res.*, *12*, 2007.

Crutzen, P. J., and M. O. Andreae, Biomass burning in the tropics: impact on atmospheric chemistry and biogeochemical cycles, *Science*, *250*, 1669–1678, 1990.

Damoah, R., et al., A case study of pyro-convection using transport model and remote sensing data, *Atmos. Chem. and Phys.*, *6*, 173–185, 2006.

de Gouw, J. A., et al., Volatile organic compounds composition of merged and aged forest fire plumes from Alaska and western Canada, *J. Geophys. Res.*, *111*, 2006.

De Smedt, I., J.-F. Mller, T. Stavrakou, R. van der A, H. Eskes, and M. Van Roozendael, Twelve years of global observation of formaldehyde in the troposphere using GOME and SCIAMACHY sensors, *Atmos. Chem. and Phys.*, *8*, 7555–7608, 2008.

DeBell, L. J., R. W. Talbot, J. E. Dibb, J. W. Munger, E. V. Fischer, and S. E. Frolking, A major regional air pollution event in the northeastern United States caused by extensive forest fires in Quebec, Canada, *J. Geophys. Res.*, *109*, 2004.

Draper, N. R., and H. Smith, *Applied Regression Analysis*, John Wiley & Sons, Inc., 1998.

Draxler, R., and G. Rolph, HYSPLIT4 (HYbrid Single-Particle Lagrangian Integrated Trajectory) model, http://www.arl.noaa.gov/ready/hysplit4.html, 2003, NOAA Air Resources Laboratory, Silver Spring, Maryland.

Dufour, G., F. Wittrock, M. Camredon, M. Beekmann, A. Richter, B. Aumont, and J. P. Burrows, SCIAMACHY formaldehyde observations: constraint for isoprene emission estimates over Europe?, *Atmos. Chem. and Phys.*, *9*, 1647–1664, 2009.

Duncan, B. N., R. V. Martin, A. C. Staudt, R. Yevich, and J. A. Logan, Interannual and seasonal variability of biomass burning emissions constrained by satellite observations, *J. Geophys. Res.*, *108*, 2003.

ECMWF, Users guide to ECMWF products 4.0, *Tech. Rep. Meteorological Bulletin M3.2*, European Center for Medium-Range Weather Forecasts (ECMWF), Reading, UK, 2005.

Edwards, D. P., et al., Observations of carbon monoxide and aerosols from the TERRA satellite: Northern Hemisphere variability, *J. Geophys. Res.*, *109*, 2004.

Flannigan, M. D., K. A. Logan, B. D. Amiro, W. R. Skinner, and B. Stocks, Future area burned in Canada, *Clim. Change*, *72*, 1–16, 2005.

Forster, C., et al., Transport of boreal forest fire emissions from Canada to Europe, *J. Geophys. Res.*, *106*, 22,887–22,906, 2001.

French, N., E. Kasischke, M. R. Turetsky, W. de Groot, R. Honrath, and R. Ottmar, Carbon, trace gas, and particulate emissions from wildfires in the boreal regions of North America, in *Proc. 16th International Emission Inventory Conference*, Raleigh, North Carolina, 2007.

French, N. H. F., P. Goovaerts, and E. S. Kasischke, Uncertainty in estimating carbon emissions from boreal forest fires, *J. Geophys. Res.*, *109*, 2004.

Fried, A., et al., Formaldehyde over North America and the North Atlantic during the summer 2004 INTEX campaign: Methods, observed distributions, and measurement-model comparisons, *J. Geophys. Res.*, *113*, 2008.

Fromm, M., R. Bevilacqua, R. Servranckx, J. Rosen, J. P. Thayer, J. Herman, and D. Larko, Pyro-cumulonimbus injection of smoke to the stratosphere: Observations and impact of a super blowup in northwestern Canada on 3-4 august 1998, *J. Geophys. Res.*, *110*, 2005.

Fromm, M. D., and R. Bevilacqua, New directions: eruptive transport to the stratosphere: add fire-convection to volcanoes, *Atmos. Environ.*, *38*, 163–164, 2004.

Fromm, M. D., and R. Servanckx, Transport of forest fire smoke above the tropopause by cupercell convection, *Geophys. Res. Lett.*, *30*, 2003.

Fu, T.-M., D. J. Jacob, P. I. Palmer, K. Chance, Y. X. Wang, B. Barletta, D. R. Blake, J. C. Stanton, and M. J. Pilling, Space-based formaldehyde measurements as constraints on volatile organic compound emissions in east and south Asia and implications for ozone, *J. Geophys. Res.*, *112*, 2007.

Galanter, M., H. Levy II, and G. R. Carmichael, Impacts of biomass burning on tropospheric CO, NO_x, and O_3, *J. Geophys. Res.*, *105*, 6633–6653, 2000.

Generoso, S., I. Bey, J.-L. Attie, and F.-M. Breon, A satellite-and model-based assessment of the 2003 Russian fires: Impact on the Arctic region, *J. Geophys. Res.*, *112*, 2007.

Giglio, L., Characterization of the tropical diurnal fire cycle using VIRS and MODIS observations, *Remote Sens. Environ.*, *108*, 407–421, 2007.

Gillet, N. P., A. J. Weaver, F. W. Zwiers, and M. D. Flannigan, Detecting the effect of climate change on Canadian forest fires, *Geophys. Res. Lett.*, *31*, 2004.

Goode, J. G., R. J. Yokelson, D. E. Ward, R. A. Susott, R. E. Babbitt, M. A. Davies, and W. M. Hao, Measurements of excess O_3, CO, CH_4, C_2H_4,C_2H_2, HCN,

NO, NH_3, HCOOH, CH_3COOH, HCHO, and CH_3OH in 1997 Alaskan biomass burning plumes by airborne Fourier transform infrared spectroscopy (AFTIR), *J. Geophys. Res.*, *105*, 22,147–22,166, 2000.

Guenther, A., T. Karl, P. Harley, C. Wiedinmyer, P. I. Palmer, and C. Geron, Estimates of global terrestrial isoprene emissions using megan (model of emissions of gases and aerosols from nature), *Atmospheric Chemistry and Physics*, *6*, 3181–3210, 2006.

Hassol, S. J., *Impacts of a warming Arctic: Arctic climate impact assessment*, Cambridge University Press, 2004.

Honrath, R. E., R. C. Owen, M. Val Martín, J. S. Reid, K. Lapina, P. Fialho, M. P. Dziobak, J. Kleissl, and D. L. Westphal, Regional and hemispheric impacts of anthropogenic and biomass burning emissions on summertime CO and O_3 in the North Atlantic lower free troposphere, *J. Geophys. Res.*, *109*, 2004.

Honrath, R. E., D. Helmig, R. C. Owen, D. D. Parrish, and D. M. Tanner, Nonmethane hydrocarbons at Pico Mountain, Azores: 2. Event-specific analyses of the impacts of mixing and photochemistry on hydrocarbon ratios, *J. Geophys. Res.*, *113*, 2008.

Houghton, J. T., Y. Ding, D. J. Griggs, M. Noguer, P. J. van der Linden, X. Dai, K. Maskell, and C. A. Johnson, *Climate Change 2001: The scientific basis. Contribution of Working Group I to the Third Assessment Report of the Intergovernmental Panel on Climate Change*, Cambridge University Press, 2001.

Hudman, R. C., et al., Surface and lightning sources of nitrogen oxides over the United States: magnitudes, chemical evolution, and outflow, *J. Geophys. Res.*, 2007.

Hyer, E. J., E. S. Kasischke, and D. J. Allen, Effects of source temporal resolution on transport simulations of boreal fire emissions, *J. Geophys. Res.*, *112*, 2007a.

Hyer, E. J., E. S. Kasischke, and D. J. Allen, Examining injection properties of boreal forest fires using surface and satellite measurements of CO transport, *J. Geophys. Res.*, 2007b, in press.

IPCC, Climate Change 2007: The Physical Science Basis, http://www.ipcc.ch/SPM2feb07.pdf, 2007.

Jacob, D. J., et al., Summertime photochemistry of the troposphere at high northern latitudes, *J. Geophys. Res.*, *97*, 16,421–16,431, 1992.

Jaffe, D., I. Bertschi, L. Jaeglé, P. Novelli, J. S. Reid, H. Tanimoto, R. Vingarzan, and D. L. Westphal, Long-range transport of Siberian biomass burning emissions and impact on surface ozone in western North America, *Geophys. Res. Lett.*, *31*, 2004.

Jost, H.-J., et al., In-situ observations of mid-latitude forest fire plumes deep in the stratosphere, *Geophys. Res. Lett.*, *31*, 2004.

Kasischke, E. S., and L. P. Bruhwiller, Emissions of carbon dioxide, carbon monoxide, and methane from boreal forest fires in 1998, *J. Geophys. Res.*, *108*, 2002.

Kasischke, E. S., and J. F. Johnstone, Variation in postfire organic layer thickness in a black spruce forest complex in interior alaska and its effects on soil temperature and moisture, *Can. J. For. Res.*, *35*, 2164–2177, 2005.

Kasischke, E. S., and M. R. Turetsky, Recent changes in the fire regime across the North American boreal region—Spatial and temporal patterns of burning across Canada and Alaska, *Geophys. Res. Lett.*, *33*, 2006.

Kasischke, E. S., D. Williams, and D. Barry, Analysis of the patterns of large fires in the boreal forest region of Alaska, *Int. J. Wildland Fire*, *11*, 131–144, 2002.

Kasischke, E. S., E. Hyer, P. Novelli, L. Bruhwiler, N. French, A. Sukhinin, J. Hewson, and B. Stock, Influences of boreal fire emissions on Northern Hemisphere atmospheric carbon and carbon monoxide, *Glob. Biogeochem. Cycles*, *19*, 2005.

Kleissl, J., M. P. Dziobak, and R. E. Honrath, The influence of orographic flows on PICO-NARE trace-gas measurements, *Eos Trans. AGU*, *86*, 2005, Fall Meet. Suppl., Abstract A51D-0110.

Kleissl, J., R. Honrath, M. Dziobak, D. Tanner, Val Martín, R. Owen, and D. Helmig, The occurrence of upslope flows at the Pico mountaintop observatory: A case study of orographic flows on small, volcanic island, *J. Geophys. Res.*, *112*, 2007.

Lapina, K., R. E. Honrath, R. C. Owen, M. Val Martín, and G. Pfister, Evidence of significant large-scale impacts of boreal fires on ozone levels in the midlatitude Northern Hemisphere free troposphere, *Geophys. Res. Lett.*, 2006.

Lapina, K., R. E. Honrath, R. C. Owen, Val Martín, E. J. Hyer, and P. Fialho, Late summer changes in burning conditions in the boreal regions and their implications for NOx and CO emissions from boreal fires, *J. Geophys. Res.*, *113*, 2008.

Lavoue, D., C. Liousse, H. Cachier, B. J. Stocks, and J. G. Goldammer, Modeling of carbonaceous particles emitted by boreal and temperature wildfires at northern latitudes, *J. Geophys. Res.*, *98*, 26,871–26,890, 2000.

Law, K., et al., Evidence for long-range transport of North American anthropogenic and wildfire emissions to Europe from airborne and ground based lidar measurements during European ITOP (IGAC Lagrangian 2K4, ICARTT), *Eos Trans. AGU*, *86*, 2005, Fall Meet. Suppl., Abstract A41D-01.

Law, K. S., and A. Stohl, Arctic Air Pollution: Origins and Impacts, *Science*, *1537–1540*, 2007.

Lee, M., B. G. Heikes, D. J. Jacob, G. Sachse, and B. Anderso, Hydrogen peroxide, organic hydroperoxide, and formaldehyde as primary pollutants from biomass burning, *J. Geophys. Res.*, *102*, 1301–1309, 1997.

Lee, M., B. G. Heikes, and D. J. Jacob, Enhancements of hydroperoxides and formaldehyde from biomass burning impacted air and their effect on atmospheric oxidant cycles, *J. Geophys. Res.*, *103*, 13,201–13,212, 1998.

Leung, F.-Y., J. A. Logan, R. Park, E. Hyer, E. Kasischke, D. Streets, and L. Yurganov, Impacts of biomass burning in the boreal forests on tropospheric chemistry and the sensitivity of model results to injection height, *J. Geophys. Res.*, *112*, 2007.

Levine, J. S., and W. R. Cofer III, Boreal forest fire emissions and the chemistry of the atmosphere, in *Fire, Climate Change and Carbon Cycling in the Boreal Forests*, edited by E. S. Kasischke and B. Stocks, vol. 138 of *Ecological Studies Series*, pp. 31–48, Springer-Verlag, New York, 2000.

Li, Q., D. J. Jacob, J. W. Munger, R. M. Yantosca, and D. D. Parrish, Export of NO_y from the North American boundary layer: Reconciling aircraft observations and global model budgets, *J. Geophys. Res.*, *109*, 2004.

Lobert, J. M., D. H. Scharffe, W. M. Hao, T. A. Kuhlbusch, R. Seuwen, P. Warneck, and P. J. Crutzen, Experimental evaluation of biomass burning emissions: Nitrogen and carbon containing compounds, in *Global Biomass Burning: Atmospheric, Climatic, and Biospheric Implications*, edited by J. S. Levine, chap. 36, pp. 289–307, MIT Press, Cambridge, MA, USA, 1991.

Luderer, G., J. Trentmann, T. Winterrath, C. Textor, M. Herzog, H. F. Graf, and M. O. Andreae, Modeling of biomass smoke injection into the lower stratosphere by a large forest fire (Part II): Sensitivity studies, *Atmos. Chem. and Phys.*, *6*, 5261–5277, 2006.

Macdonald, A. M., P. A. Makar, K. G. Anlauf, K. L. Hayden, J. W. Bottenheim, D. Wang, and T. Dann, Summertime formaldehyde at a high-elevation site in Quebec, *J. Geophys. Res.*, *106*, 32,361–32,374, 2001.

Marbach, T., S. Beirle, J. Hollwedel, U. Platt, and T. Wagner, Identication of tropospheric emissions sources from satellite observations: Synergistic use of trace gas meassurements of formaldehyde (HCHO), and nitrogen dioxide (NO2), in *Proc. of the 2004 Envisat and ERS Symposium 6-10 September 2004*, Salzburg, Austria, 2005.

Martin, R. V., D. J. Jacob, K. Chance, T. P. Kurosu, P. I. Palmer, and M. J. Evans, Global inventory of nitrogen oxide emissions constrained by space-based observations of NO_2 columns, *J. Geophys. Res.*, *108*, 2003.

Mason, S. A., R. J. Field, R. J. Yokelson, M. A. Kochivar, M. R. Tinsley, D. E. Ward, and W. M. Hao, Complex effects arising in smoke plume simulations due to inclusion of direct emissions of oxygenated organic species from biomass combustion, *J. Geophys. Res.*, *106*, 12,527–12,539, 2001.

Mason, S. A., J. Trentmann, T. Winterrath, R. J. Yokelson, T. J. Christian, L. J. Carlson, T. R. Warner, L. C. Wolfe, and M. O. Andreae, Intercomparison of two box models of the chemical evolution in biomass-burning smoke plumes, *J. Atmos. Chem.*, *55*, 273–297, 2006.

Mauzerall, D. L., et al., Photochemistry in biomass burning plumes and implications for tropospheric ozone over the tropical South Atlantic, *J. Geophys. Res.*, *103*, 8401–8423, 1998.

Mazzoni, D., J. A. Logan, D. Diner, R. Kahn, L. Tong, and Q. Li, A data-mining approach to associating misr smoke plume heights with modis fire measurements, *Remote Sens. Environ.*, *107*, 138–148, 2007.

McKeen, S. A., G. Wotawa, D. D. Parrish, J. S. Holloway, M. P. Buhr, G. Hübler, F. C. Fehsenfeld, and J. F. Meagher, Ozone production from Canadian wildfires during June and July of 1995, *J. Geophys. Res.*, *107*, 2002.

Meyer-Arnek, J., A. Ladstatter-Weienmayer, A. Richter, F. Wittrock, and J. P. Burrows, A study of the trace gas columns of O_3, NO_2 and HCHO over Africa in September 1997, *Faraday Discuss.*, *130*, 387–405, 2005.

Millet, D. B., D. J. Jacob, K. F. Boersma, T. M. Fu, T. P. Kurosu, K. Chance, C. L. Heald, and A. Guenther, Spatial distribution of isoprene emissions from North America derived from formaldehyde column measurements by the OMI satellite sensor, *J. Geophys. Res.*, *113*, 2008.

Miyanishi, K., Duff consumption, in *Forest fires: behavior and ecological effects*, edited by E. A. Johnson and K. Miyanishi, pp. 437–475, Academic Press, San Diego, Calif, 2001.

Morris, G. A., et al., Alaskan and Canadian forest fires exacerbate ozone pollution over Houston, Texas, on 19 and 20 July 2004, *J. Geophys. Res.*, *111*, 2006.

Nance, J. D., P. V. Hobbs, L. F. Radke, and D. E. Ward, Airborne measurements of gases and particles from an Alaskan wildfire, *J. Geophys. Res.*, *98*, 14,873–14,882, 1993.

Novelli, P. C., K. A. Masarie, P. M. Lang, B. D. Hall, R. C. Myers, and J. W. Elkins, Reanalysis of tropospheric CO trends: Effects of the 1997-1998 wildfires, *J. Geophys. Res.*, *108*, 2003.

Olivier, J., and J. Berdowski, Global emissions sources and sinks, in *The Climate System*, edited by J. Berdowski, R. R. Guicherit, and B. Heij, vol. 33–78, A.A. Balkema Publishers / Swets and Zeitlinger Publishers, Lisse, The Netherlands, 2001.

Owen, R., O. Cooper, A. Stohl, and R. Honrath, An analysis of the mechanisms of transport of North American emissions to the Central North Atlantic, *J. Geophys. Res.*, *111*, 2006.

Palmer, P., D. Jacob, A. Fiore, R. Martin, K. Chance, and T. Kurosu, Mapping isoprene emissions over North America using formaldehyde column observations from space, *J. Geophys. Res.*, *108*, 2003.

Palmer, P. I., et al., Quantifying the seasonal and interannual variability of North American isoprene emissions using satellite observations of the formaldehyde column, *J. Geophys. Res.*, *111*, 2006.

Parrish, D. D., A. Stohl, C. Forster, E. L. Atlas, D. R. Blake, P. D. Goldan, W. C. Kuster, and J. A. de Geow, Effects of mixing on evolution of hydrocarbon ratios in the troposphere, *J. Geophys. Res.*, *112*, 2007.

Parrish, D. D., et al., Fraction and composition of NO_y transported in air masses lofted from the North American boundary layer, *J. Geophys. Res.*, *109*, 2004.

Pfister, G., P. G. Hess, K. Emmons, J.-F. Lamarque, C. Wiedinmyer, D. P. Edwards, G.Pétron, J. C. Gille, and G. W. Sachse, Quantifying CO emissions from the 2004 Alaskan wildfires using MOPITT CO data, *Geophys. Res. Lett.*, *32*, 2005.

Pfister, G., et al., Ozone production from the 2004 north american boreal fires, *J. Geophys. Res.*, *111*, 2006.

Pfister, G. G., C. Wiedinmyer, and L. K. Emmons, Impacts of the fall 2007 California wildfires on surface ozone: Integrating local observations with global model simulations, *Geophys. Res. Lett.*, *35*, 2008.

Real, E., et al., Processes influencing ozone levels in Alaskan forest fire plumes during long-range transport over the North Atlantic, *J. Geophys. Res.*, *112*, 2007.

Richter, A., and J. P. Burrows, Retrieval of Tropospheric NO2 from GOME Measurements, *Adv. Space Res.*, *29*, 1673–1683, 2002.

Richter, A., J. P. Burrows, H. Nüß, C. Granier, and U. Niemeier, Increase in tropospheric nitrogen dioxide over China observed from space, *Nature*, *437*, 129–132, 2005.

Roy, B., G. A. Pouliot, A. Gilliland, T. Pierce, S. Howard, P. V. Bhave, and W. Benjey, Refining fire emissions for air quality modeling with remotely sensed fire counts: A wildfire case study, *Atmos. Environ.*, *41*, 655–665, 2007.

Sapkota, A., et al., Impact of the 2002 Canadian forest fires on particulate matter air quality in Baltimore city, *Environ. Sci. Technol.*, *39*, 24–32, 2005.

Seibert, P., and A. Frank, Source-receptor matric calculation with a Lagrangian particle disperion model in backward mode, *Atmos. Chem. and Phys.*, *4*, 51–63, 2004.

Seinfeld, J. H., and S. N. Pandis, *Atmospheric Chemistry and Physics: From Air Pollution to Climate Change*, John Wiley, New York, 1998.

Simmonds, P., A. Manning, R. Derwent, P. Ciais, M. Ramonet, V. Kazan, and D. Ryall, A burning question. Can recent growth rate anomalies in the greenhouse gases be attributed to large-scale biomass burning events?, *Atmos. Environ.*, *39*, 2513–2517, 2005.

Singh, H. B., et al., Reactive nitrogen distribution and partiti oning in the North American troposphere and lowermost stratosphere, *J. Geophys. Res.*, *112*, 2007.

Soja, A. J., et al., Climate-induced boreal forest change: Predictions versus current observations, *Global and Planetary Change*, *56*, 274–296, 2007.

Spichtinger, N., M. Wenig, P. James, T. Wagner, U. Platt, and A. Stohl, Satellite detection of a continental-scale plume of nitrogen oxides from boreal forest fires, *Geophys. Res. Lett.*, *28*, 4579–4582, 2001.

Spichtinger, N., R. Damoah, S. Eckhardt, C. Forster, P. James, S. Beirle, T. Wagner, P. Novelli, and A. Stohl, Boreal forest fires in 1997 and 1998: a seasonal comparison using transport model simulations and measurement data, *Atmos. Chem. and Phys.*, *4*, 1857–1868, 2004.

Spracklen, D. V., J. A. Logan, L. J. Mickley, R. Y. R. J. Park, A. L. Westerling, and D. A. Jaffe, Wildfires drive interannual variability of organic carbon aerosol in the western U.S. in summer, *Geophys. Res. Lett.*, *34*, 2007.

Stavrakou, T., J.-F. Müller, I. De Smedt, M. Van Roozendael, G. R. van der Werf, L. Giglio, and A. Guenther, Evaluating the performance of pyrogenic and biogenic emission inventories against one decade of space-based formaldehyde columns, *Atmos. Chem. and Phys.*, *9*, 1037–1060, 2009.

Stocks, B., et al., Climate change and forest fire potential in Russian and Canadian boreal forests, *Clim. Change*, *38*, 1–13, 1998.

Stocks, B. J., et al., Large forest fires in Canada, 1959-1997, *J. Geophys. Res.*, *108*, 2003.

Stohl, A., S. Eckhardt, C. Forster, P. James, N. Spichtinger, and P. Seibert, A replacement for simple back trajectory calculations in the interpretation of atmospheric trace substance measurements, *Atmos. Environ.*, *36*, 4635–4648, 2002.

Stohl, A., C. Forster, A. Frank, P. Seibert, and G. Wotawa, Technical note: The Lagrangian particle dispersion model FLEXPART version 6.2, *Atmos. Chem. and Phys.*, *5*, 2461–2474, 2005, sRef-ID:1680-7324/acp/2005-5-2461.

Stohl, A., et al., Pan-arctic enhancements of light absorbing aerosol concentrations due to north american boreal forest fires during summer 2004, *J. Geophys. Res.*, *111*, 2006.

Stunder, B., NCEP model output—FNL archive data: TD-6141, Tech. rep., available at http://www.arl.noaa.gov/ready-bin/fnl.pl, 1997, NOAA-Air Resources Laboratory, Silver Spring, MD 20910.

Tabazadeh, A., R. J. Yokelson, H. B. Singh, P. V. Hobbs, J. H. Crawford, and L. T. Iraci, Heterogeneous chemistry involving methanol in tropospheric clouds, *Geophys. Res. Lett.*, *31*, 2004.

Tanimoto, H., Y. Kajii, J. Hirokawa, H. Akimoto, and N. P. Minko, The atmospheric impact of boreal forest fires in far eastern Siberia on the seasonal variation of carbon monoxide: Observations at Rishiri, a northern remote island in Japan, *J. Geophys. Res.*, *27*, 4073–4076, 2000.

Trentmann, J., G. Luderer, T. Winterrath, M. D. Fromm, R. Servranckx, C. Textor, M. Herzog, H. F. Graf, and M. O. Andreae, Modeling of biomass smoke injection into the lower stratosphere by a large forest fire (Part I): Reference simulation, *Atmos. Chem. and Phys.*, *6*, 5247–5260, 2006.

Turetsky, M. R., B. D. Amiro, E. Bosch, and J. S. Bhatti, Historical burn area in western canadian peatlands and its relationship to fire weather indices, *Global Biogeochem. Cycles*, *18*, 2004.

Turquety, S., et al., Inventory of boreal fire emissions for North America in 2004: the importance of peat burning and pyro-convective injection, *J. Geophys. Res.*, *112*, 2007.

Val Martín, M., R. Honrath, R. C. Owen, G. Pfister, P. Fialho, and F. Barata, Significant enhancements of nitrogen oxides, ozone and aerosol black carbon in the North Atlantic lower free troposphere resulting from North American boreal wildfires, *J. Geophys. Res.*, *111*, 2006.

Val Martín, M., R. E. Honrath, R. C. Owen, and K. Lapina, Large-scale impacts of anthropogenic pollution and boreal wildfires on the nitrogen oxides over the central North Atlantic region, *J. Geophys. Res.*, *113*, 2008.

Val Martín M., R. Honrath, R. Owen, J. Kleissl, P. Fialho, G. Pfister, and K. Lapina, Large enhancements of NO_x over the central North Atlantic lower free troposphere resulting from boreal wildfires: Observations at the PICO-NARE station during summer 2004, *Eos Trans. AGU*, *86*, 2005, Fall Meet. Suppl., Abstract A41D-02.

Van der Werf, G. R., J. T. Randerson, G. J. Collatz, L. Giglio, P. S. Kasibhatla, A. F. Arellano Jr., S. C. Olsen, and E. S. Kasischke, Continental-scale partitioning of fire emissions during the 1997 to 2001 El Nino/La Nina period, *Science*, *303*, 73–76, 2004.

Verma, S., et al., Ozone production in boreal fire smoke plumes using observations from the Tropospheric Emission Spectrometer and the Ozone Monitoring Instrument, *J. Geophys. Res.*, *114*, 2009.

Wittrock, F., The retrieval of oxygenated volatile organic compounds by remote sensing techniques, Ph.D. thesis, Institute of Environmental Physics, University of Bremen, Bremen, available at http://nbn-resolving.de/urn:nbn:de:gbv:46-diss000104818, 2006.

Wittrock, F., et al., Simultaneous global observations of glyoxal and formaldehyde from space, *Geophys. Res. Lett.*, *33*, 2006.

Wofsy, S. C., S.-M. Fan, D. R. Blake, J. D. Bradshaw, S. T. Sandholm, H. B. Singh, G. W. Sachse, and R. C. Harriss, Factors influencing atmospheric composition over subarctic North America during summer, *J. Geophys. Res.*, *99*, 1887–1897, 1994.

Wofsy, S. C., et al., Atmospheric chemistry in the arctic and subarctic: Influence of natural fires, industrial emissions, and stratospheric inputs, *J. Geophys. Res.*, *97*, 16,731–16,746, 1992.

Wotawa, G., P. C. Novelli, M. Trainer, and C. Granier, Inter-annual variability of summertime CO concentrations in the northern hemisphere explained by boreal forest fires in North America and Russia, *Geophys. Res. Lett.*, *28*, 4575–4578, 2001.

W.Thomas, E. Hegels, S. Slijkhuis, R. Spurr, and K. Chance, Detection of biomass burning combustion products in Southeast Asia from backscatter data taken by the GOME spectrometer, *Geophys. Res. Lett.*, *25*, 1317–1320, 1998.

Yokelson, R., et al., Emissions from biomass burning in the Yucatan, *Atmos. Chem. and Phys. Discussions*, *9*, 767–835, 2009.

Yokelson, R. J., D. W. T. Griffith, and D. E. Ward, Open-path Fourier transform infrared studies of large-scale laboratory biomass fire, *J. Geophys. Res.*, *101*, 21,067–21,080, 1996.

Yokelson, R. J., R. Susott, D. E. Ward, J. Reardon, and D. W. T. Griffith, Emissions from smoldering combustion of biomass measured by open-path fourier transform infrared spectroscopy, *J. Geophys. Res.*, *102*, 18,865–18,878, 1997.

Yokelson, R. J., I. T. Bertschi, T. J. Christian, P. V. Hobbs, D. E. Ward, and W. M. Hao, Trace gas measurements in nascent, aged, and cloud-processed smoke from African savanna fires by airborne Fourier transform infrared spectroscopy (AFTIR), *J. Geophys. Res.*, *108*, 2003.

Yurganov, L. N., et al., A quantitative assessment of the 1998 carbon monoxide emission anomaly in the Northern Hemisphere based on total column and surface concentration measurement, *J. Geophys. Res.*, *109*, 2004.

Appendix A

Figures

This document includes supplementary figures and results used for the analysis discussed in Chapter 4 of this work. Figures A.1, A.2, A.3, A.4 and A.5 present daily SCIAMACHY observations of HCHO columns, gridded on a $1^\circ \times 1^\circ$ grid. They demonstrate a sparse coverage of the measurements (section 4.2), which is the main reason for the use of 5-day composites in the analysis.

The locations used to compare the SCIAMACHY signal over the regions of high-isoprene and low-isoprene regions (section 4.4.1.1) are shown in Figures A.6 and A.7. Table A.1 presents statistics for the HCHO measurements in the analyzed regions. The last column of Table A.1 contains the difference between the average HCHO columns in the high- and low-isoprene regions.

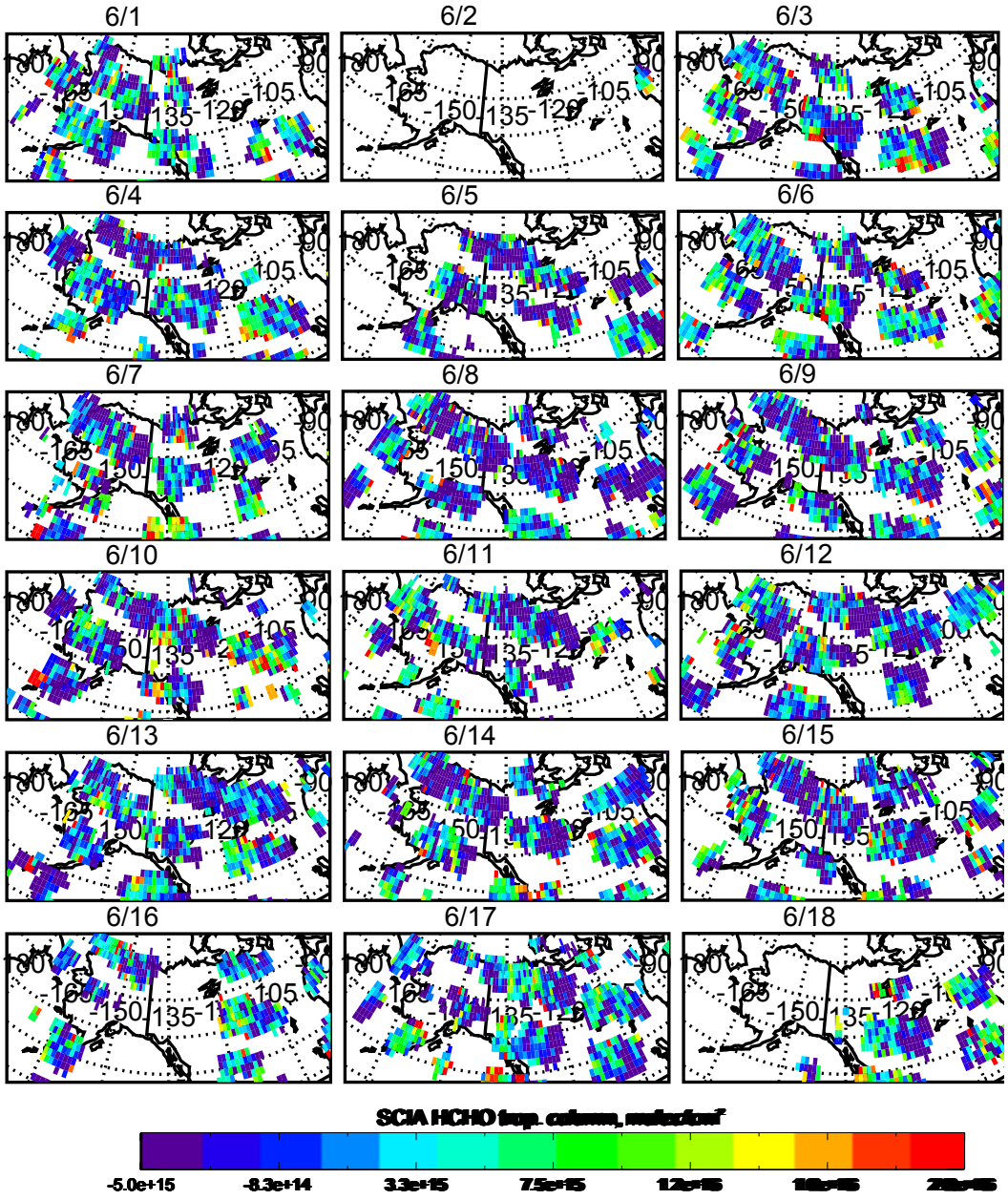

Figure A.1 Daily SCIAMACHY observations of HCHO, for the period from June 1 untill June 17, 2004. White areas inside the study region indicate missing satellite observations.

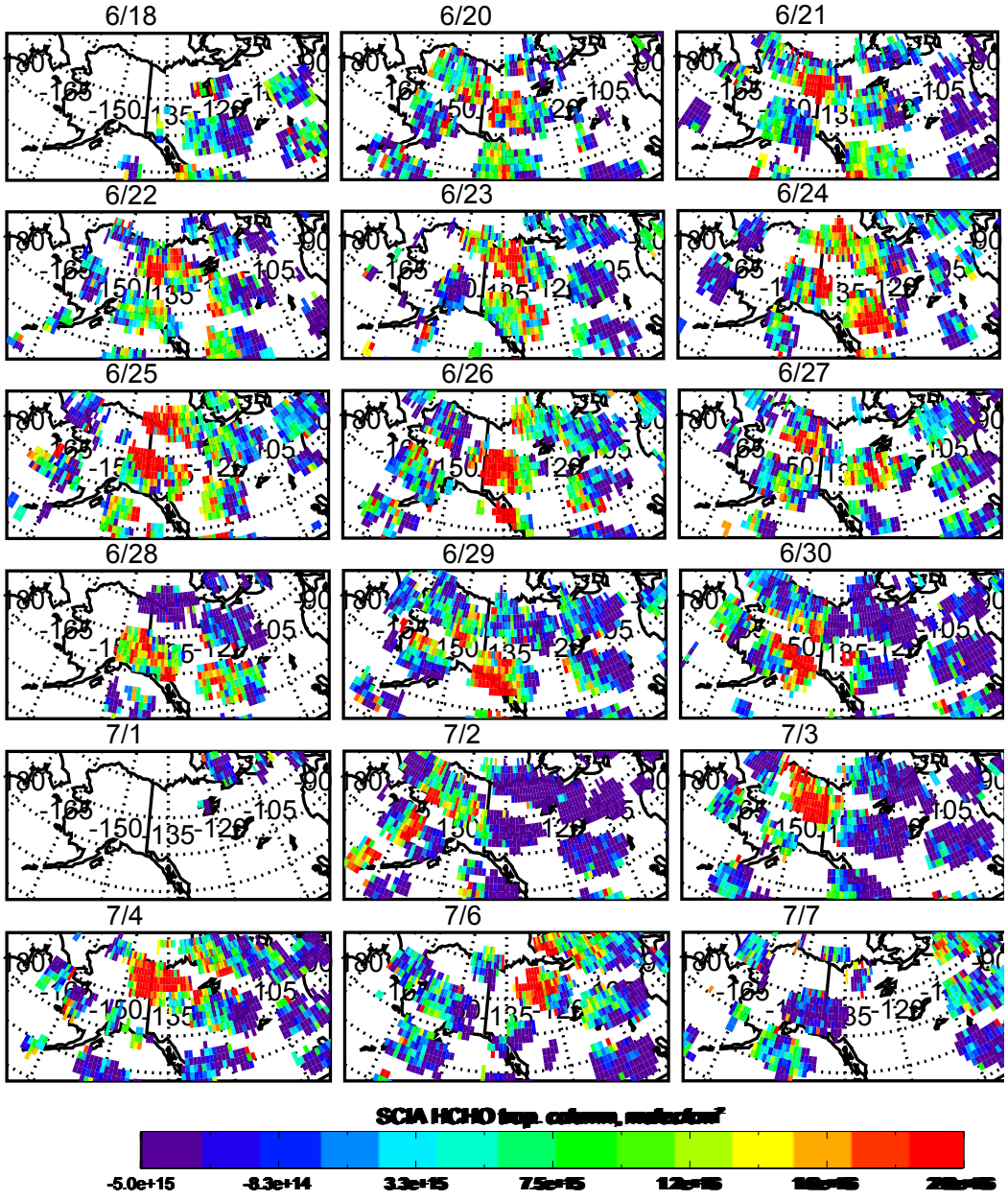

Figure A.2 Daily SCIAMACHY observations of HCHO, for the period from June 18 untill July 7, 2004. White areas inside the study region indicate missing satellite observations.

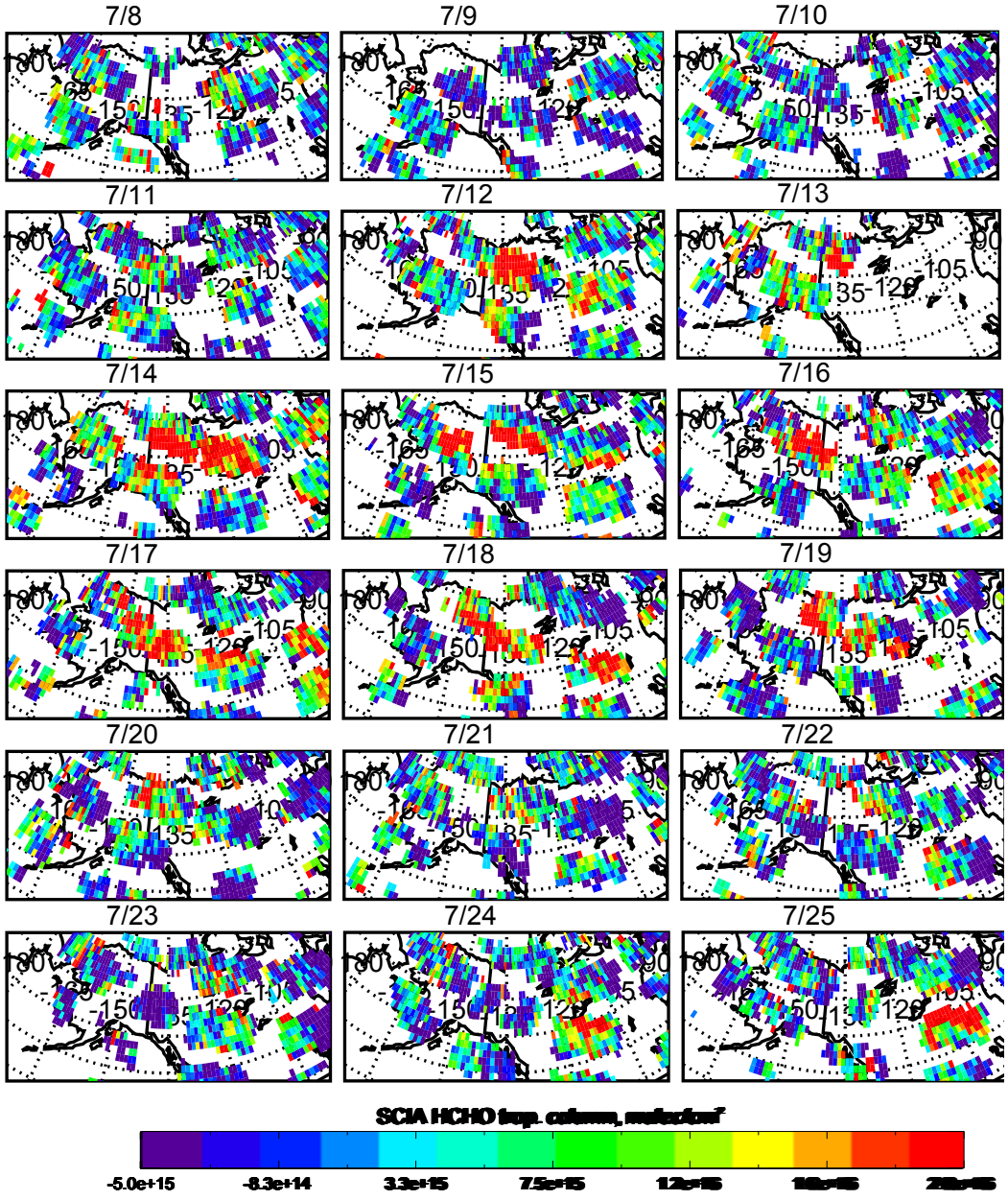

Figure A.3 Daily SCIAMACHY observations of HCHO, for the period from July 8 untill July 25, 2004. White areas inside the study region indicate missing satellite observations.

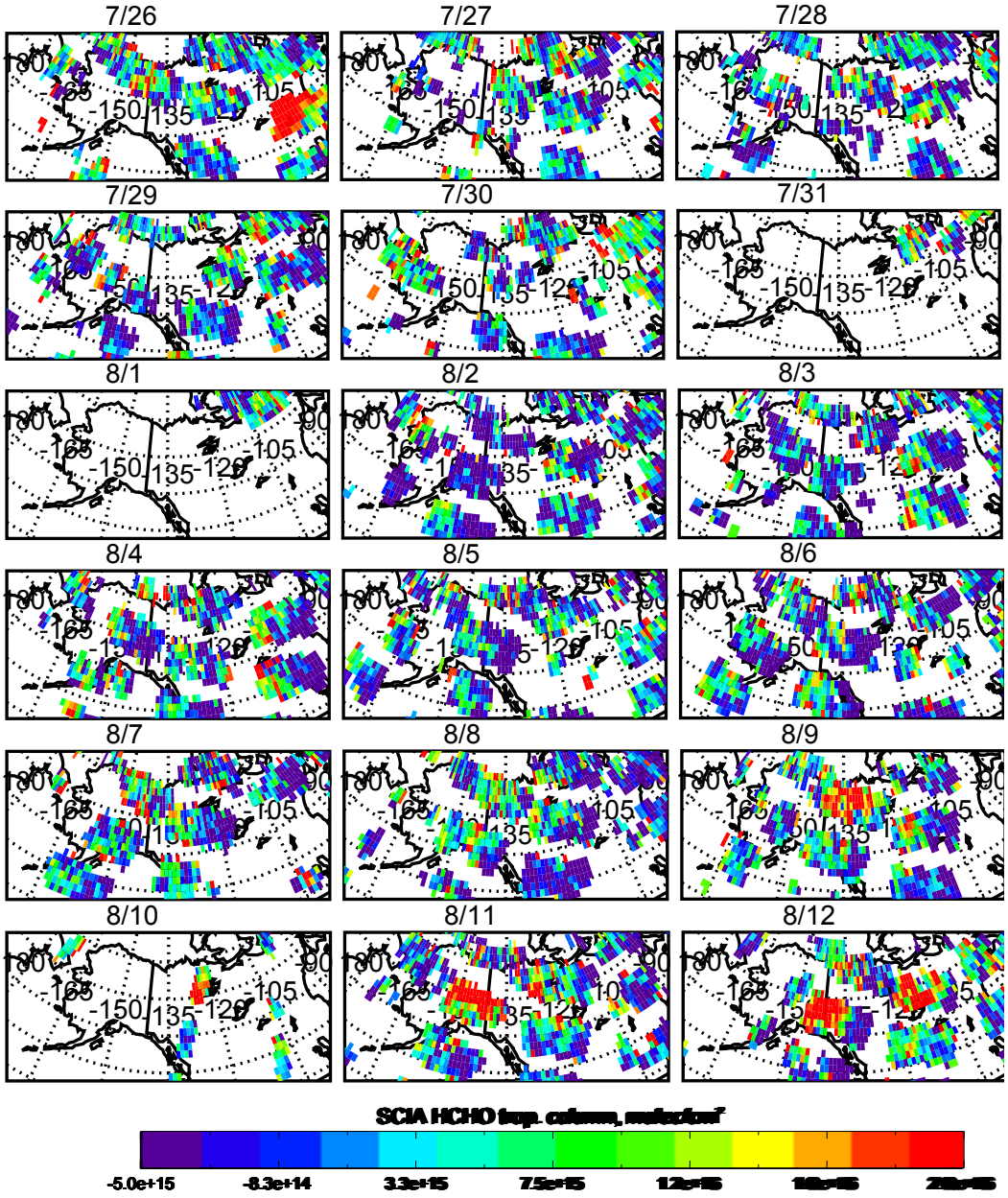

Figure A.4 Daily SCIAMACHY observations of HCHO, for the period from July 26 untill August 12, 2004. White areas inside the study region indicate missing satellite observations.

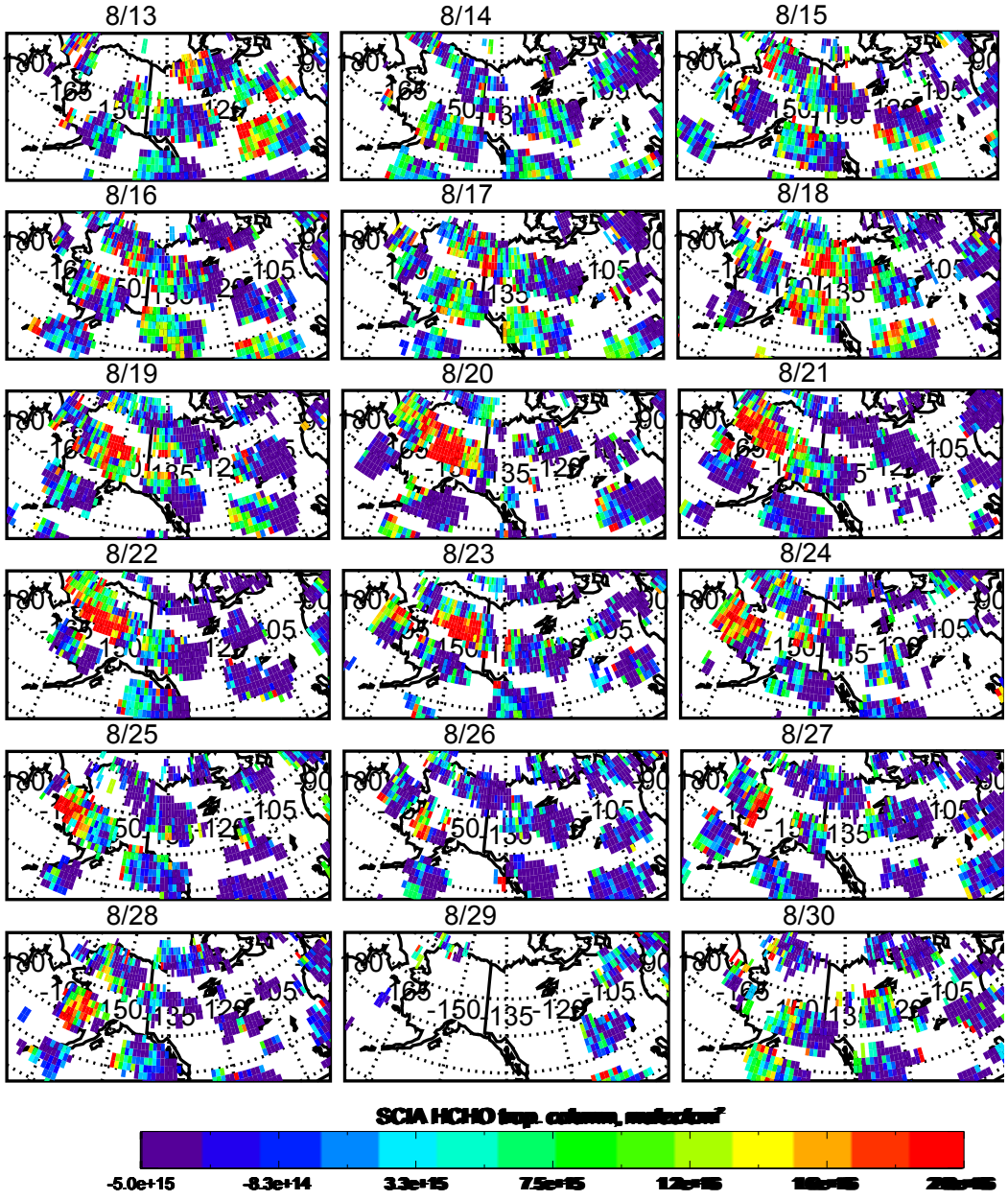

Figure A.5 Daily SCIAMACHY observations of HCHO, for the period from August 13 untill August 30, 2004. White areas inside the study region indicate missing satellite observations.

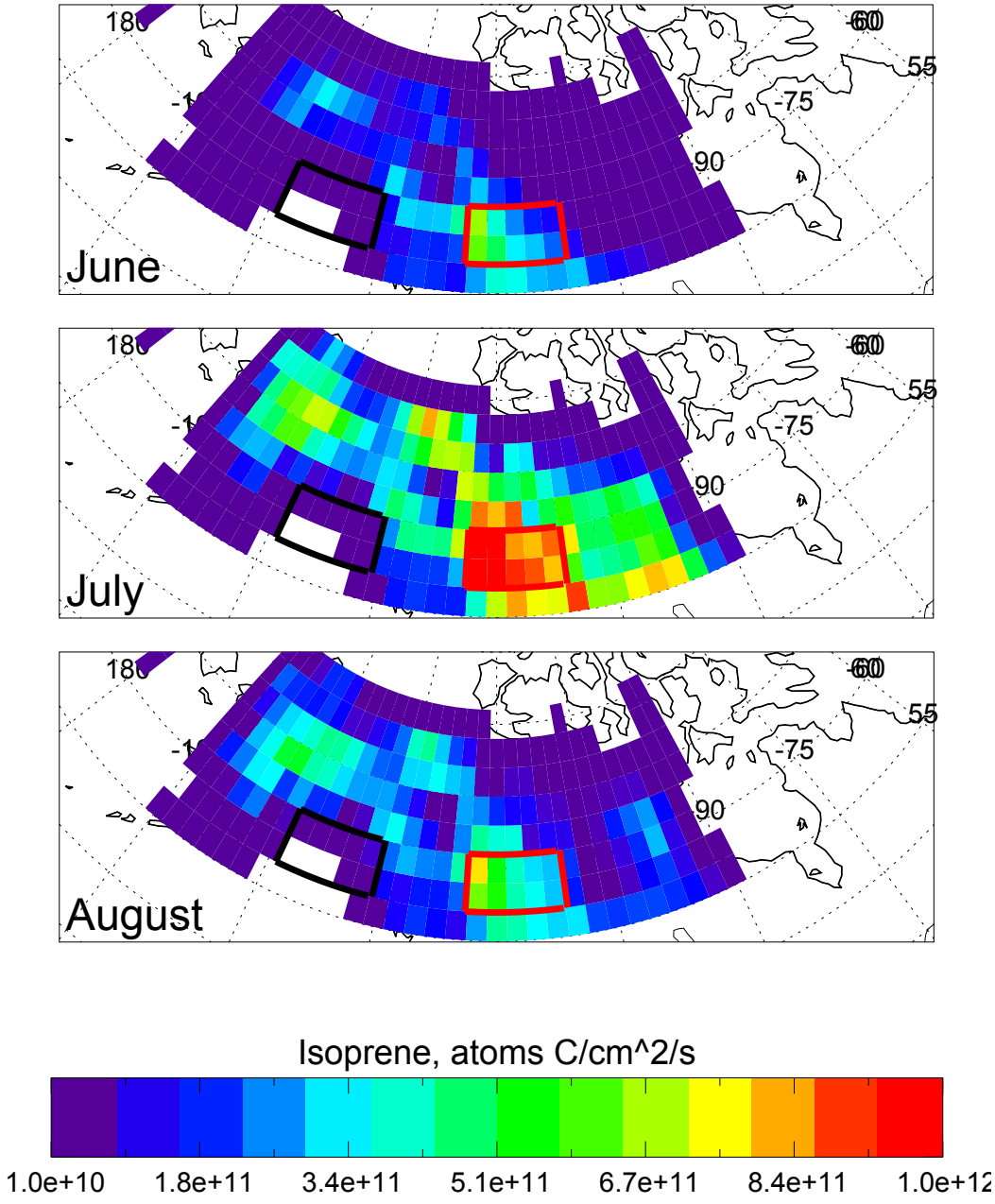

Figure A.6 Monthly-mean modeled isoprene emission fluxes in units of atoms/C/cm^2. The areas used for comparison of HCHO columns between the high-isoprene and low-isoprene regions during the periods of low fire activity are overplotted in red (high-isoprene) and black (low-isoprene). High-isoprene region indicated in this figure was also used for computing the average daily isoprene flux.

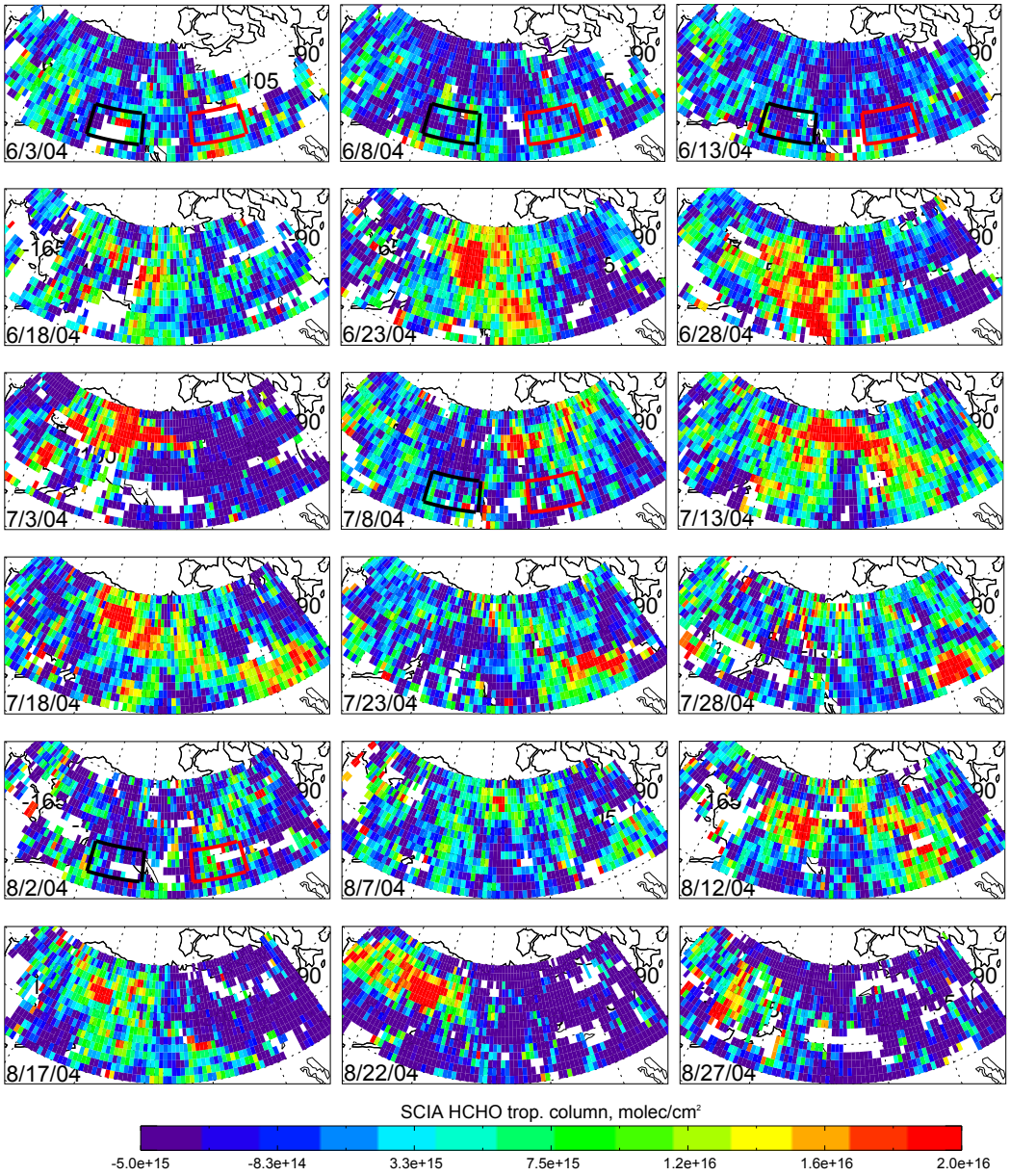

Figure A.7 SCIAMACHY HCHO 5-day composites. The areas used for comparison of HCHO columns between the high-isoprene and low-isoprene regions during the periods of low fire activity are overploted in red (high-isoprene) and black (low-isoprene).

Table A.1 Statistics of HCHO SCIAMACHY tropospheric columns in the high- and low-isoprene regions.

	Low-isoprene			High-isoprene			Difference between
Day	N	Mean	Std. dev.	N	Mean	Std. dev.	means (high-low)
June 3, 2004	71	3.6e15	8.4e15	54	2.5e15	4.9e15	-1.1e15
June 8, 2004	84	2.4e15	5.7e15	70	3.2e15	3.6e15	0.8e15
June 13, 2004	80	1.4e15	6.6e15	70	-7.5e13	3.6e15	-1.4e15
July 8, 2004	83	1.9e15	5.9e15	68	1.8e15	6.1e15	-0.1e15
August 2, 2004	70	-5.4e13	7.6e15	59	4.0e15	8.5e14	4.e15

Appendix B

Copyright permissions and information

This section contains copyright information for Chapters 2 and 3, which are based on the articles *Lapina et al.* [2006] and *Lapina et al.* [2008].

B.1 Documentation for Chapter 2

Chapter 2 is based entirely on *Lapina et al.* [2006], the copyright of which is held by the American Geophysical Union. The two following subsections contain the email sent to request permission and information regarding reproduction of the paper in this dissertation and the response granting that right.

B.1.1 Email requesting for reproduction permission

Subject: Use of paper in dissertation

Sent By "Kateryna Lapina" klapina@mtu.edu

On: April 17, 2009 6:23 PM

To: grl@agu.org

Dear Sir/Madam,

I am completing a doctoral dissertation at Michigan Technological University entitled "Boreal forest fire impacts on lower troposphere CO and ozone levels at the regional to hemispheric scales" and I am seeking permission to reprint as a chapter in my dissertation the contents from my GRL paper

Lapina K., R. E. Honrath, R. C. Owen, M. Val Martn, G. Pfister (2006), Evidence of significant large-scale impacts of boreal fires on ozone levels in the midlatitude Northern Hemisphere free troposphere, Geophys. Res. Lett., 33, L10815, doi:10.1029/2006GL025878.

Thank you very much.

Sincerely,

Kateryna Lapina

B.1.2 Email granting reproduction permission

Subject: permission

Sent By "Michael Connolly" MConnolly@agu.org

On: April 20, 2009 1:19 PM

To: klapina@mtu.edu

We are pleased to grant permission for the use of the material requested for inclusion in your thesis. The following non-exclusive rights are granted to AGU authors:

All proprietary rights other than copyright (such as patent rights). The right to present the material orally. The right to reproduce figures, tables, and extracts, appropriately cited. The right to make hard paper copies of all or part of the paper for classroom use. The right to deny subsequent commercial use of the paper.

Further reproduction or distribution is not permitted beyond that stipulated. The copyright credit line should appear on the first page of the article or book chapter. The following must also be included, Reproduced by permission of American Geophysical Union. To ensure that credit is given to the original source(s) and that authors receive full credit through appropriate citation to their papers, we recommend that the full bibliographic reference be cited in the reference list. The standard credit line for journal articles is: "Author(s), title of work, publication title, volume number, issue number, citation number (or page number(s) prior to 2002), year. Copyright [year] American Geophysical Union."

If an article was placed in the public domain, in which case the words Not subject to U.S. copyright appear on the bottom of the first page or screen of the article, please substitute published for the word copyright in the credit line mentioned above.

Copyright information is provided on the inside cover of our journals. For permission for any other use, please contact the AGU Publications Office at AGU, 2000 Florida Ave., N.W., Washington, DC 20009.

Michael Connolly

Journals Publications Specialist

B.2 Documentation for Chapter 3

Chapter 3 is based entirely on *Lapina et al.* [2008], the copyright of which is held by the American Geophysical Union. The two following subsections contain the email sent to request permission and information regarding reproduction of the paper in this dissertation and the response granting that right.

B.2.1 Email requesting for reproduction permission

Subject: Use of paper in dissertation

Sent By "Kateryna Lapina" klapina@mtu.edu

On: April 17, 2009 6:20 PM

To: jgr-atmospheres@agu.org

Dear Sir/Madam,

I am completing a doctoral dissertation at Michigan Technological University entitled "Boreal forest fire impacts on lower troposphere CO and ozone levels at the regional to hemispheric scales".

First, I am seeking permission to reprint as a chapter in my dissertation the contents from my JGR Atmospheres article: Lapina K., R. E. Honrath, R. C. Owen, M. Val Martn, E. J. Hyer, P. Fialho (2008), Late summer changes in burning conditions in the boreal regions and their implications for NO x and CO emissions from boreal fires, J. Geophys. Res., 113, D11304, doi:10.1029/2007JD009421.

Second, I am planning to submit one of the chapters of my dissertation (which will be published within the next month) for the publication in the JGR. Will then PhD dissertation be counted as a "prior publication?"

Any information or assistance you can provide regarding this issue would be appreciated.

Sincerely,

Kateryna Lapina

B.2.2 Email granting reproduction permission

Subject: permission

Sent By "Michael Connolly" MConnolly@agu.org

On: April 20, 2009 1:39 PM

To: klapina@mtu.edu

We are pleased to grant permission for the use of the material requested for inclusion in your thesis. The following non-exclusive rights are granted to AGU authors:

All proprietary rights other than copyright (such as patent rights). The right to present the material orally. The right to reproduce figures, tables, and extracts, appropriately cited. The right to make hard paper copies of all or part of the paper for classroom use. The right to deny subsequent commercial use of the paper.

Further reproduction or distribution is not permitted beyond that stipulated. The copyright credit line should appear on the first page of the article or book chapter. The following must also be included, Reproduced by permission of American Geophysical Union. To ensure that credit is given to the original source(s) and that authors receive full credit through appropriate citation to their papers, we recommend that the full bibliographic reference be cited in the reference list. The standard credit line for journal articles is: "Author(s), title of work, publication title, volume number, issue number, citation number (or page number(s) prior to 2002), year. Copyright [year] American Geophysical Union."

If an article was placed in the public domain, in which case the words Not subject to U.S. copyright appear on the bottom of the first page or screen of the article, please substitute published for the word copyright in the credit line mentioned above.

Copyright information is provided on the inside cover of our journals. For permission for any other use, please contact the AGU Publications Office at AGU, 2000 Florida Ave., N.W., Washington, DC 20009.

Michael Connolly

Journals Publications Specialist